US012395109B2

(12) **United States Patent**
Elshormbably et al.

(10) **Patent No.: US 12,395,109 B2**
(45) **Date of Patent: Aug. 19, 2025**

(54) **PREDICTIVE CURRENT CONTROL METHOD FOR A SIX-PHASE INDUCTION MOTOR**

(71) Applicant: **KING FAHD UNIVERSITY OF PETROLEUM AND MINERALS**, Dhahran (SA)

(72) Inventors: **Mohamed Mamdouh Mohamed Elshormbably**, Dhahran (SA); **Mohamed Ali Yousef Abido**, Dhahran (SA)

(73) Assignee: **KING FAHD UNIVERSITY OF PETROLEUM AND MINERALS**, Dhahran (SA)

(*) Notice: Subject to any disclaimer, the term of this patent is extended or adjusted under 35 U.S.C. 154(b) by 174 days.

(21) Appl. No.: **18/498,753**

(22) Filed: **Oct. 31, 2023**

(65) **Prior Publication Data**

US 2025/0141380 A1 May 1, 2025

(51) **Int. Cl.**
H02P 21/22 (2016.01)
H02P 21/18 (2016.01)
(Continued)

(52) **U.S. Cl.**
CPC ***H02P 21/22*** (2016.02); ***H02P 21/18*** (2016.02); ***H02P 25/107*** (2013.01); ***H02P 27/06*** (2013.01)

(58) **Field of Classification Search**
CPC H02P 21/18; H02P 21/22; H02P 2207/01; H02P 25/107; H02P 27/06; H02P 21/00;
(Continued)

(56) **References Cited**

U.S. PATENT DOCUMENTS

11,119,457 B2 9/2021 El Shormbably et al.
2020/0409320 A1 12/2020 El Shormbably et al.
(Continued)

FOREIGN PATENT DOCUMENTS

CN 107565872 A 1/2018
CN 109347389 A 2/2019
CN 115037213 A 9/2022

OTHER PUBLICATIONS

Osvaldo Gonzalez, et al., "Model Predictive Current Control of Six-Phase Induction Motor Drives Using Virtual Vectors and Space Vector Modulation", IEEE Transactions on Power Electronics, vol. 37, Issue 7, Jan. 7, 2022, pp. 7617-7628 (Abstract only).

Primary Examiner — Antony M Paul
(74) *Attorney, Agent, or Firm* — Oblon, McClelland, Maier & Neustadt, L.L.P.

(57) **ABSTRACT**

A predictive current control method for a six-phase induction motor (6PIM) includes initializing a six-phase inverter at a present switching state, measuring a stator current and a rotor speed, transforming the stator current to αβ and xy orthogonal frame, estimating a pair of currents in αβ and xy frame based upon the measured and an estimated rotor speed, and calculating a future stator current for a future control sample of the inverter. The method further includes selecting four voltage vectors (VV) from αβ and xy frames, implementing a cost function to calculate an error between the predicted future and a reference stator current, calculating a plurality of cost function results of each of the four VV, identifying a future VV that provides a minimum cost function results for the future control sample, saving the future VV to be used as an input to the lookup table for the next control sample and controlling the 6PIM by applying the future control sample as the switching state of the inverter.

14 Claims, 30 Drawing Sheets

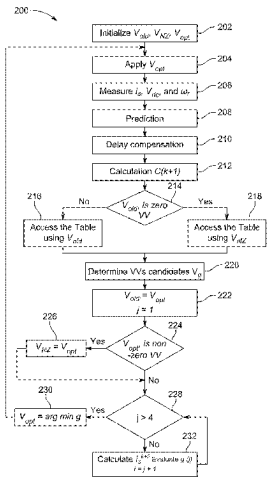

(51) **Int. Cl.**
H02P 25/10 (2006.01)
H02P 27/06 (2006.01)

(58) **Field of Classification Search**
CPC H02P 21/0003; H02P 21/0021; H02P 21/0085; H02P 21/14; H02P 21/34; H02P 21/50; H02P 21/30; H02P 23/07; H02P 27/08; H02P 25/062
See application file for complete search history.

(56) **References Cited**

U.S. PATENT DOCUMENTS

2021/0344292 A1* 11/2021 Sahin H02M 7/53873
2023/0006582 A1* 1/2023 Wang H02M 1/0009

* cited by examiner

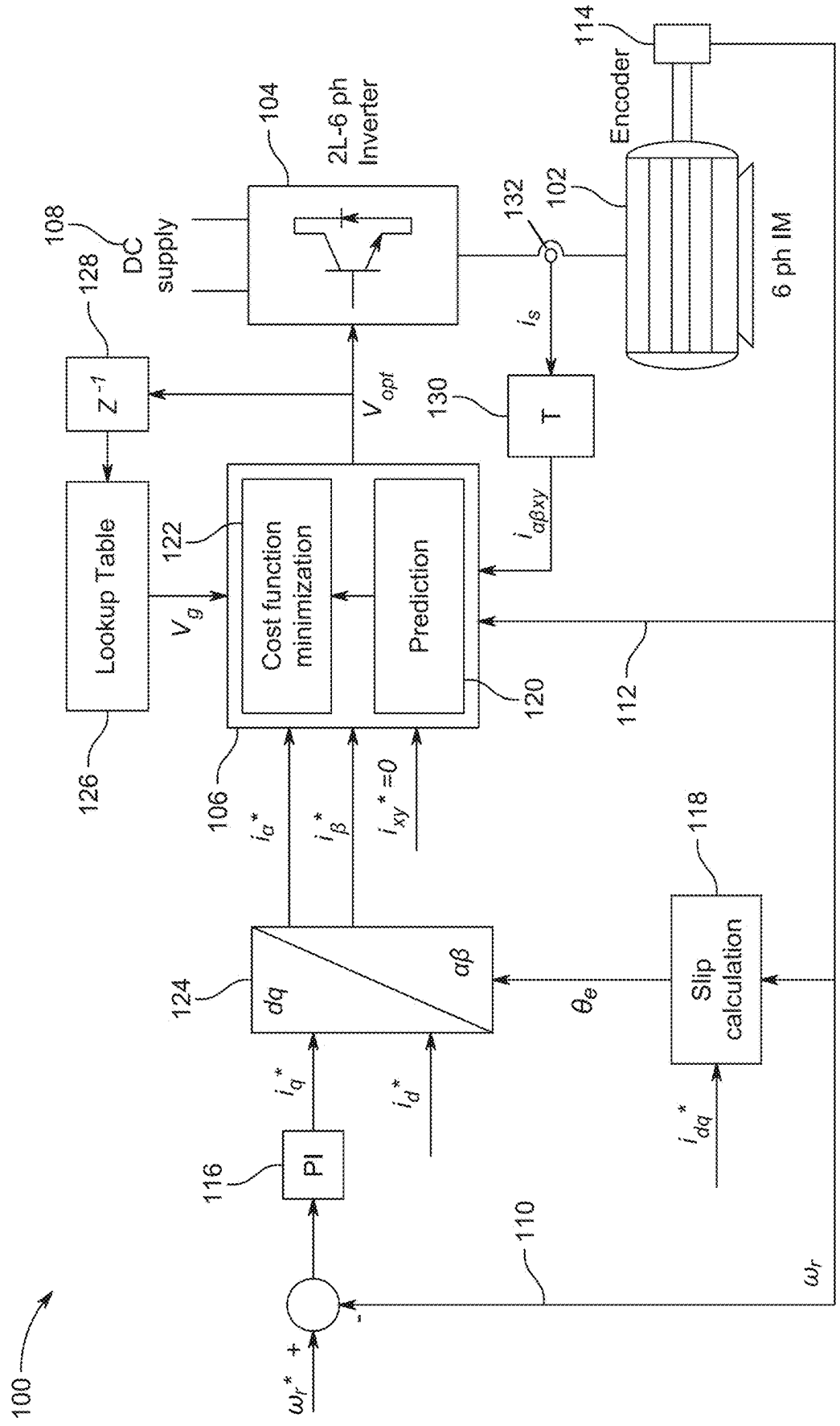
100
ω_r^*
+
-
110
PI
116
i_q^*
i_d^*
124
dq
αβ
θ_e
Slip calculation
118
i_{dq}^*
ω_r
i_α^*
i_β^*
$i_{xy}^*=0$
106
126
Lookup Table
V_g
122
Cost function minimization
Prediction
120
112
$i_{\alpha\beta xy}$
T
130
i_s
V_{opt}
Z^{-1}
128
108
DC supply
104
2L-6 ph Inverter
132
102
6 ph IM
Encoder
114

FIG. 1

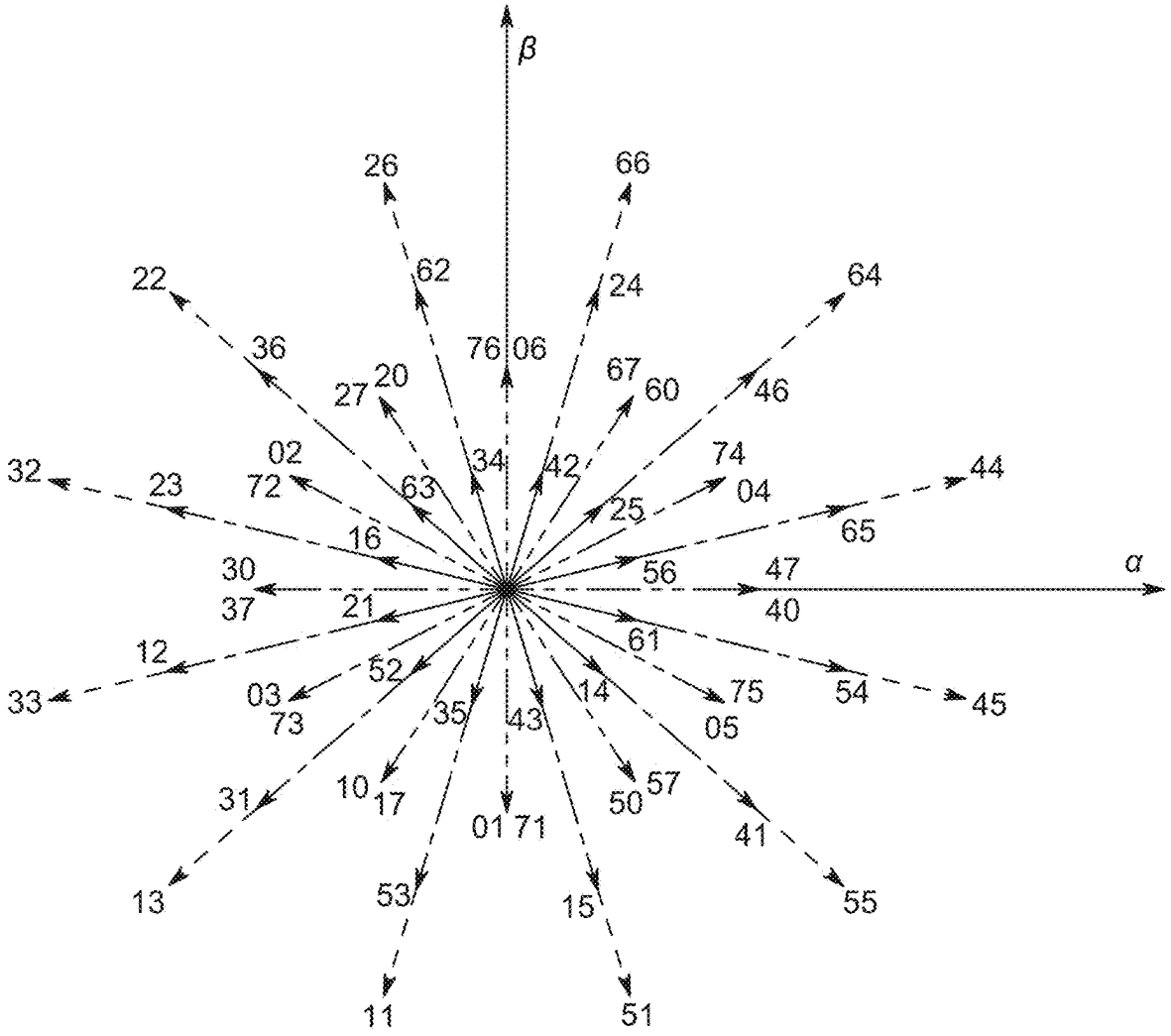
β
α
26
66
62
24
22
64
36
76
06
27
20
67
60
46
02
74
32
23
72
63
34
42
04
44
25
16
65
30
56
47
37
21
40
12
61
52
33
03
14
75
54
45
73
35
43
05
31
10
17
50
57
01
71
41
13
53
15
55
11
51

FIG. 2A

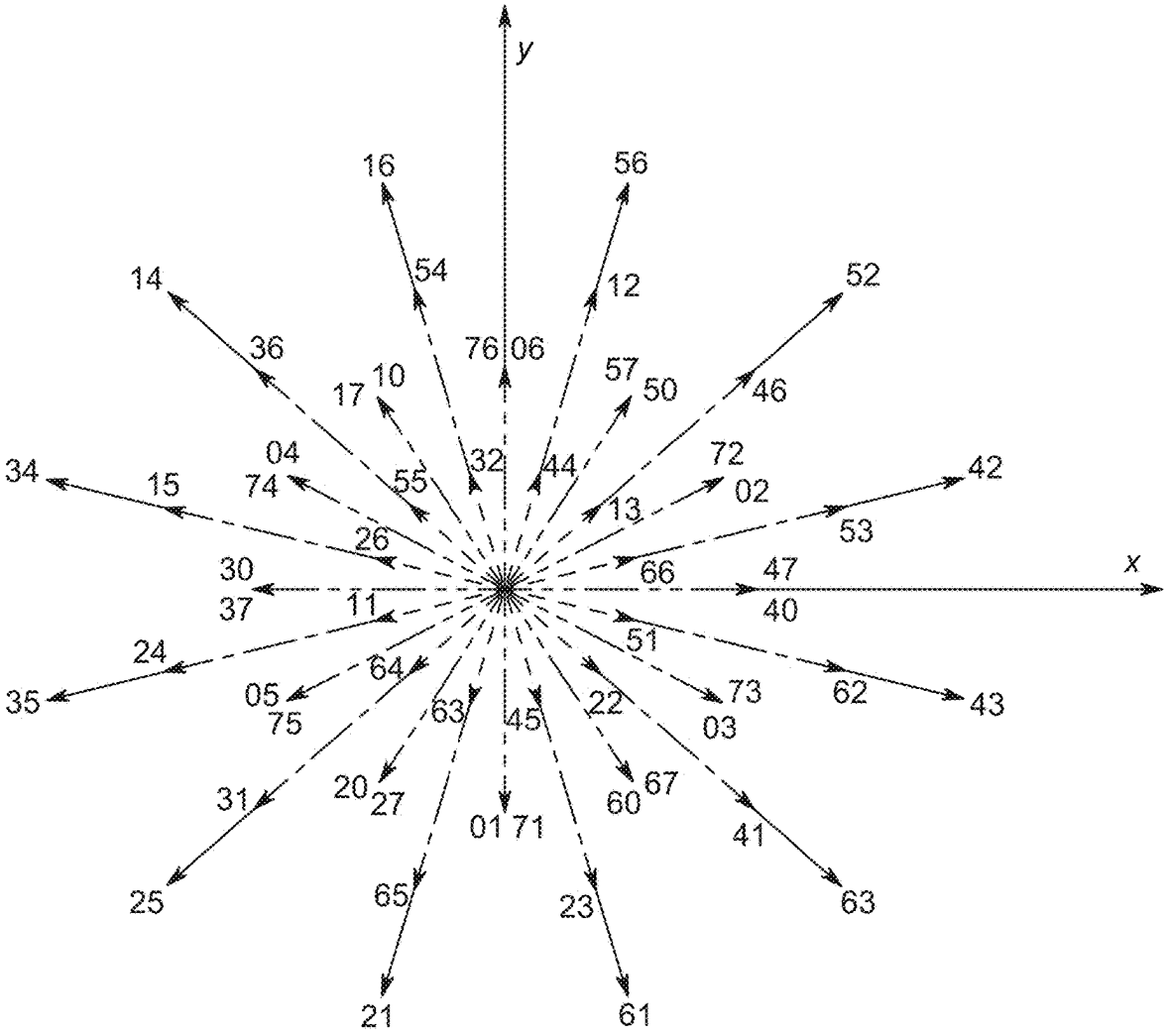
y
x
16
56
54
12
14
52
36
76
06
10
57
17
50
46
04
72
34
32
44
42
15
74
55
02
13
26
53
30
66
47
37
11
40
24
51
64
35
05
73
62
43
75
63
45
22
03
31
20
27
60
67
01
71
41
25
65
23
63
21
61

FIG. 2B

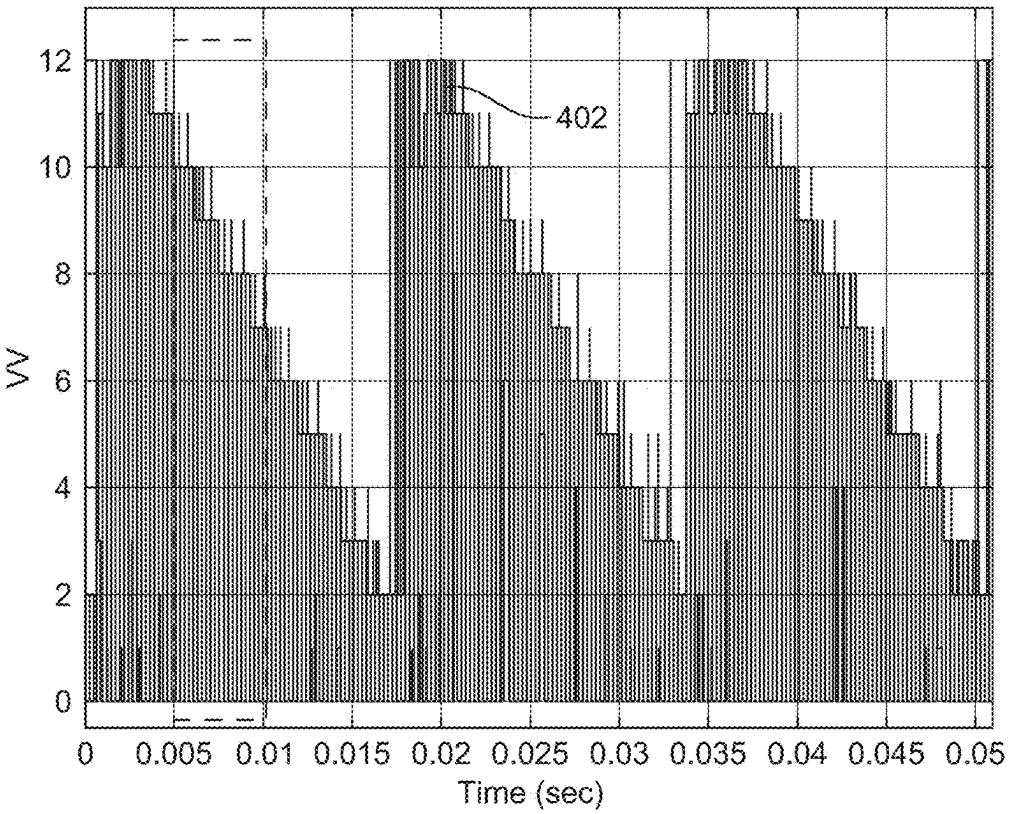
402
12
10
8
6
4
2
0
VV
0
0.005
0.01
0.015
0.02
0.025
0.03
0.035
0.04
0.045
0.05
Time (sec)

FIG. 3A

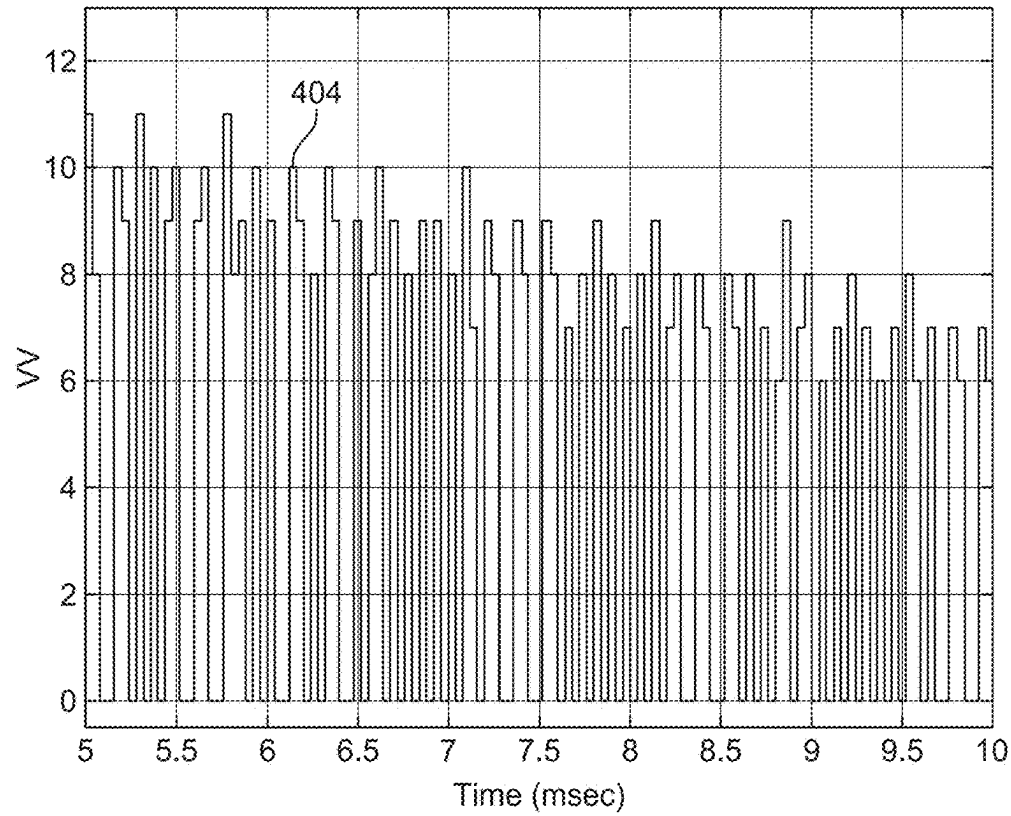
404
12
10
8
6
4
2
0
VV
5
5.5
6
6.5
7
7.5
8
8.5
9
9.5
10
Time (msec)

FIG. 3B

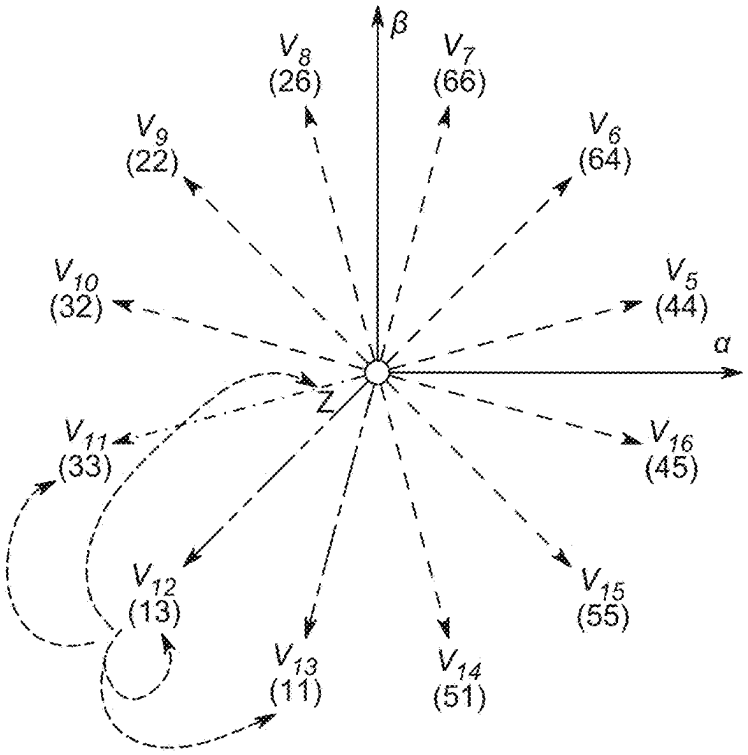
β
α
V8 (26)
V7 (66)
V9 (22)
V6 (64)
V10 (32)
V5 (44)
Z
V11 (33)
V16 (45)
V12 (13)
V15 (55)
V13 (11)
V14 (51)
Z = { V1,V2,V3,V4 }

FIG. 3C

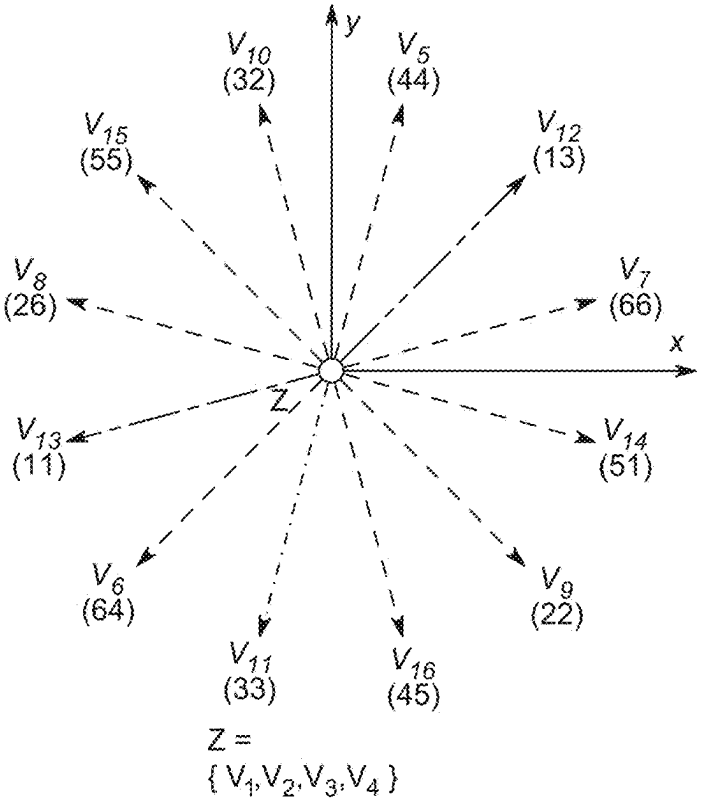
y
x
V10 (32)
V5 (44)
V15 (55)
V12 (13)
V8 (26)
V7 (66)
Z
V13 (11)
V14 (51)
V6 (64)
V9 (22)
V11 (33)
V16 (45)
Z = { V1,V2,V3,V4 }

FIG. 3D

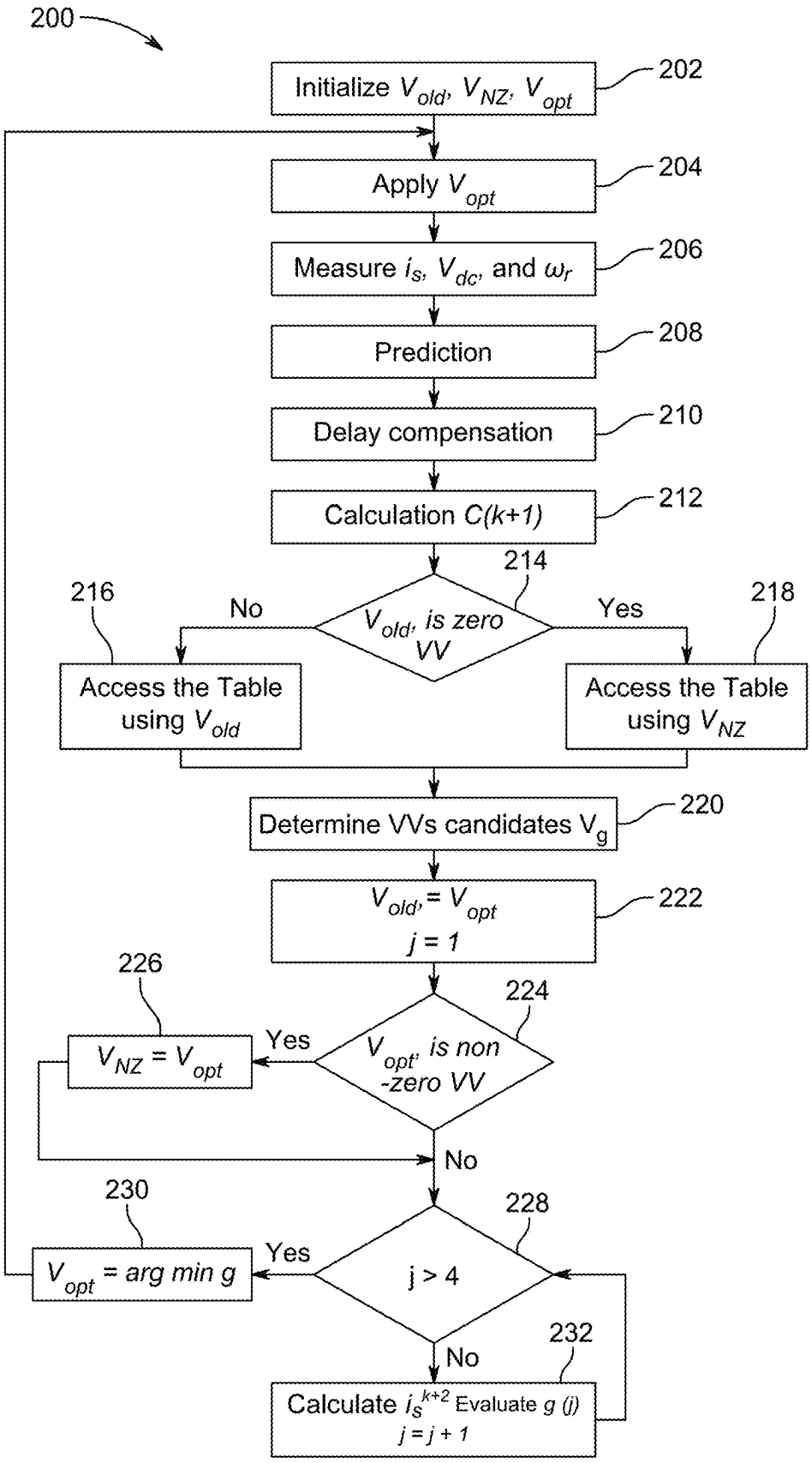
200
Initialize V_{old}, V_{NZ}, V_{opt}
202
Apply V_{opt}
204
Measure i_s, V_{dc}, and ω_r
206
Prediction
208
Delay compensation
210
Calculation C(k+1)
212
214
V_{old}, is zero VV
No
Yes
216
218
Access the Table using V_{old}
Access the Table using V_{NZ}
Determine VVs candidates V_g
220
V_{old} = V_{opt}
j = 1
222
226
224
V_{NZ} = V_{opt}
Yes
V_{opt}, is non -zero VV
No
230
228
V_{opt} = arg min g
Yes
j > 4
232
No
Calculate i_s^{k+2} Evaluate g (j)
j = j + 1

FIG. 4

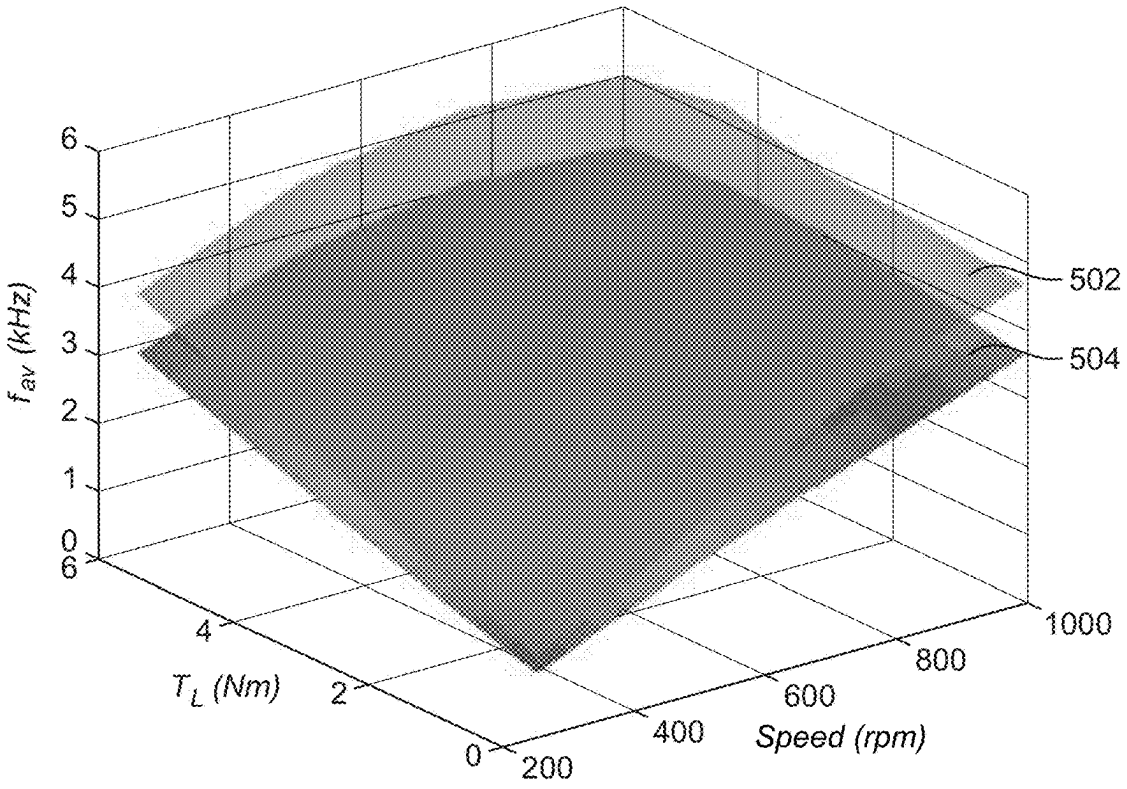
f_{av} (kHz)
6
5
4
3
2
1
0
502
504
T_L (Nm)
6
4
2
0
200
400
600
800
1000
Speed (rpm)

FIG. 5A

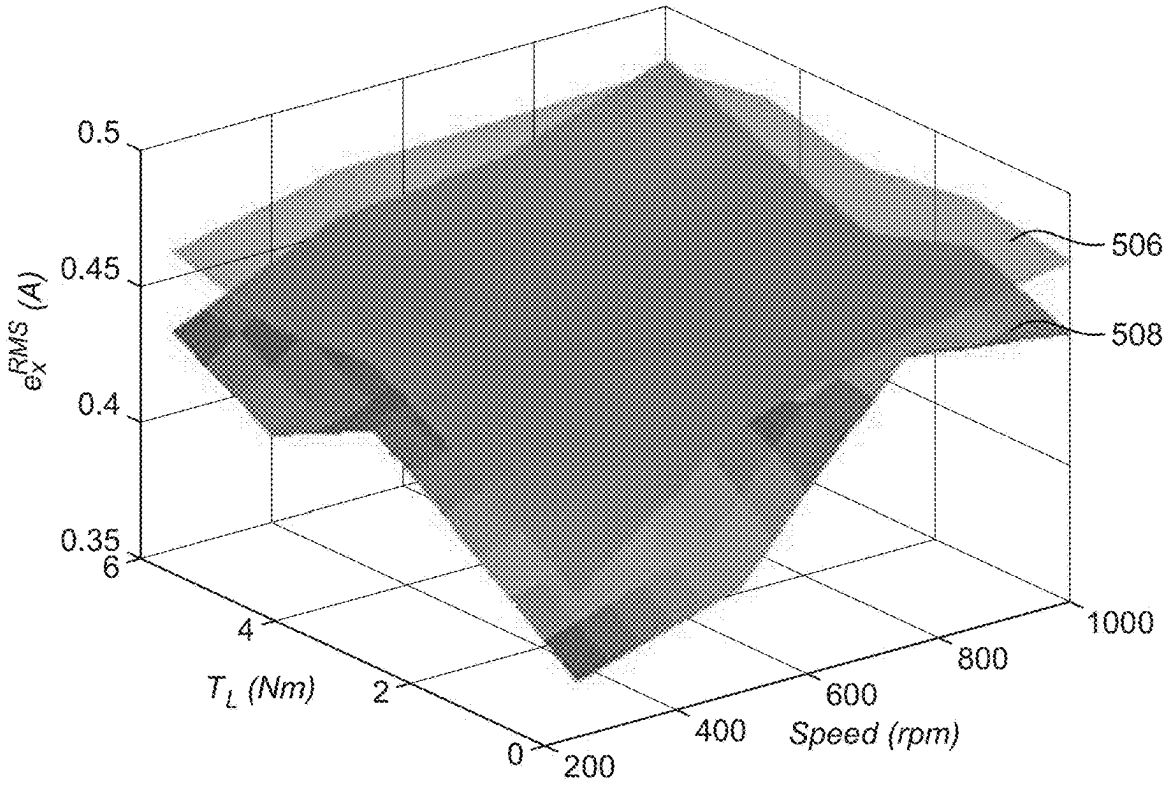
e_X^{RMS} (A)
0.5
0.45
0.4
0.35
506
508
T_L (Nm)
6
4
2
0
200
400
600
800
1000
Speed (rpm)

FIG. 5B

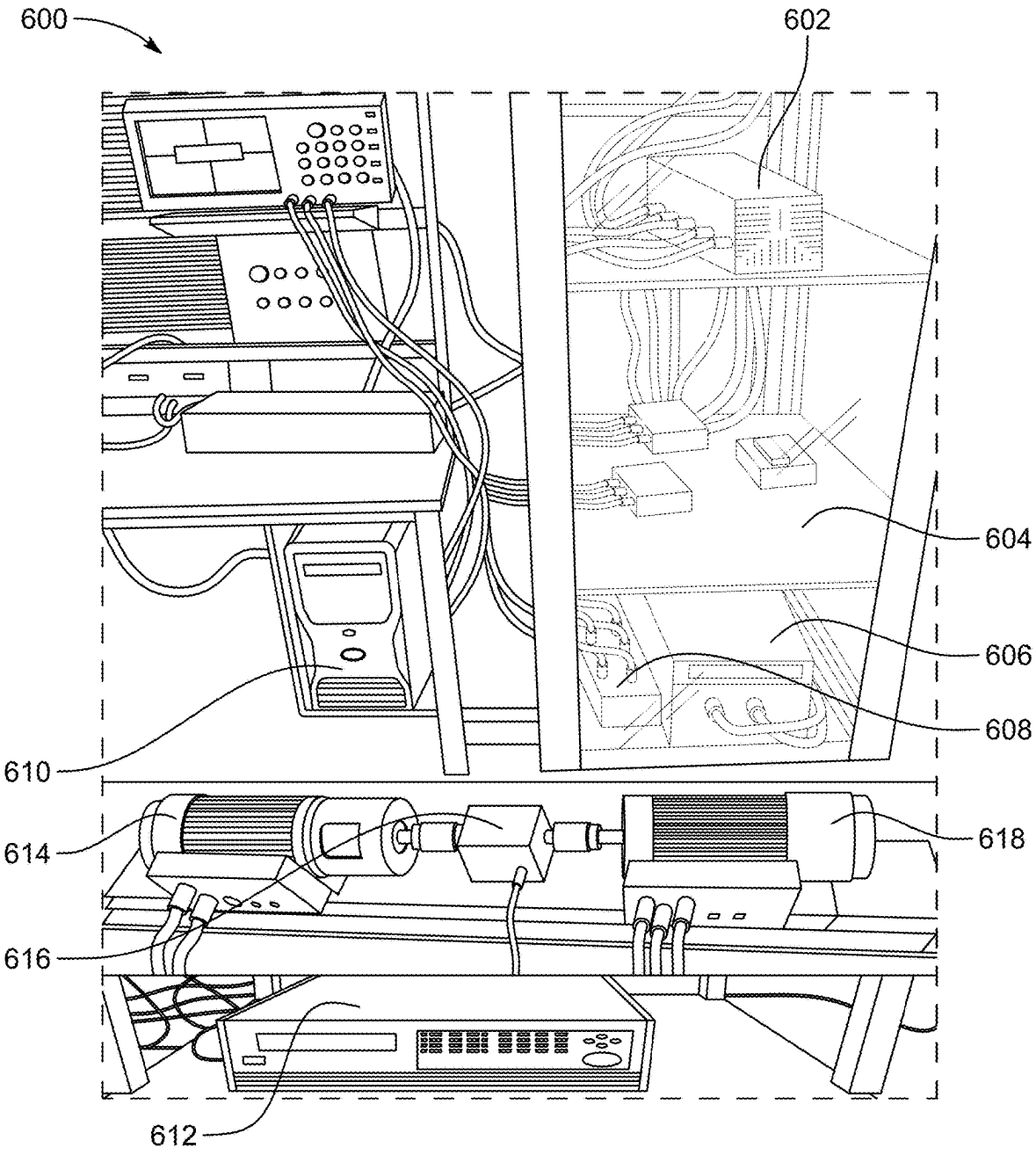

FIG. 6

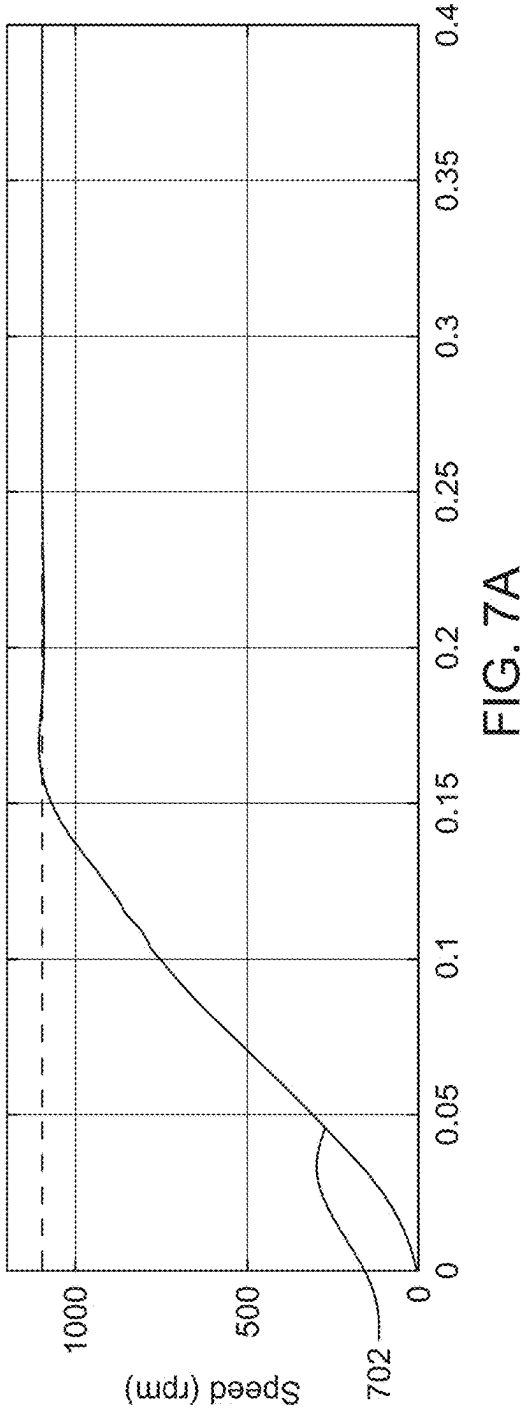
Speed (rpm)
1000
500
0
0
0.05
0.1
0.15
0.2
0.25
0.3
0.35
0.4
702

FIG. 7A

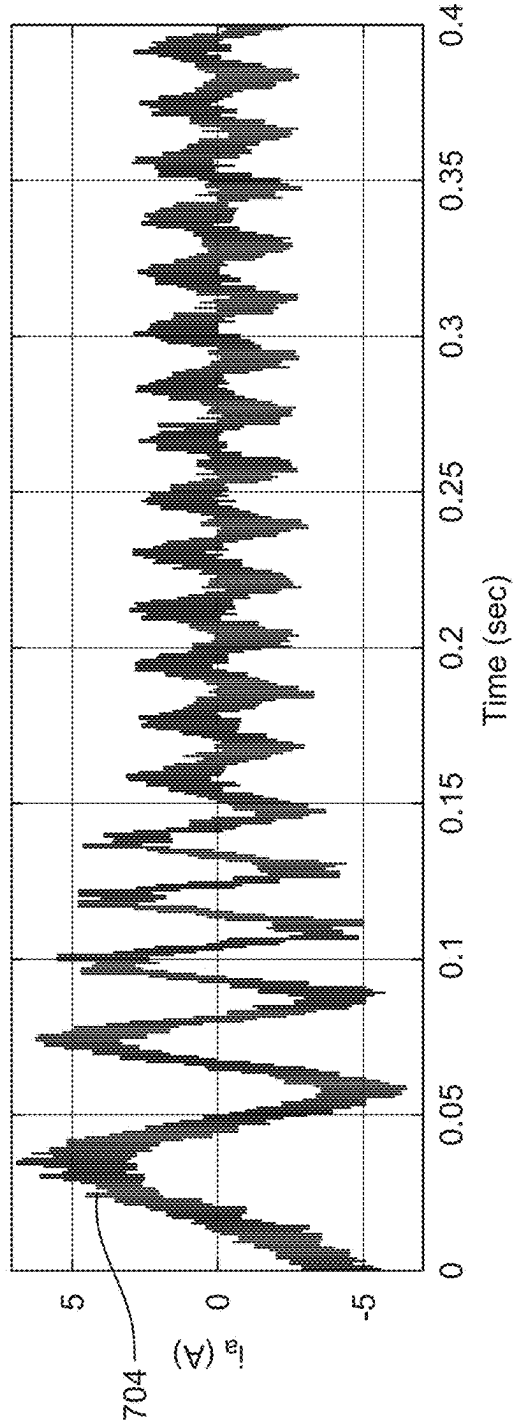
i_a (A)
5
0
-5
0
0.05
0.1
0.15
0.2
0.25
0.3
0.35
0.4
Time (sec)
704

FIG. 7B

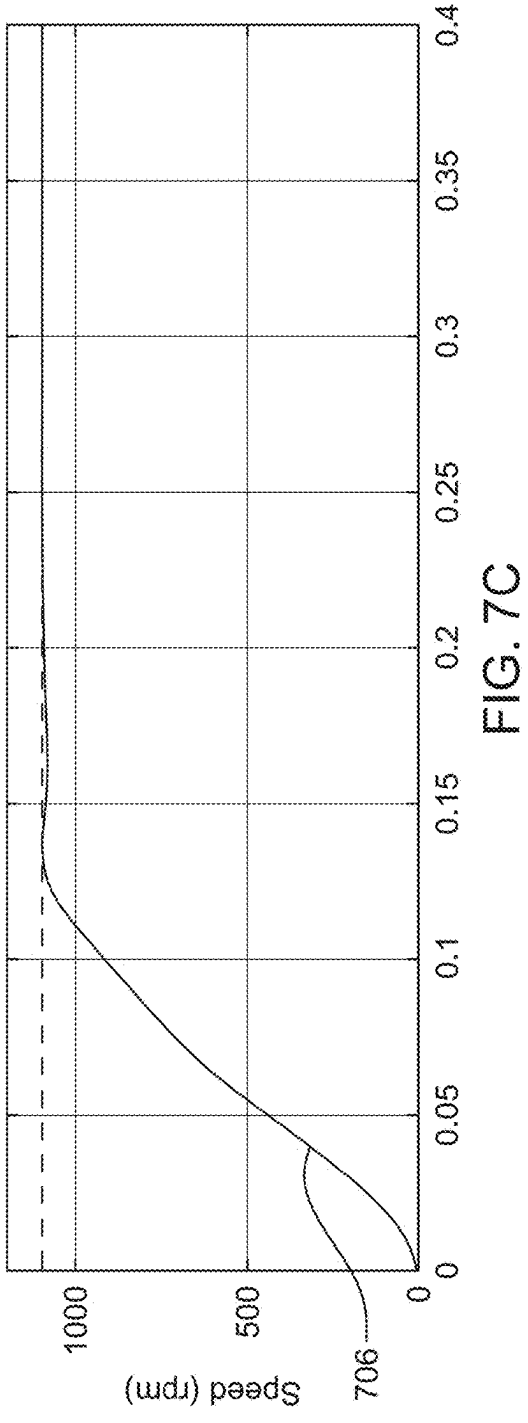
Speed (rpm)
1000
500
0
706
0
0.05
0.1
0.15
0.2
0.25
0.3
0.35
0.4

FIG. 7C

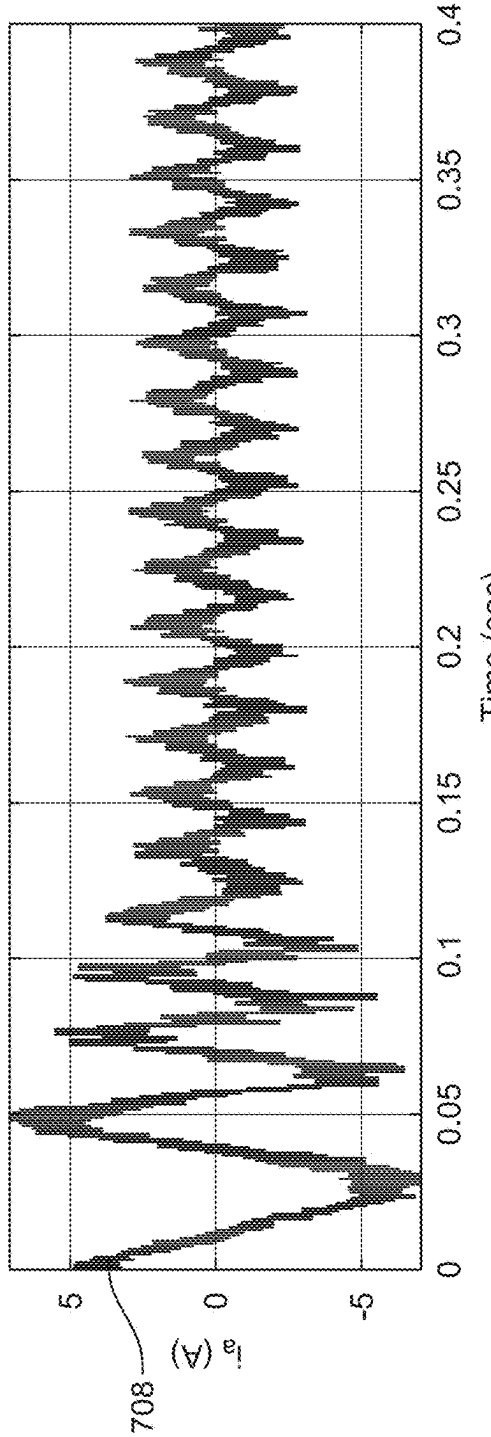
i_a (A)
5
0
-5
708
0
0.05
0.1
0.15
0.2
0.25
0.3
0.35
0.4
Time (sec)

FIG. 7D

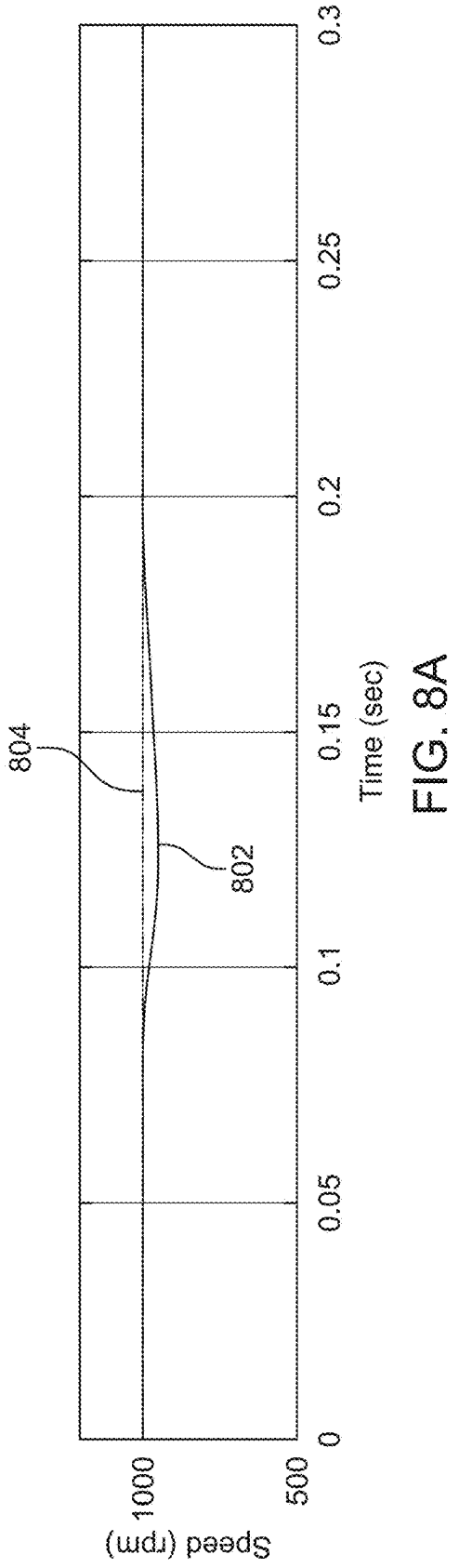
804
802
Speed (rpm)
1000
500
0
0.05
0.1
0.15
0.2
0.25
0.3
Time (sec)

FIG. 8A

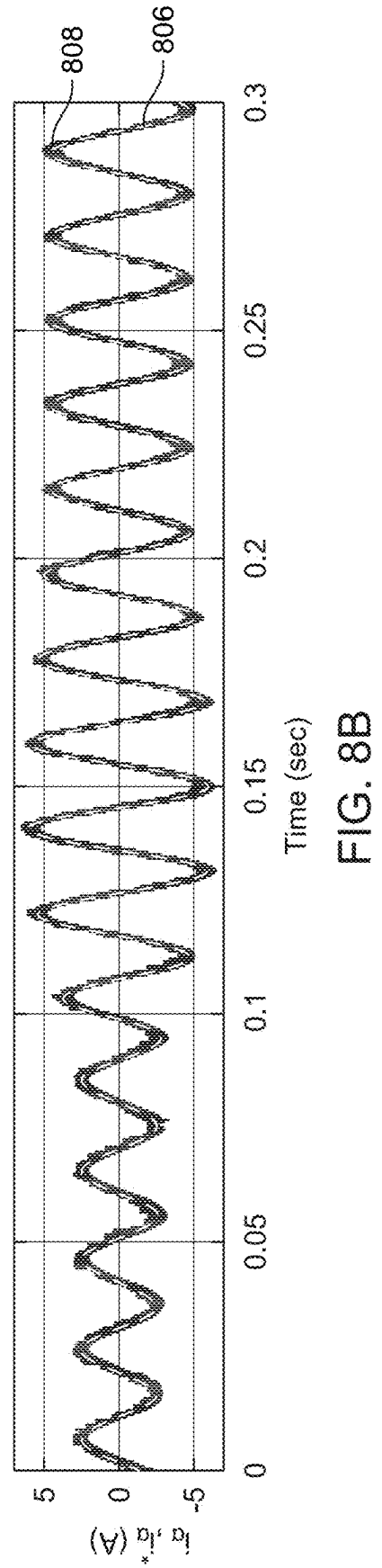
808
806
i_a ,i_a^* (A)
5
0
-5
0
0.05
0.1
0.15
0.2
0.25
0.3
Time (sec)

FIG. 8B

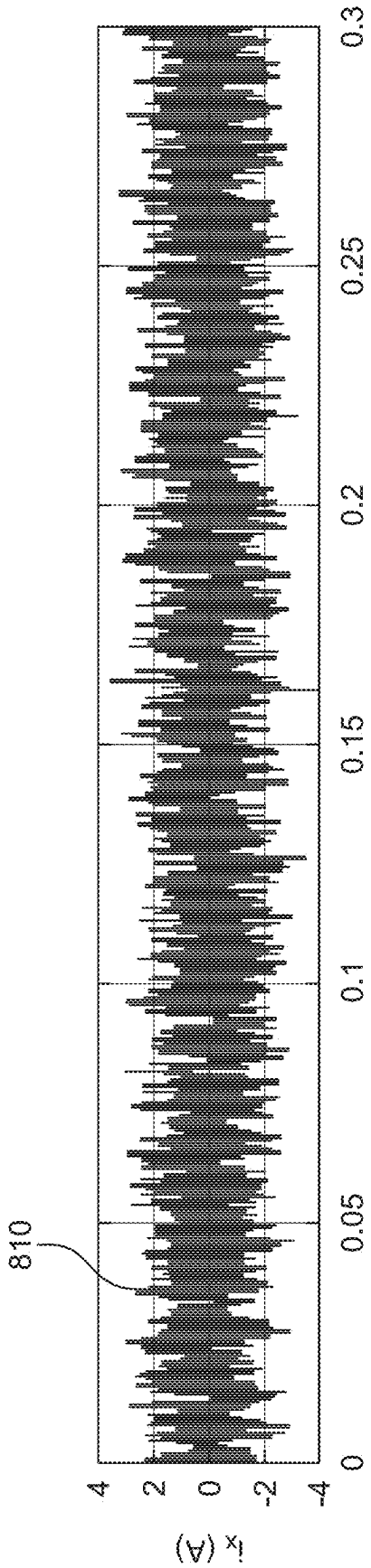
810
4
2
0
-2
-4
i_x (A)
0
0.05
0.1
0.15
0.2
0.25
0.3
Time (sec)

FIG. 8C

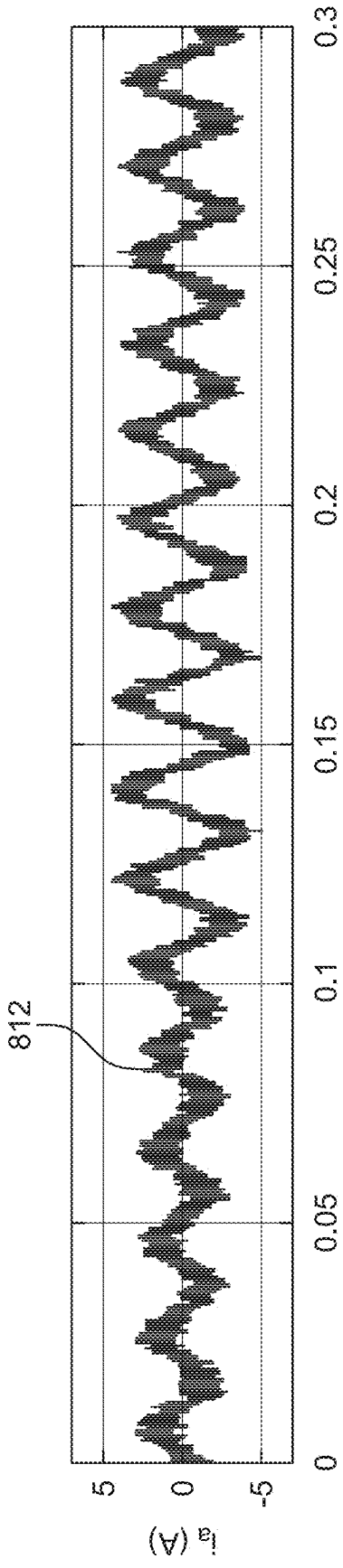
812
5
0
-5
i_a (A)
0
0.05
0.1
0.15
0.2
0.25
0.3
Time (sec)

FIG. 8D

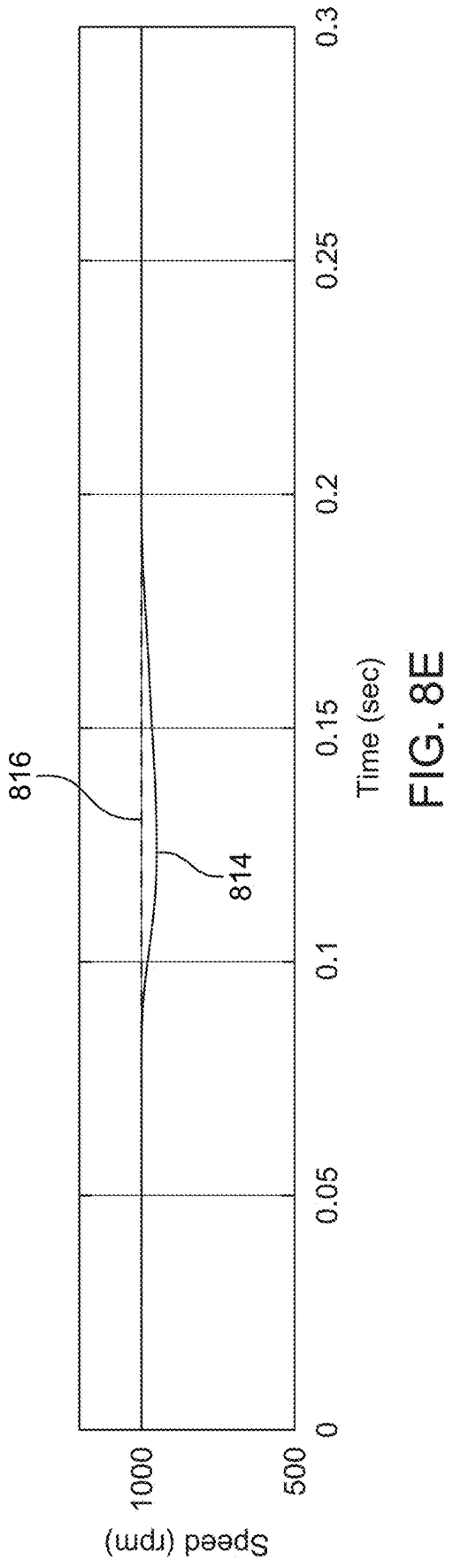
Speed (rpm)
1000
500
0
0.05
0.1
0.15
0.2
0.25
0.3
Time (sec)
816
814

FIG. 8E

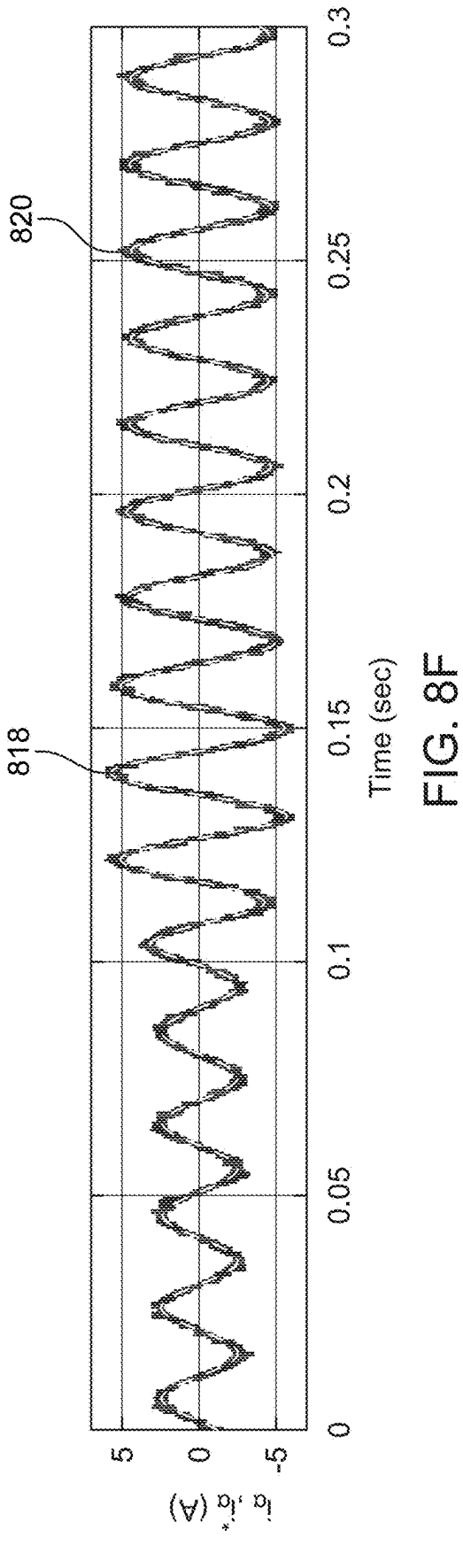
i_a ,i_a^* (A)
5
0
-5
0
0.05
0.1
0.15
0.2
0.25
0.3
Time (sec)
820
818

FIG. 8F

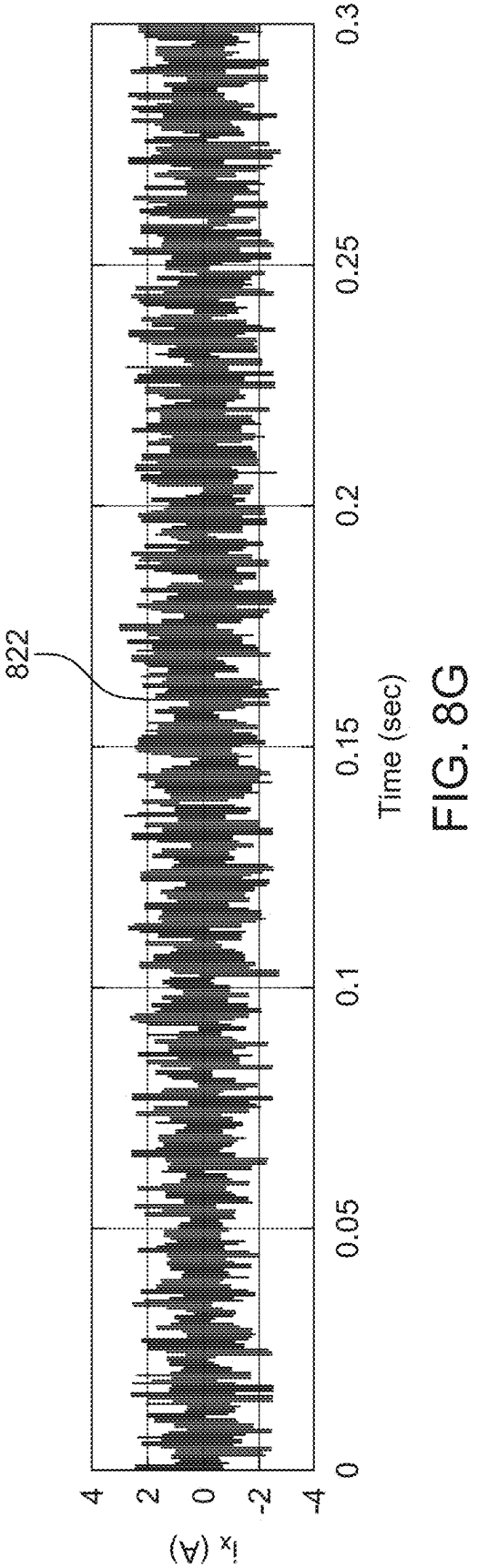
822
4
2
0
-2
-4
i_x (A)
0
0.05
0.1
0.15
0.2
0.25
0.3
Time (sec)

FIG. 8G

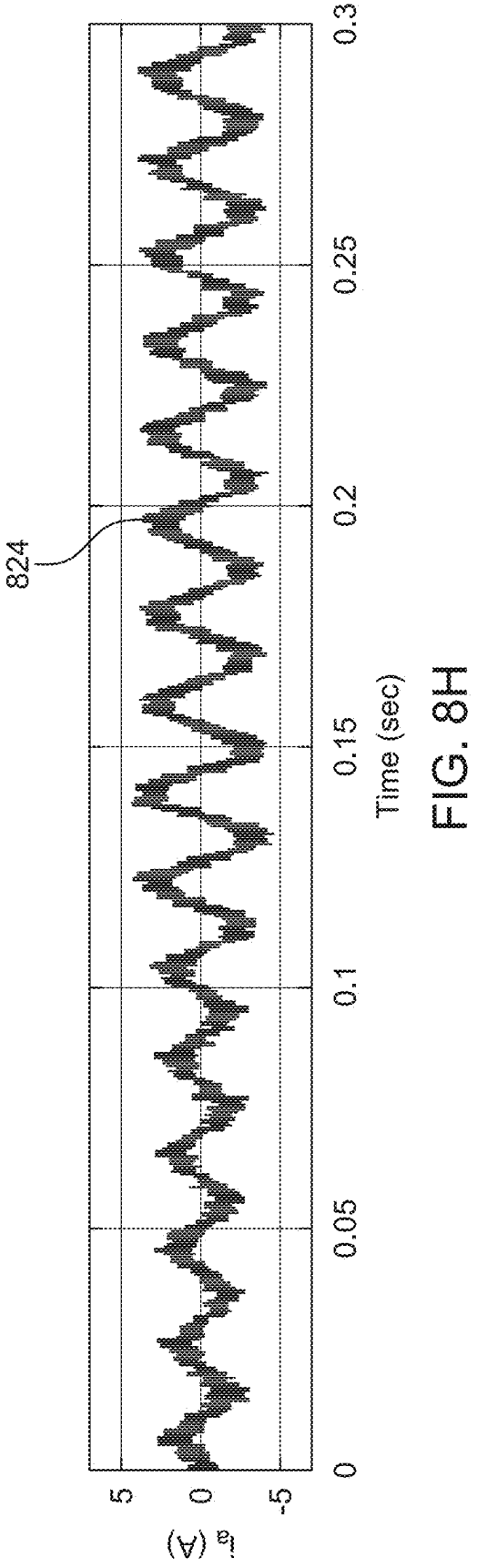
824
5
0
-5
i_a (A)
0
0.05
0.1
0.15
0.2
0.25
0.3
Time (sec)

FIG. 8H

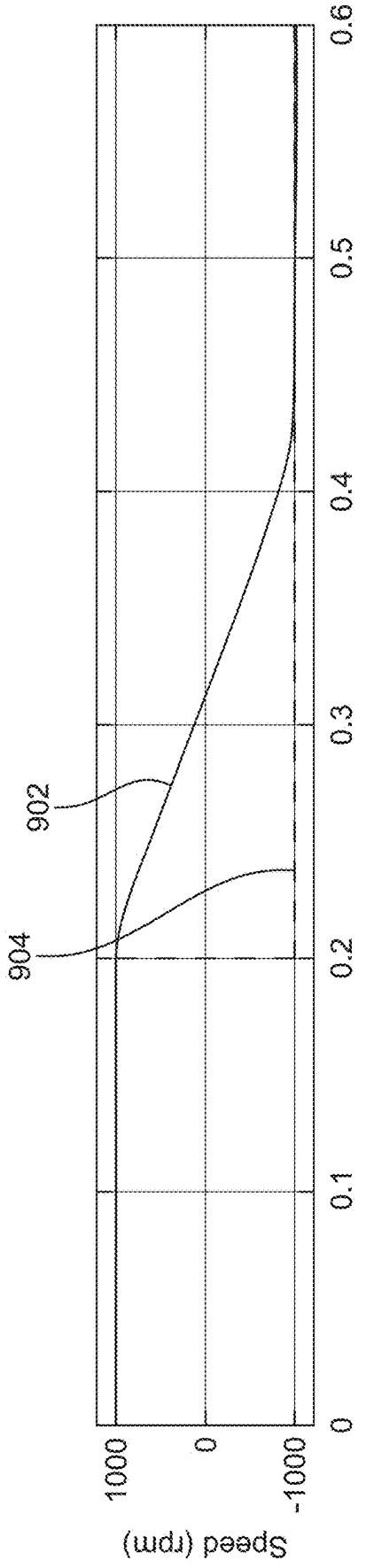
Speed (rpm)
1000
0
-1000
0
0.1
0.2
0.3
0.4
0.5
0.6
Time (sec)
902
904

FIG. 9A

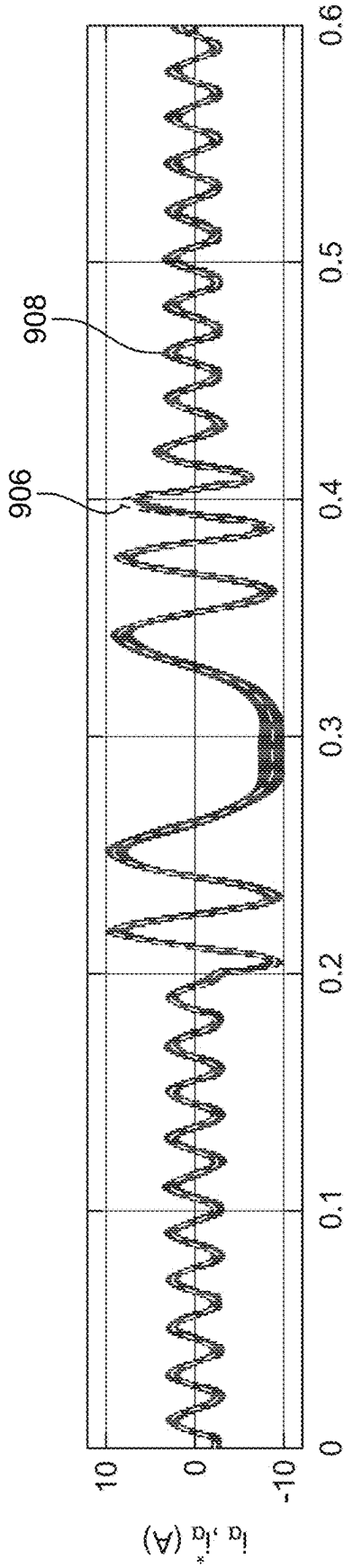
i_a ,i_a^* (A)
10
0
-10
0
0.1
0.2
0.3
0.4
0.5
0.6
Time (sec)
906
908

FIG. 9B

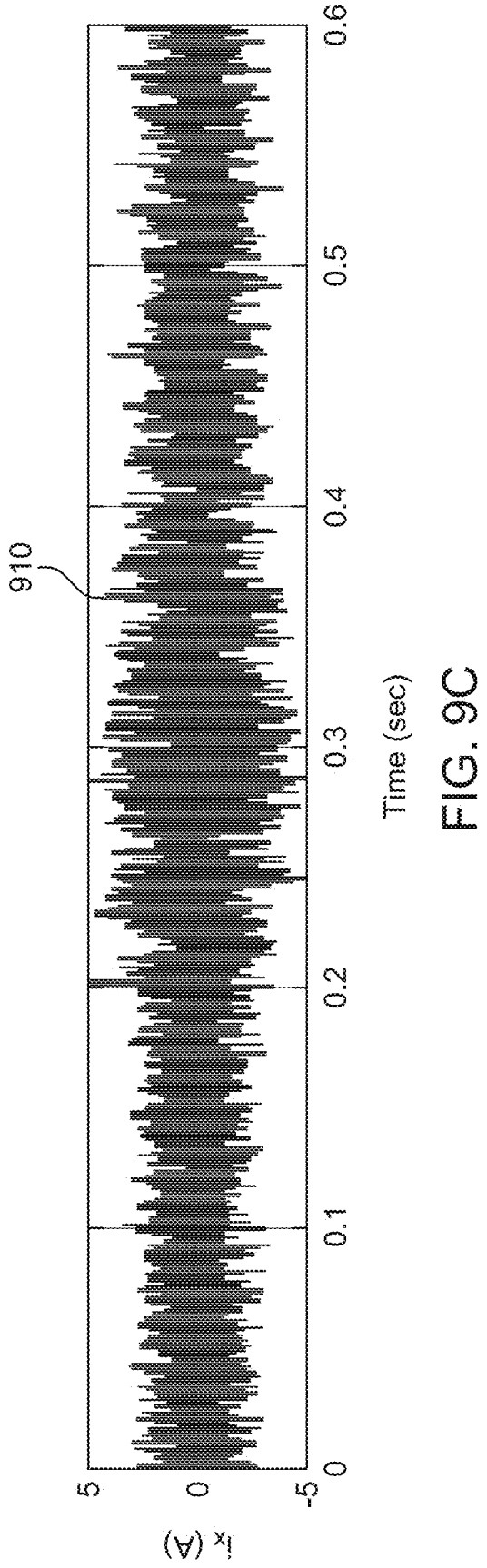
910
5
0
-5
i_x (A)
0
0.1
0.2
0.3
0.4
0.5
0.6
Time (sec)

FIG. 9C

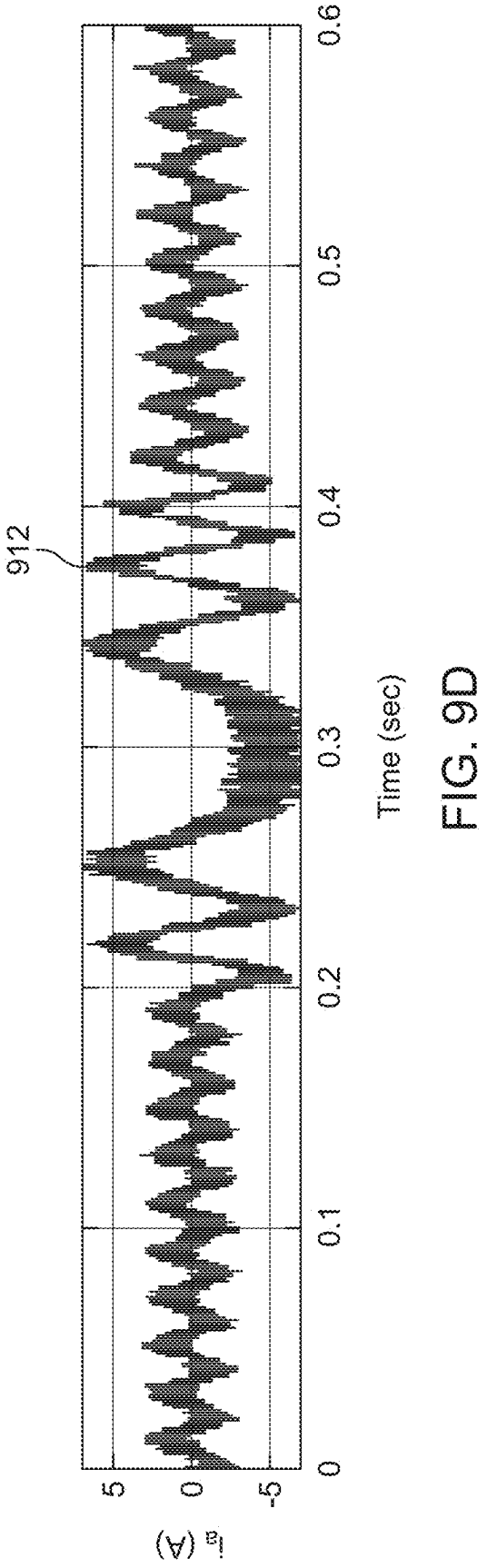
912
5
0
-5
i_a (A)
0
0.1
0.2
0.3
0.4
0.5
0.6
Time (sec)

FIG. 9D

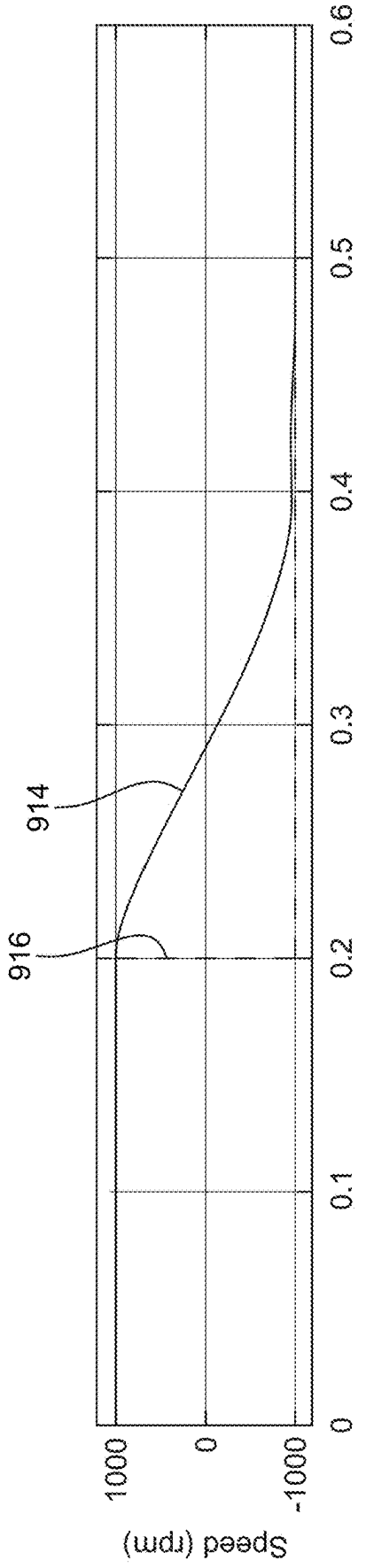
914
916
1000
0
-1000
Speed (rpm)
0
0.1
0.2
0.3
0.4
0.5
0.6
Time (sec)

FIG. 9E

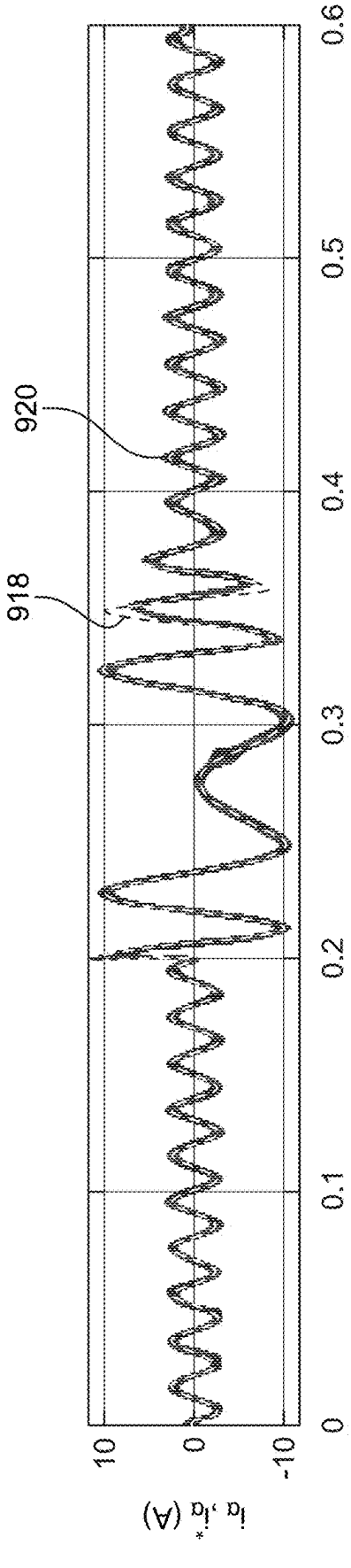
920
918
10
0
-10
i_a, i_a^* (A)
0
0.1
0.2
0.3
0.4
0.5
0.6
Time (sec)

FIG. 9F

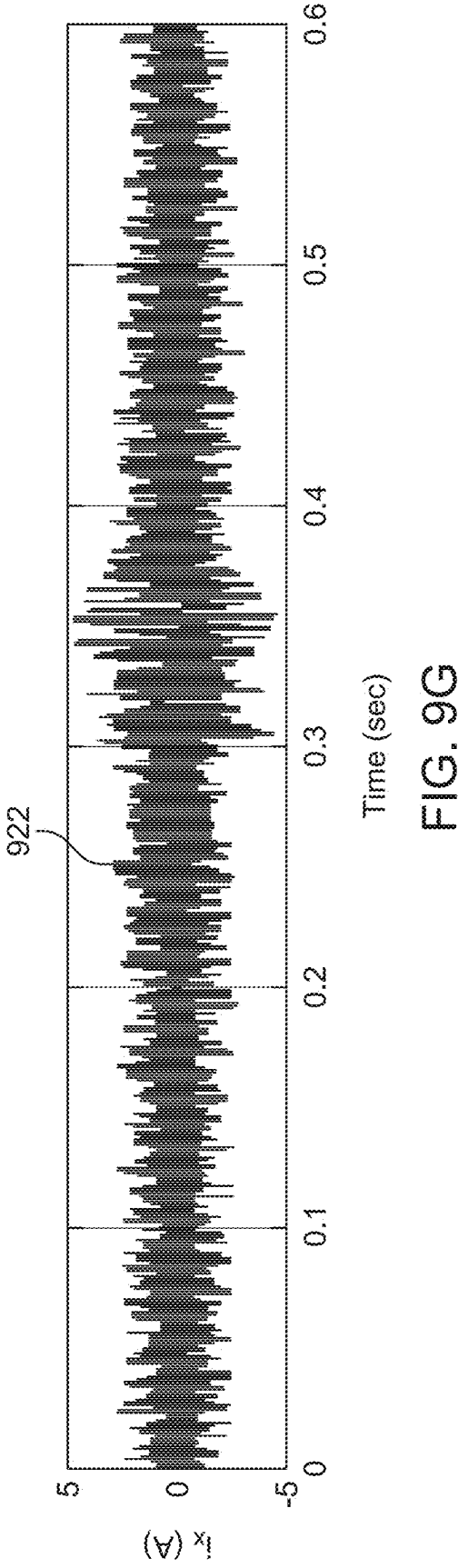
922
5
0
-5
i_x (A)
0
0.1
0.2
0.3
0.4
0.5
0.6
Time (sec)

FIG. 9G

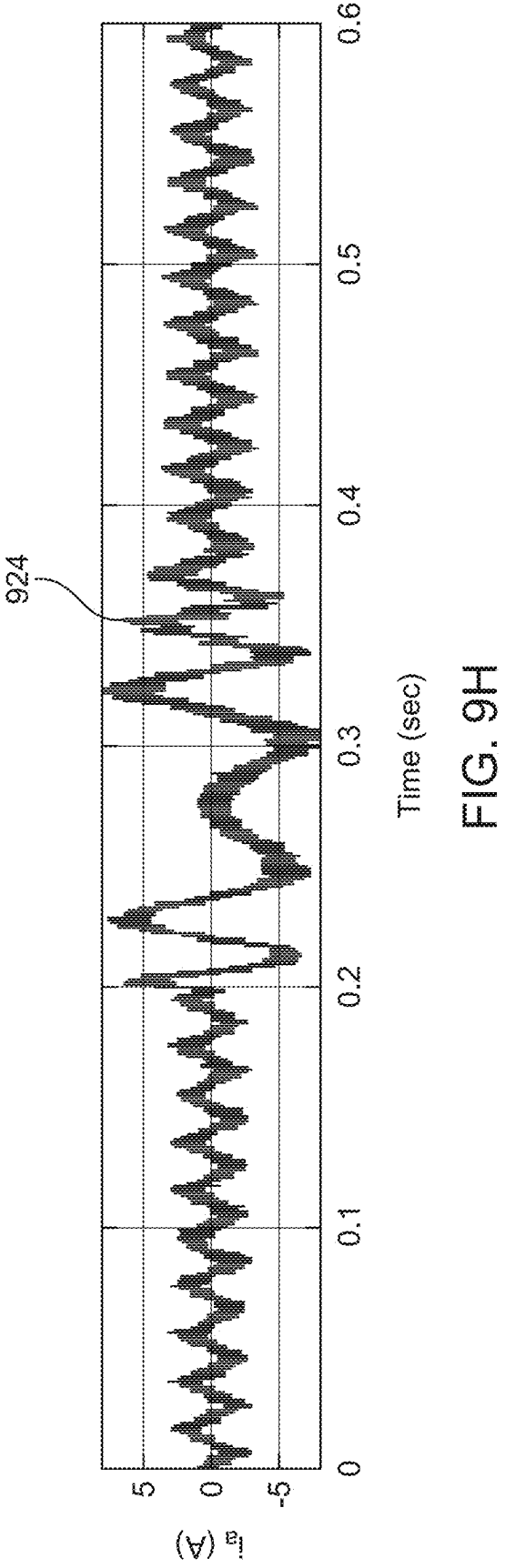
924
5
0
-5
i_α (A)
0
0.1
0.2
0.3
0.4
0.5
0.6
Time (sec)

FIG. 9H

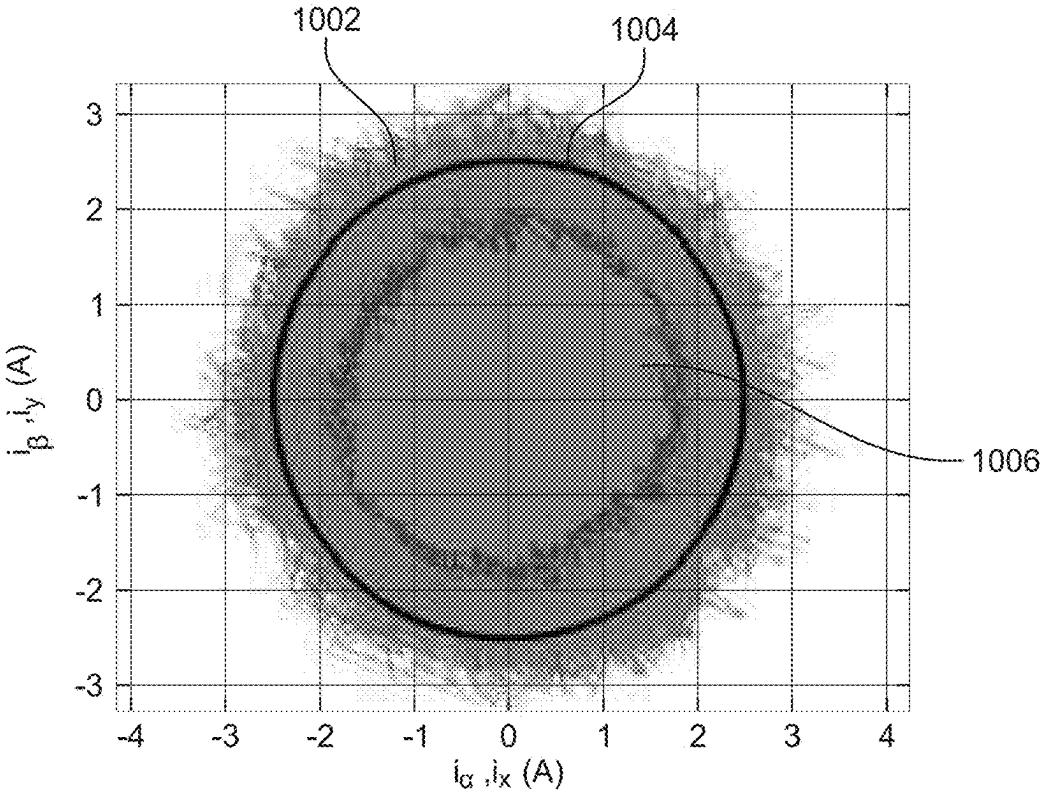

FIG. 10A

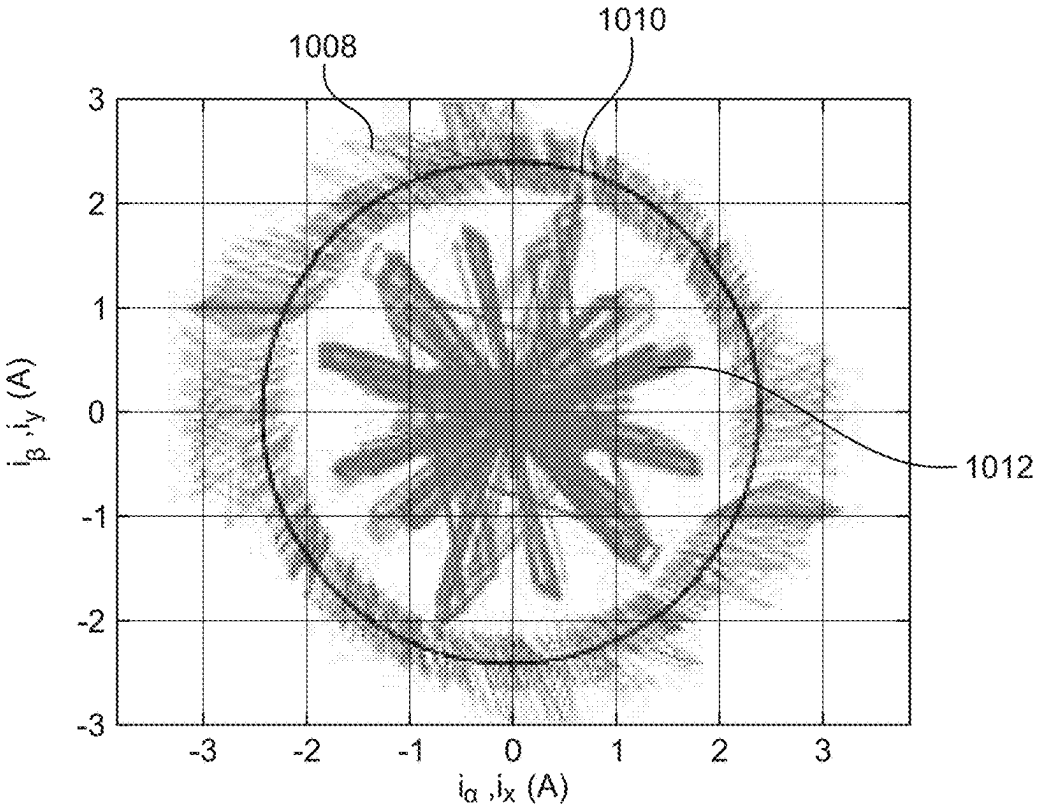

FIG. 10B

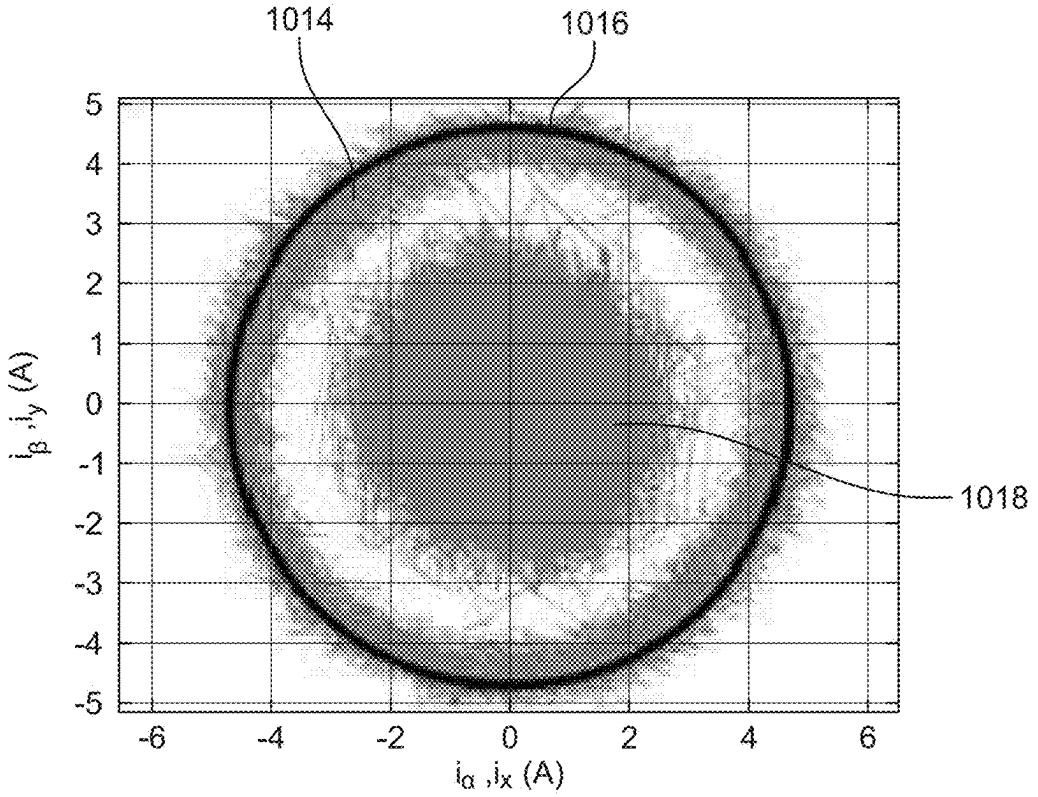

FIG. 10C

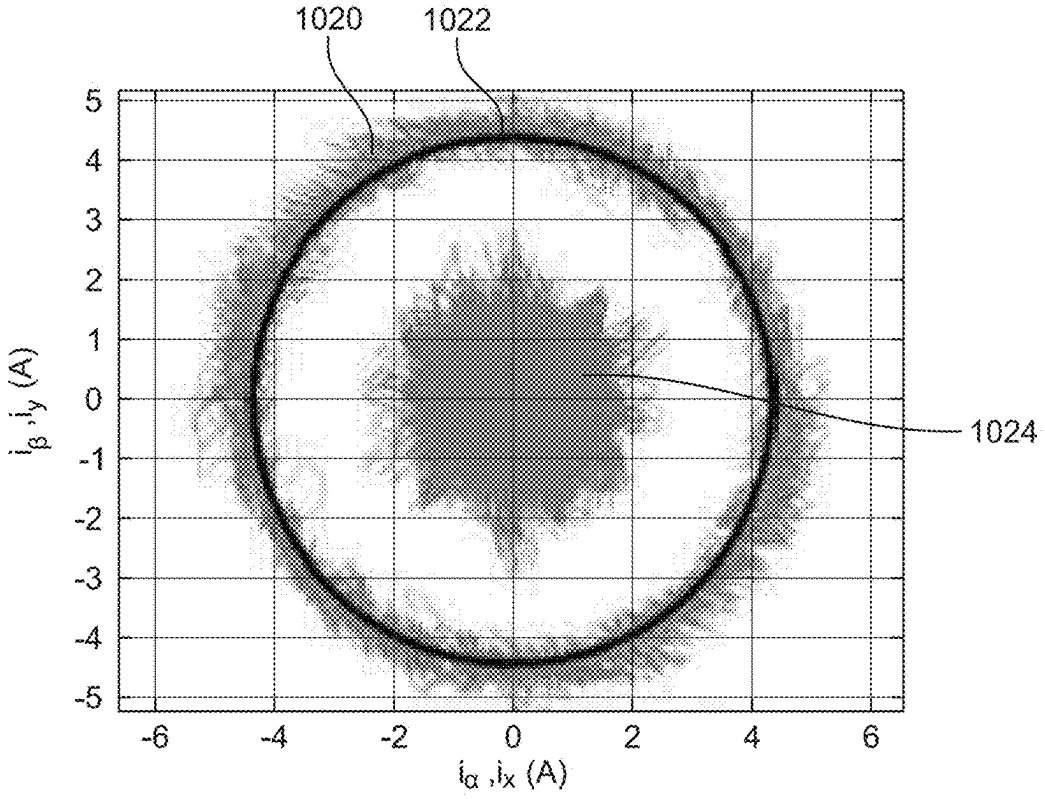

FIG. 10D

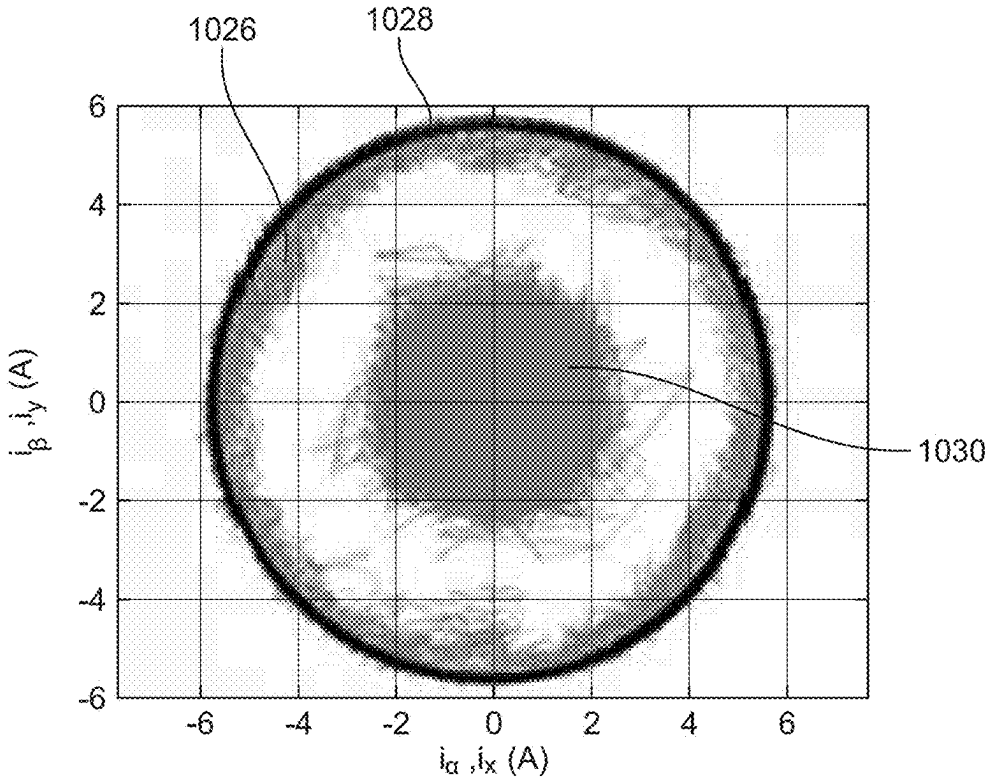

FIG. 10E

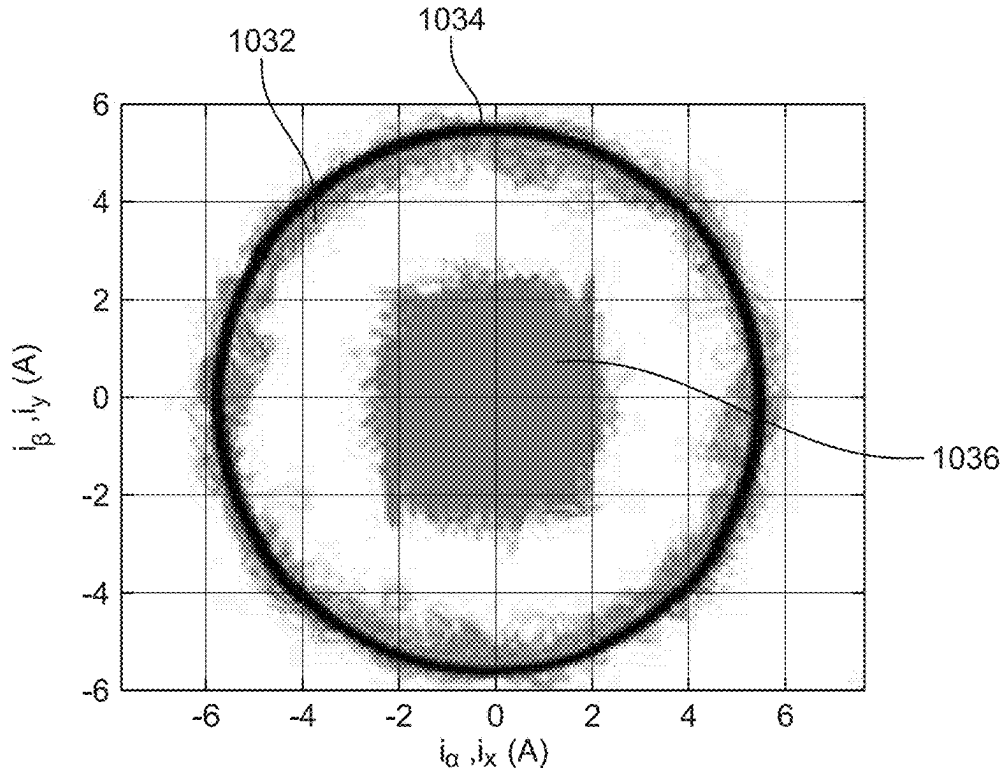

FIG. 10F

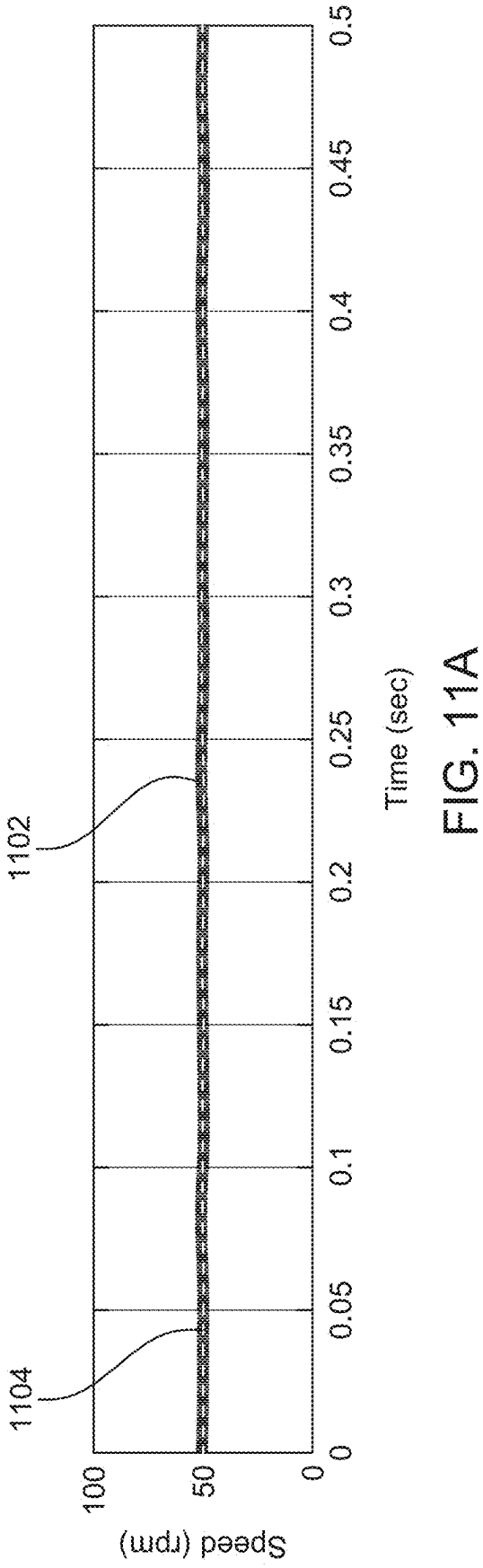

FIG. 11A

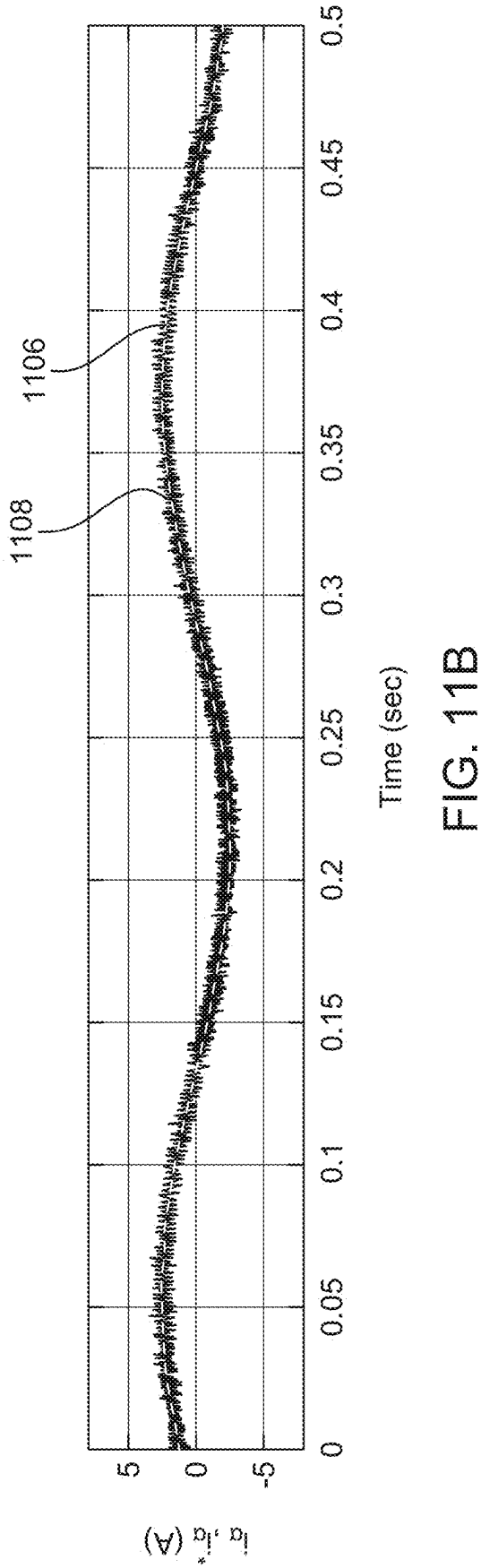

FIG. 11B

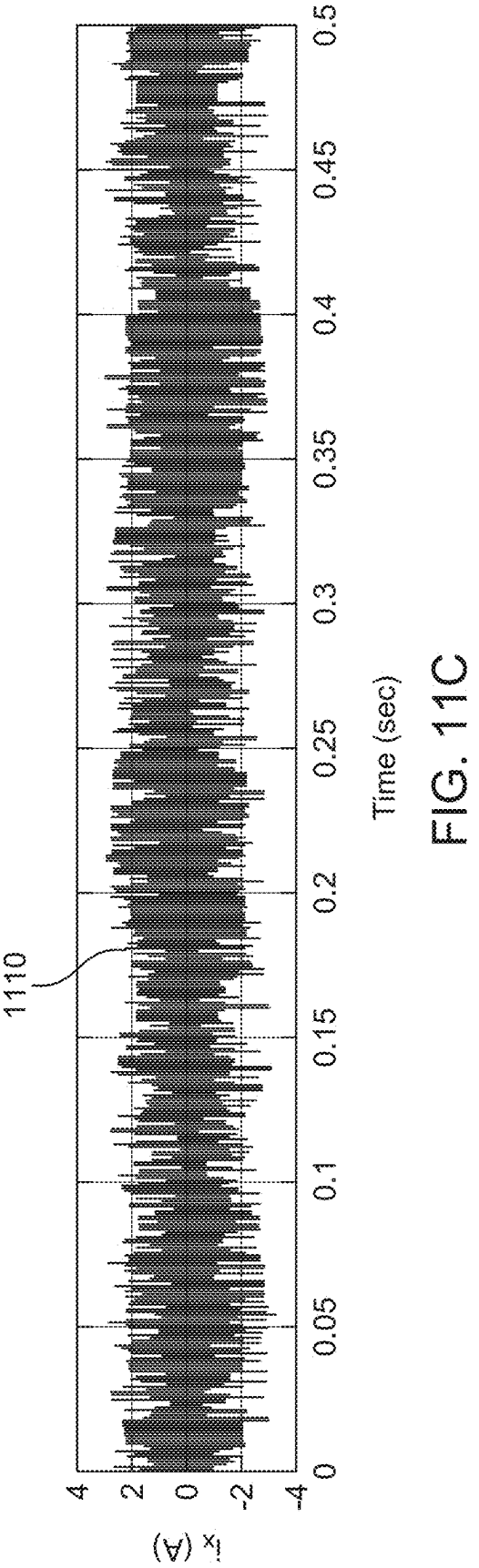

FIG. 11C

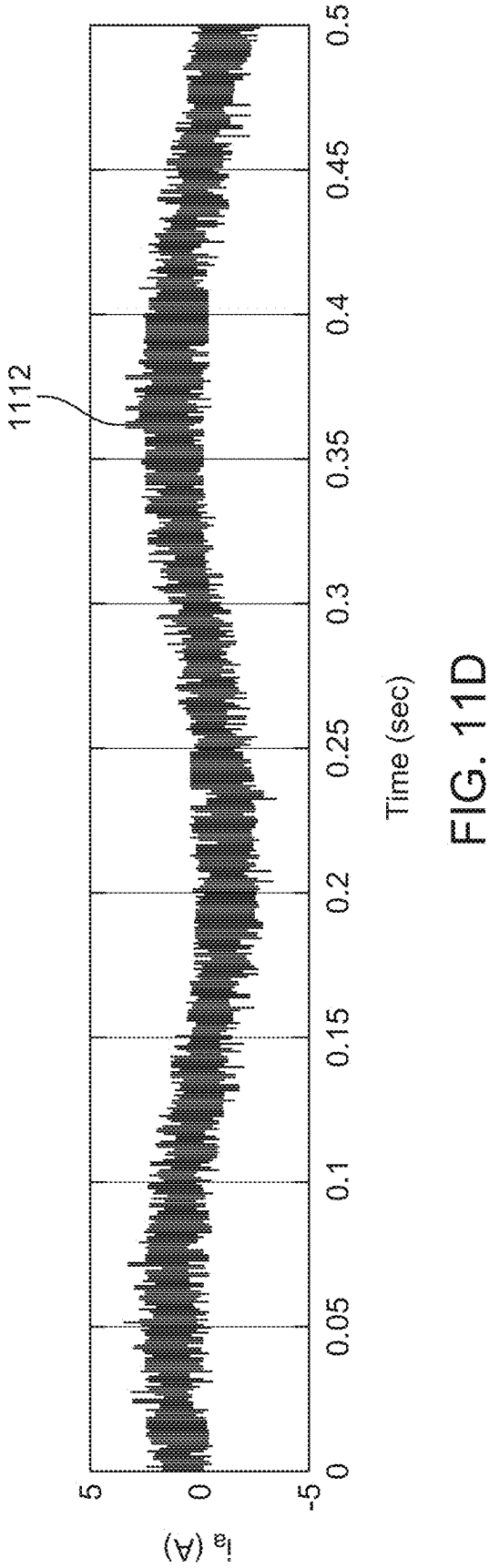

FIG. 11D

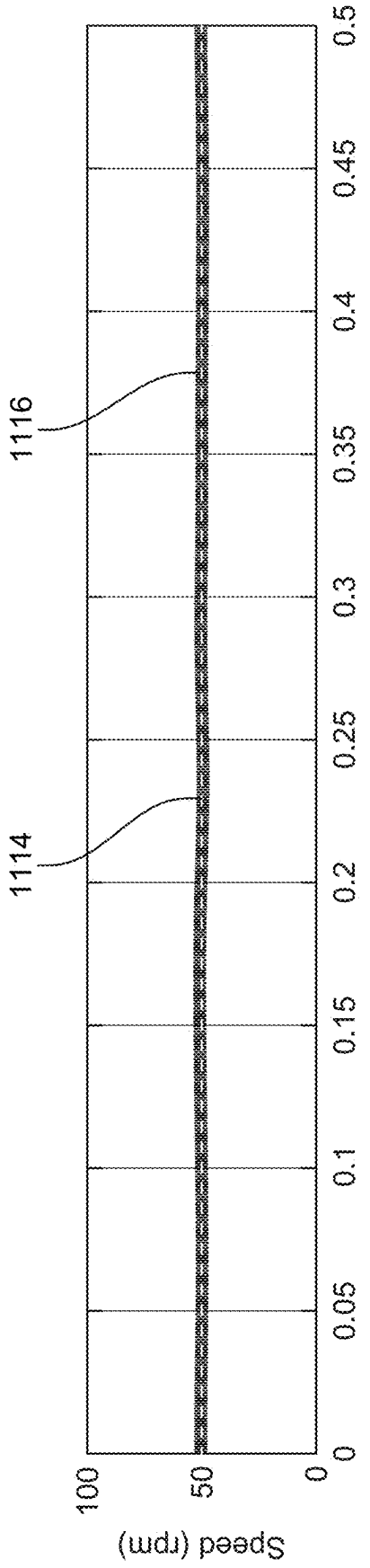

FIG. 11E

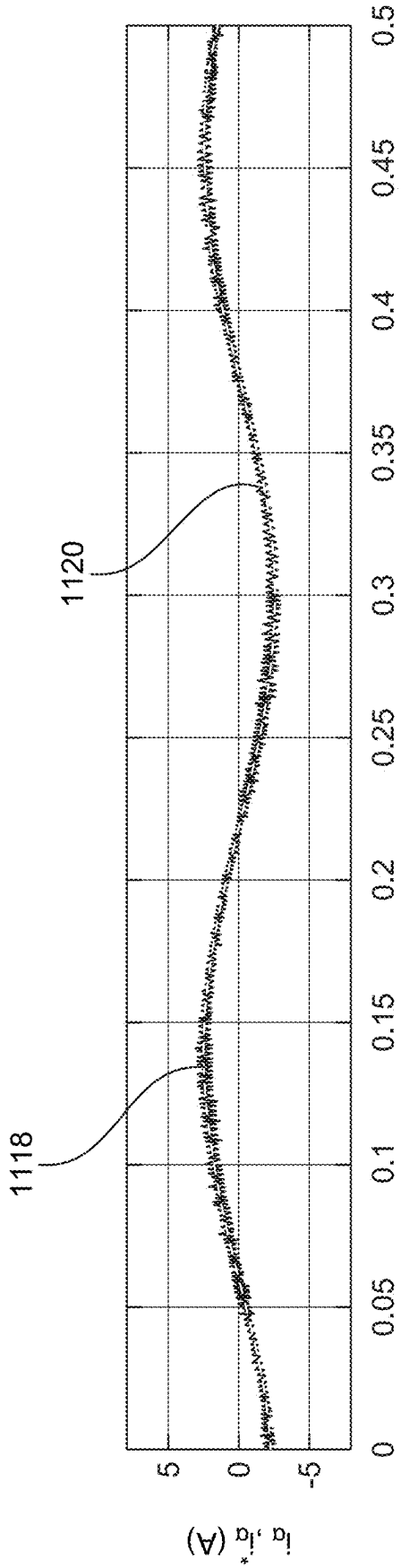

FIG. 11F

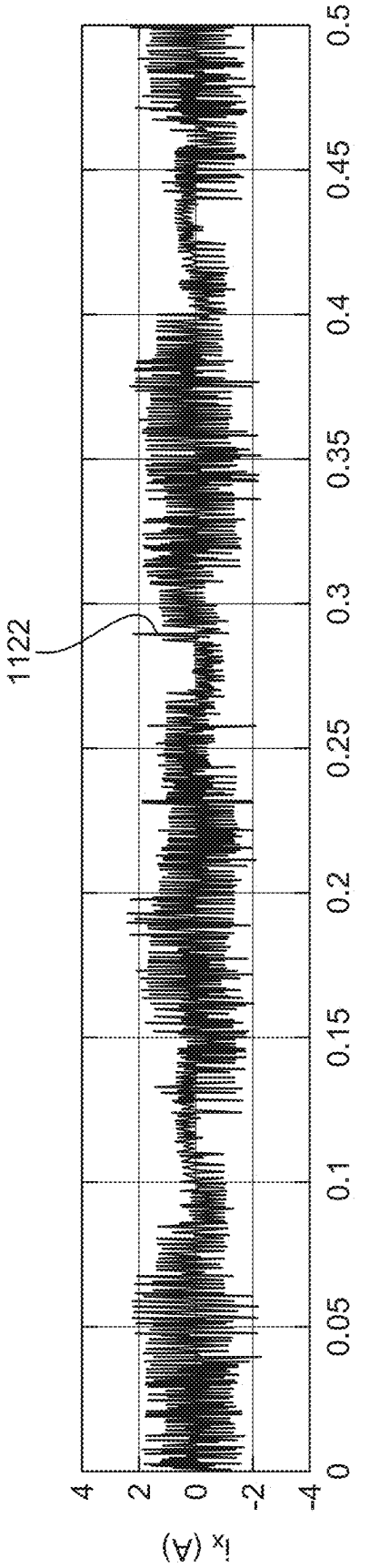

FIG. 11G

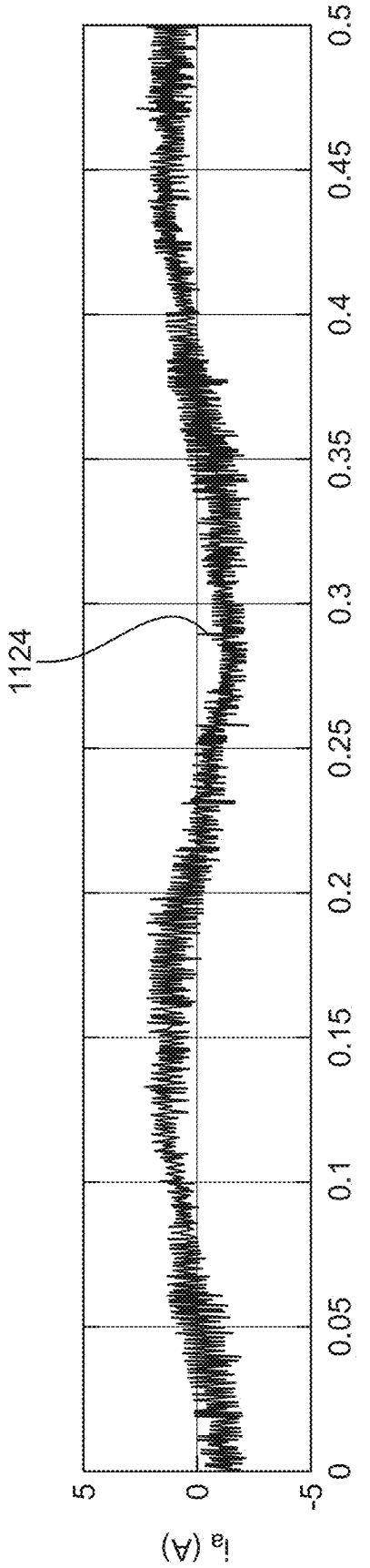

FIG. 11H

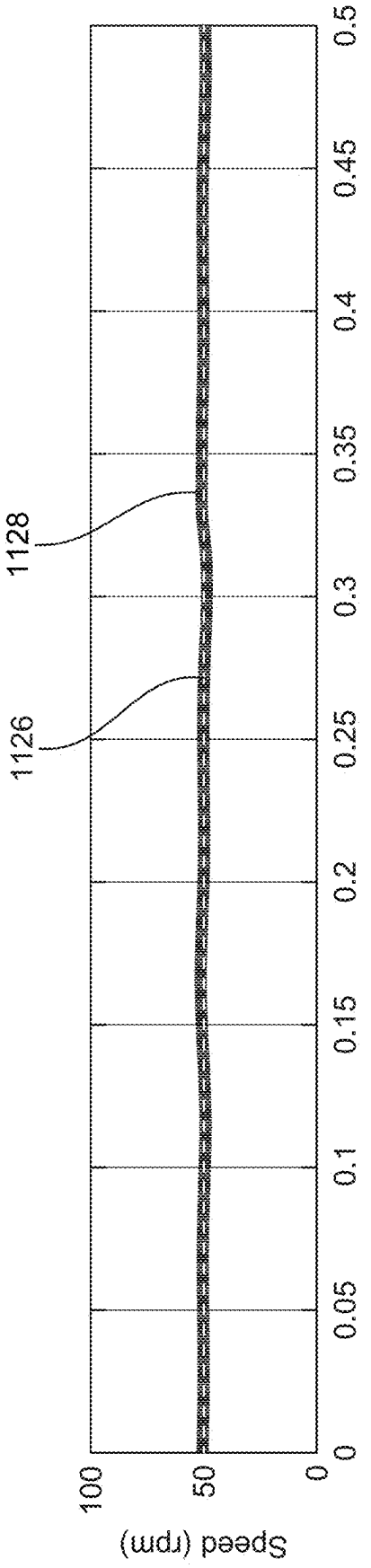

FIG. 11I

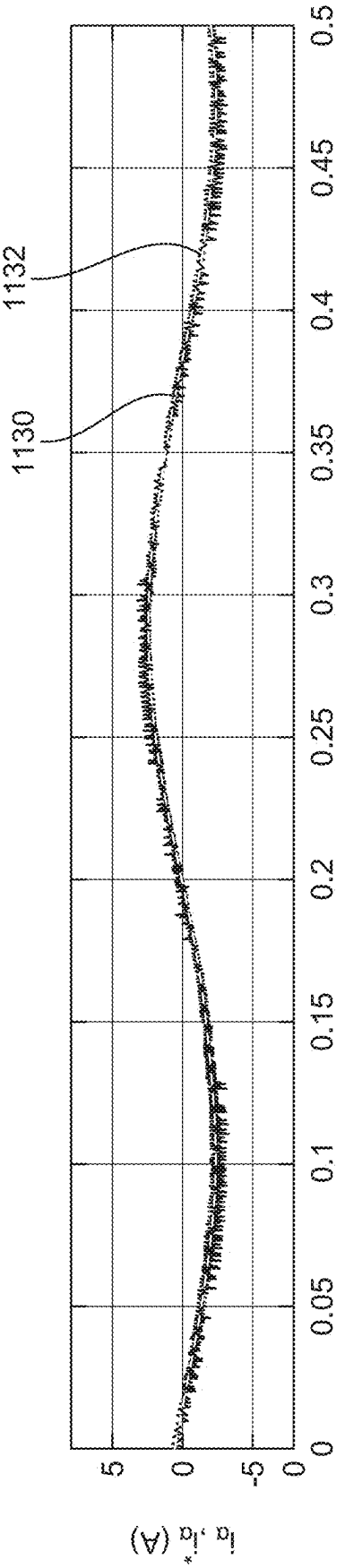

FIG. 11J

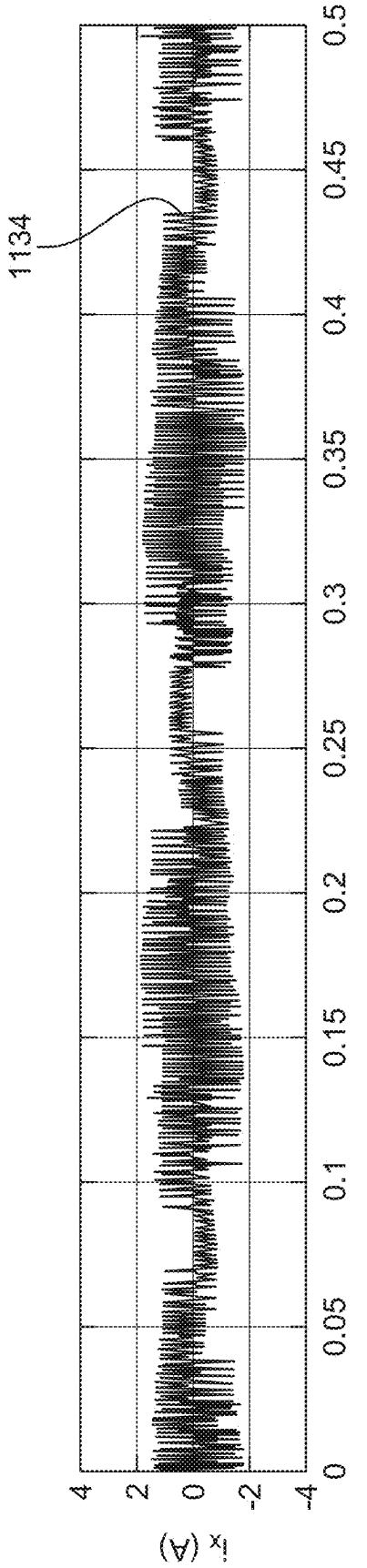

FIG. 11K

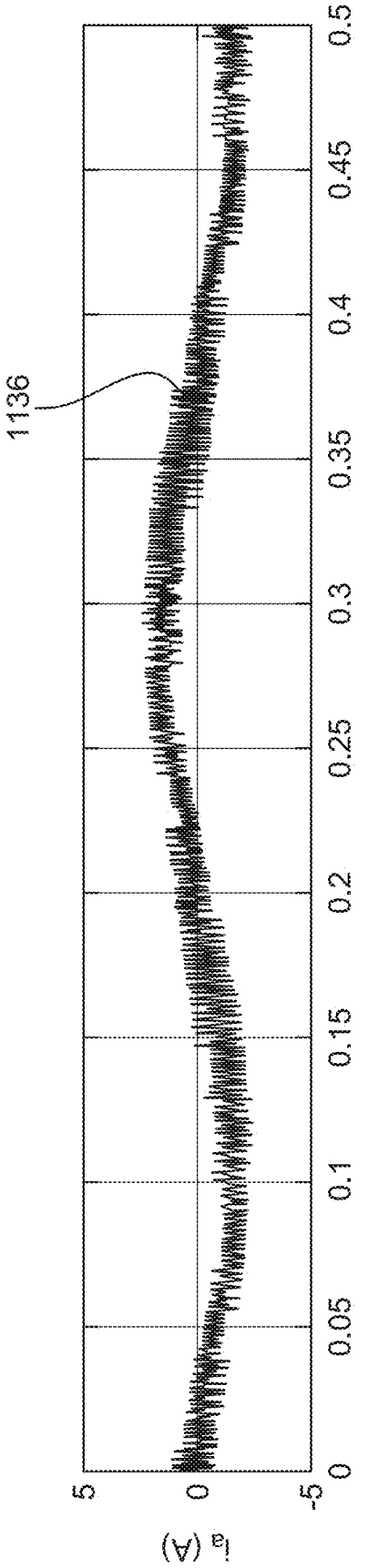

FIG. 11L

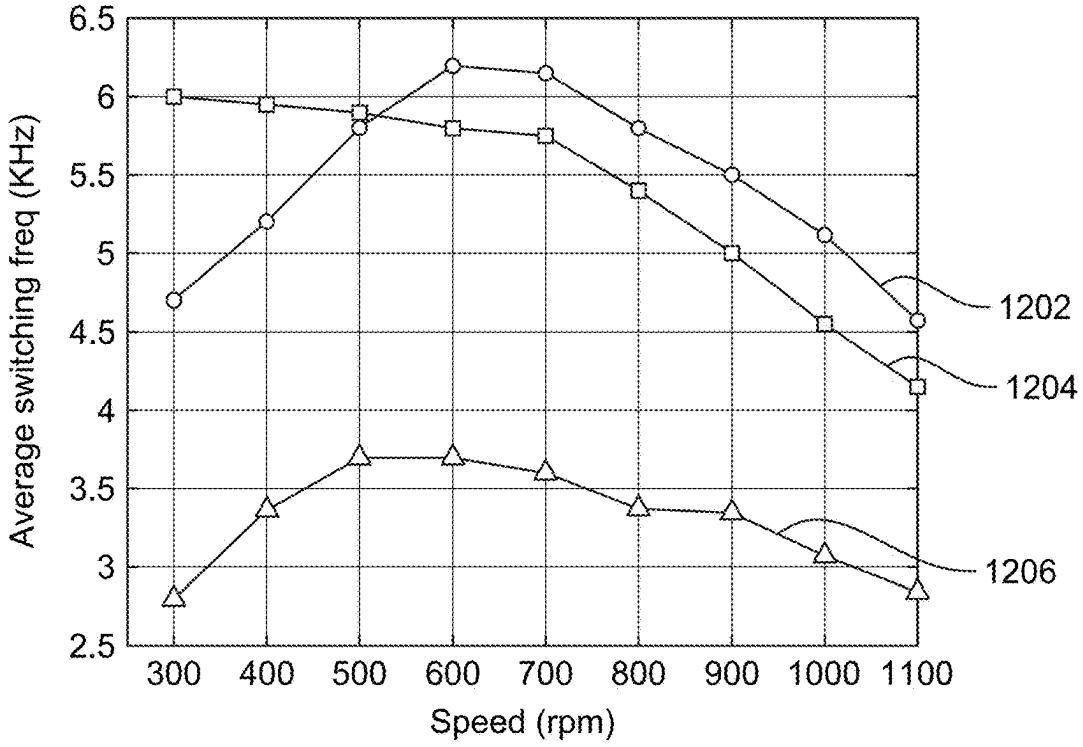

FIG. 12A

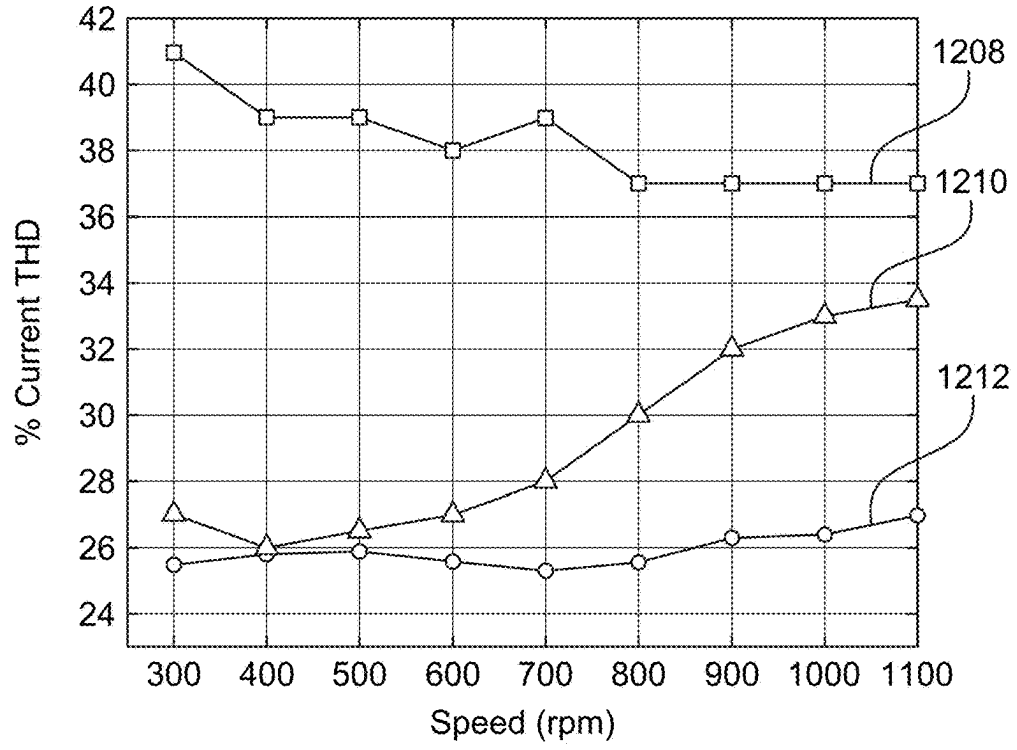

FIG. 12B

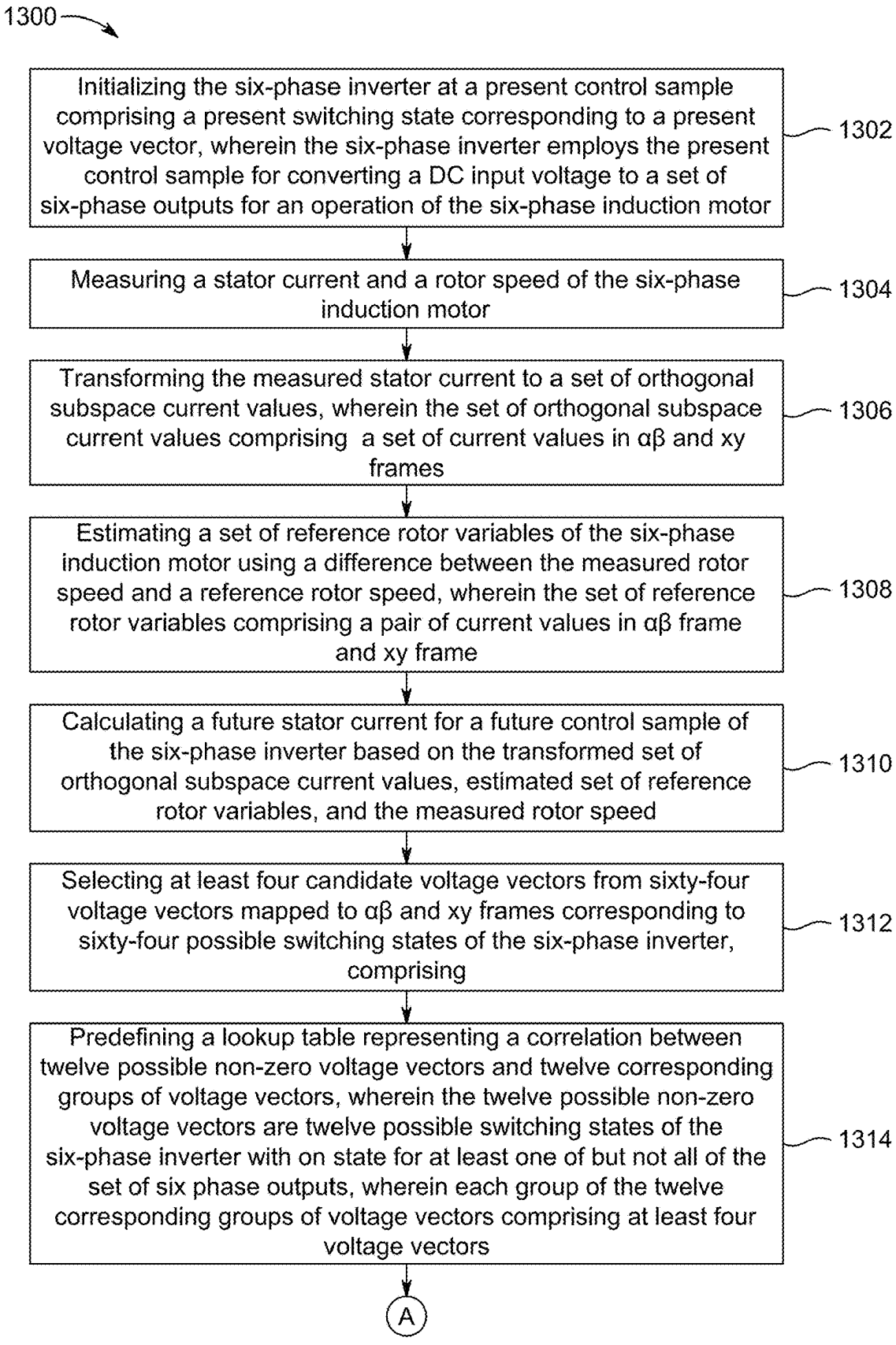
1300
Initializing the six-phase inverter at a present control sample comprising a present switching state corresponding to a present voltage vector, wherein the six-phase inverter employs the present control sample for converting a DC input voltage to a set of six-phase outputs for an operation of the six-phase induction motor
1302
Measuring a stator current and a rotor speed of the six-phase induction motor
1304
Transforming the measured stator current to a set of orthogonal subspace current values, wherein the set of orthogonal subspace current values comprising a set of current values in αβ and xy frames
1306
Estimating a set of reference rotor variables of the six-phase induction motor using a difference between the measured rotor speed and a reference rotor speed, wherein the set of reference rotor variables comprising a pair of current values in αβ frame and xy frame
1308
Calculating a future stator current for a future control sample of the six-phase inverter based on the transformed set of orthogonal subspace current values, estimated set of reference rotor variables, and the measured rotor speed
1310
Selecting at least four candidate voltage vectors from sixty-four voltage vectors mapped to αβ and xy frames corresponding to sixty-four possible switching states of the six-phase inverter, comprising
1312
Predefining a lookup table representing a correlation between twelve possible non-zero voltage vectors and twelve corresponding groups of voltage vectors, wherein the twelve possible non-zero voltage vectors are twelve possible switching states of the six-phase inverter with on state for at least one of but not all of the set of six phase outputs, wherein each group of the twelve corresponding groups of voltage vectors comprising at least four voltage vectors
1314
A

FIG. 13

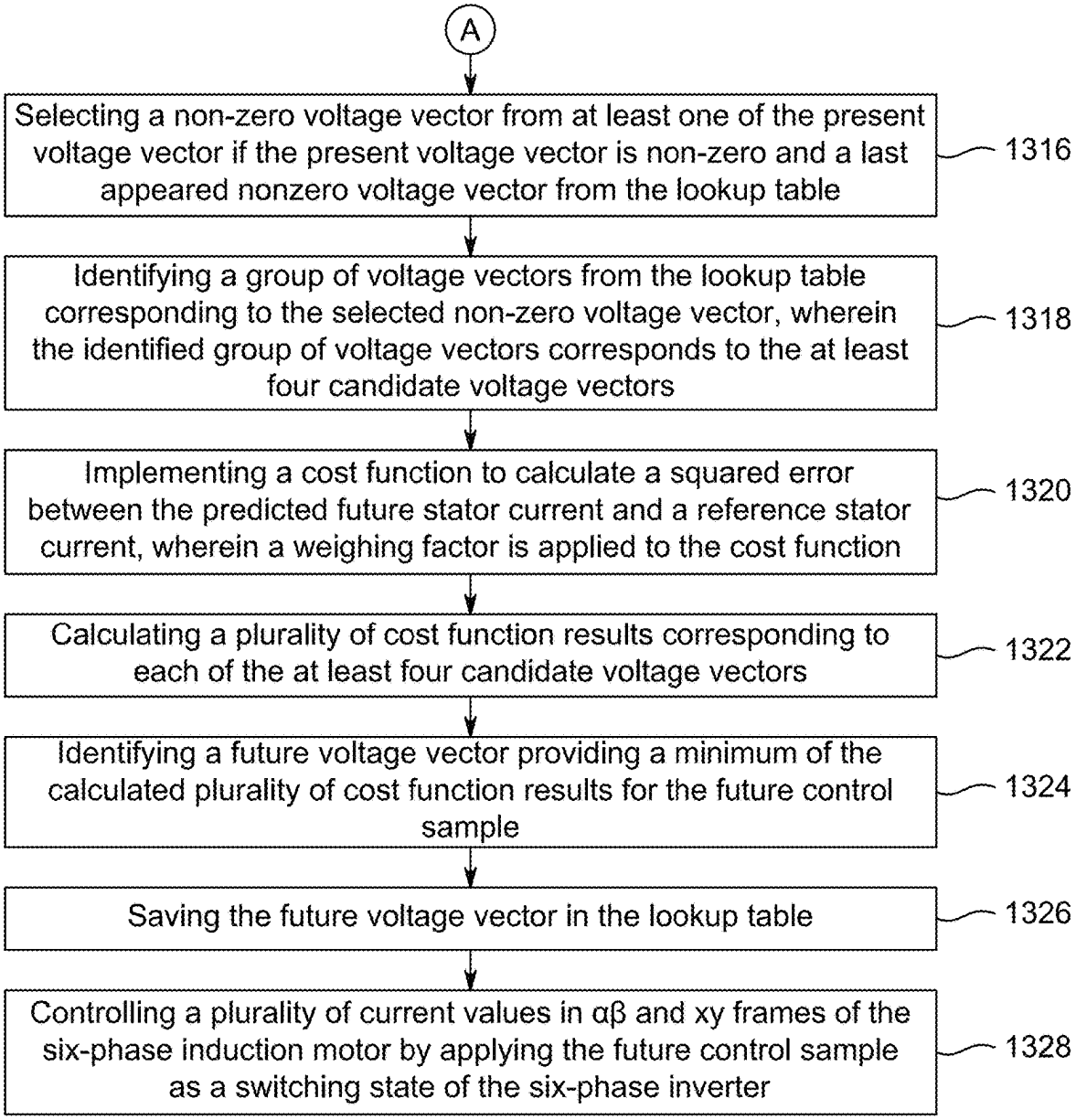
A
Selecting a non-zero voltage vector from at least one of the present voltage vector if the present voltage vector is non-zero and a last appeared nonzero voltage vector from the lookup table
1316
Identifying a group of voltage vectors from the lookup table corresponding to the selected non-zero voltage vector, wherein the identified group of voltage vectors corresponds to the at least four candidate voltage vectors
1318
Implementing a cost function to calculate a squared error between the predicted future stator current and a reference stator current, wherein a weighing factor is applied to the cost function
1320
Calculating a plurality of cost function results corresponding to each of the at least four candidate voltage vectors
1322
Identifying a future voltage vector providing a minimum of the calculated plurality of cost function results for the future control sample
1324
Saving the future voltage vector in the lookup table
1326
Controlling a plurality of current values in αβ and xy frames of the six-phase induction motor by applying the future control sample as a switching state of the six-phase inverter
1328

FIG. 13 (Cont'd)

PREDICTIVE CURRENT CONTROL METHOD FOR A SIX-PHASE INDUCTION MOTOR

STATEMENT OF PRIOR DISCLOSURE BY AN INVENTOR

Aspects of the present application were described in "Simple Predictive Current Control of Asymmetrical Six-Phase Induction Motor with Improved Performance," Mohamed Mamdouh, Mohammad Ali Abido, IEEE Transactions on Industrial Electronics, Volume 70, Issue 8, 7580-7590 Nov. 2, 2022, which is incorporated herein by reference in its entirety.

STATEMENT OF ACKNOWLEDGMENT

Support provided by the Interdisciplinary Research Center in Renewable Energy and Power Systems (IRC-REPS), King Fahd University of Petroleum & Minerals, through the funded research project #INRE2103 and KACARE Energy Research and Innovation Center (ERIC), KFUPM, Saudi Arabia is gratefully acknowledged.

BACKGROUND OF THE INVENTION

Technical Field

The present disclosure is related to a method and system for controlling electric drives and power systems. In particular, the present disclosure is related to a predictive current control method for a six-phase induction motor driven by a six-phase inverter.

Description of Related Art

The "background" description provided herein is for the purpose of generally presenting the context of the present disclosure. Work of the presently named inventors, to the extent it is described in this background section, as well as aspects of the description which may not otherwise qualify as prior art at the time of filing, are neither expressly or impliedly admitted as prior art against the present invention.

In recent times, multi-phase machines have gained large interest compared to conventional three-phase counterparts, despite their control mechanism being more complex than those of three-phase machines. Multi-phase machines are characterized by lower torque ripple, reduced current per phase and higher reliability than their three-phase counterparts. Conventional control methods such as direct torque control and field-oriented control have been successfully applied to higher-order phase machines, such as three-phase, six-phase and more. However, they suffer in regulating stator circulating currents, also known as x-y current component.

Control methods, such as, model predictive control (MPC) algorithms have emerged in the power electronic community and proved their capability for different applications. Finite control set-model predictive control (FCS-MPC) is one such convenient choice for multi-phase drives that can meet the torque and flux tracking requirements and simultaneously limit the stator circulating currents by considering a cost function. However, the FCS-MPC has other issues related to implementations such as the variable switching frequency, difficult setting of the weighting factors (WF), and high computation burden. Although, the issue of variable switching frequency is solved by adding modulation stages which also lowers total harmonic distortion (THD) and x-y currents, additional modulation stage increases the complexity of the control procedure. Further, the WF setting is also an issue for FCS-MPC. Several online and offline procedures are implemented for tuning the WF as a part of optimization step of FCS-MPC algorithms. For example, a cost function optimization is implemented, which is based on certain performance indices, followed by a discrete operating space establishment by calculating the performance indices at different operating points and different weighting factors. However, this method is time-consuming and noticeable offline work is required. A predictive current control (PCC) based double dq (2dq) method is generally used in order to eliminate the weighting factors, where a cost function consists of the four stator currents, having same priorities and equal WFs in 2dq space. Another method, such as a virtual voltage vector (VVV) concept maps the voltage vectors to $\alpha\beta$ and x-y subspaces with different magnitudes and orientations. Although, VVV simplifies the cost function design by eliminating the terms relating to x-y currents assuming them equal zero on average, the VVV method suffers from reduced DC link utilization and higher average switching frequency since more than one VV is applied in the same control sample.

FCS-MPC algorithms suffer from a high computation burden compared to other control methods. Moreover, the computation cost increases tremendously with the increased complexity of the system. For example, a six-phase machine feed from two-level voltage source inverter (2L-VSI) creates 64 voltage vectors (VVs) where a minimum of 49 iterations are required for the prediction and optimization processes.

In order to reduce the computation burden, a VSD theory introduced indicates that the largest voltage vectors in a-β subspace are mapped to the smallest ones in x-y subspace. It has also been suggested that use of the largest 12 VVs and one zero VV is efficient instead of evaluating the 49 VVs for A6P IM. A constrained search PCC of A6PIM is implemented by applying certain constraints to reduce the number of switching commutations. This results in reducing the number of admissible VV to 6 VVs at each control sample. However, these constraints lead to suboptimal solutions. For example, the PCC algorithm has better tracking and reduced switching frequency compared to the conventional PCC. However, the selection of the admissible VV is complicated and can result in either 11 or 16 VVs to be evaluated depending on the operating point. A concept of deadbeat (PCC-DC) has also been introduced in the past that indicates that it could decrease the number of admissible VVs to three and thus reducing computation burden by calculating the optimal reference voltage and select the closest admissible VV. However, this method needs the calculation of the position of the reference voltage and another optimization step to guarantee regulation of x-y currents. A two-step PCC algorithm for six-phase permanent magnet synchronous machine (PMSM) reduces the computation burden and the switching frequency. In a first step, the phase which has maximum error is identified and its switching state is reversed. In a second step, candidate VVs are formed by retaining the switching state of the first step and reversing the other five phases. This results in 6 VVs to be evaluated in each control sample. However, this method focuses only on the tracking of $\alpha\beta$ subspace and quite a number of components in the x-y subspace were observed.

As described, the existing methods suffer from one or more limitations hindering their adoption for control of multi-phase machines. For example, too many voltage vectors were to be examined. The high number of voltage

vectors to be examined causes higher computational burden on the system. Although, some of the methods somehow reduced the computational burden by reducing the number of voltage vectors to be examined, they required computation of location of reference voltage that further aided the burden on computation cost in other ways. Moreover, the average number of switching frequency were also found to be high in almost all of the methods.

Accordingly, there is a need for a control method for multi-phase machines that require only few voltage vectors to be examined, reduce the average number of switching frequencies, minimize the x-y currents and does not accumulate the additional burden of computing a location of the reference voltage vectors. The presently disclosed predictive current control method and system meet such a need by reducing the switching frequency and current total harmonic distortion and regulating the xy currents of an asynchronous six-phase induction motor.

SUMMARY

In an exemplary embodiment, the present disclosure includes a predictive current control method for a six-phase induction motor driven by a six-phase inverter. The method includes initializing the six-phase inverter at a present control sample comprising a present switching state corresponding to a present voltage vector, wherein the six-phase inverter employs the present control sample for converting a DC input voltage to a set of six-phase outputs for an operation of the six-phase induction motor. The method further includes measuring a stator current and a rotor speed of the six-phase induction motor. The method further includes transforming the measured stator current to a set of orthogonal subspace current values. The set of orthogonal subspace current values comprises a set of current values in αβ and xy frames. The method further includes estimating a set of rotor variables of the six-phase induction motor using a difference between the measured rotor speed and a reference rotor speed. The set of rotor variables comprises a pair of current values in αβ frame and xy frame. The method further includes calculating a future stator current for a future control sample of the six-phase inverter based on the transformed set of orthogonal subspace current values, estimated set of rotor variables, and the measured rotor speed. The method further includes selecting four candidate voltage vectors from sixty-four voltage vectors mapped to αβ and xy frames corresponding to sixty-four possible switching states of the six-phase inverter. The method of selecting four candidate voltage vectors includes three additional steps. The first step includes (1) predefining a lookup table representing a correlation between twelve possible non-zero voltage vectors and twelve corresponding groups of voltage vectors. The twelve possible non-zero voltage vectors are twelve possible switching states of the six-phase inverter with on state for at least one of but not all of the set of six phase outputs. Each group of the twelve corresponding groups of voltage vectors comprises four voltage vectors. The second step includes (2) selecting a non-zero voltage vector from at least one of the present voltage vector if the present voltage vector is non-zero and a last appeared nonzero voltage vector from the lookup table, and the third step includes (3) identifying a group of voltage vectors from the lookup table corresponding to the selected non-zero voltage vector. The identified group of voltage vectors corresponds to the four candidate voltage vectors. The method further includes implementing a cost function to calculate a squared error between the predicted future stator current and a reference stator current. A weighing factor is applied to the cost function. The method further includes calculating a plurality of cost function results corresponding to each of the four candidate voltage vectors. The method further includes identifying a future voltage vector providing a minimum of the calculated plurality of cost function results for the future control sample. The method further includes saving the future voltage vector as an optimal voltage vector to be used as an input to the lookup table for the next control sample. The method further includes controlling a plurality of current values in αβ and xy frames of the six-phase induction motor by applying the future control sample as a switching state of the six-phase inverter.

In another exemplary embodiment, the future control sample comprises at least two future control samples corresponding to the present control sample.

In another exemplary embodiment, the method further includes identifying a control sample with up to one commutation of a set of switches of the six-phase inverter.

In another exemplary embodiment, the method further includes mapping of a plurality of largest voltage vectors in αβ orthogonal subspace to a plurality of lowest voltage vectors in xy orthogonal subspace.

In another exemplary embodiment, the applied weighing factor corresponds to controlling a current in xy orthogonal subspace.

In another exemplary embodiment, the weighing factor is a value selected from a range of 0.01 up to 0.2.

In another exemplary embodiment, the twelve possible switching states of the six-phase inverter correspond to twelve largest voltage vectors in αβ orthogonal subspace.

In another exemplary embodiment, the four candidate voltage vectors comprise three active voltage vectors and one zero voltage vector.

In another exemplary embodiment, the three active voltage vectors correspond to three consecutive switching states of the six-phase inverter.

In another exemplary embodiment, the one zero voltage vector is selected from four zero voltage vectors corresponding to four zero switching states of the six-phase inverter.

In another exemplary embodiment, the six-phase inverter comprises two three-phase two level-voltage source inverters (2L-VSI) connected in parallel.

In another exemplary embodiment, the measuring of the rotor speed of the six-phase induction motor utilizing an encoder coupled to the six-phase induction motor.

In another exemplary embodiment, the estimating of the set of rotor variables utilizing a proportional-integral controller.

In another exemplary embodiment, the predictive current control method is performed utilizing a computer module.

The foregoing general description of the illustrative embodiments and the following detailed description thereof are merely exemplary aspects of the teachings of this disclosure, and are not restrictive.

BRIEF DESCRIPTION OF THE DRAWINGS

A more complete appreciation of this disclosure and many of the attendant advantages thereof will be readily obtained as the same becomes better understood by reference to the following detailed description when considered in connection with the accompanying drawings, wherein:

FIG. **1** illustrates a schematic diagram of an electric drive system, according to certain embodiments;

FIG. **2**A illustrates a mapping of resultant voltage vectors (VVs) to αβ subspaces for 49 voltage vectors (VVs), according to certain embodiments;

FIG. **2**B illustrates a mapping of resultant voltage vectors (VVs) to xy subspaces for 49 voltage vectors (VVs), according to certain embodiments;

FIG. **3**A illustrates selected optimal voltage vectors (VVs) for conventional predictive current control (PCC) at 1100 rpm and 3 Nm for three electric cycles, according to certain embodiments;

FIG. **3**B illustrates a zoomed view of the selected optimal voltage vectors (VVs) for conventional PCC at 1100 rpm and 3 Nm for three electric cycles, according to certain embodiments;

FIG. **3**C illustrates a mapping of voltage vectors (VVs) in αβ subspaces for all 16 voltage vectors (VVs) (12 Non-zero and four zero vectors), according to certain embodiments;

FIG. **3**D illustrates a mapping of voltage vectors (VVs) in the xy subspaces for all 16 VVs (12 Non-zero and four zero vectors), according to certain embodiments;

FIG. **4** illustrates an exemplary flowchart of main steps of the method of predictive current control for six-phase induction motor driven by six-phase inverter, according to certain embodiments;

FIG. **5**A illustrates a comparison between conventional and proposed predictive current control (PCC) methods based on average switching frequency, according to certain embodiments;

FIG. **5**B illustrates a comparison between conventional and proposed predictive current control (PCC) methods based on the root mean square (RMS) error of x current, according to certain embodiments;

FIG. **6** illustrates an experimental setup used to demonstrate the dynamic and steady-state analysis of an electric drive system, according to certain embodiments;

FIG. **7**A illustrates the starting response as a dynamic response of the electric drive system from a standstill to 1100 rpm at no load for a conventional predictive current control (PCC) method using 13 voltage vectors, according to certain embodiments;

FIG. **7**B illustrates a starting response as a dynamic response of the electric drive system for a stator current at no-load for a conventional predictive current control (PCC) method using 13 voltage vectors, according to certain embodiments;

FIG. **7**C illustrates starting response as a dynamic response of the electric drive system from standstill to 1100 rpm at no-load for the proposed predictive current control (PCC) method using 4 voltage vectors, according to certain embodiments;

FIG. **7**D illustrates starting response as a dynamic response of the electric drive system for a stator current at no-load for the proposed predictive current control (PCC) method using 4 voltage vectors, according to certain embodiments;

FIG. **8**A illustrates a loading response of the electric drive system for conventional predictive current control (PCC) method using 13 voltage vectors for rotation speed, according to certain embodiments;

FIG. **8**B illustrates a loading response of the electric drive system for conventional predictive current control (PCC) method using 13 voltage vectors for subspace currents i_α, according to certain embodiments;

FIG. **8**C illustrates a loading response of the electric drive system for conventional predictive current control (PCC) method using 13 voltage vectors for subspace currents i_x, according to certain embodiments;

FIG. **8**D illustrates a loading response of the electric drive system for conventional predictive current control (PCC) method using 13 voltage vectors for phase currents i_a, according to certain embodiments;

FIG. **8**E illustrates a loading response of the electric drive system for the proposed predictive current control (PCC) method using 4 voltage vectors for rotation speed, according to certain embodiments;

FIG. **8**F illustrates a loading response of the electric drive system for the proposed predictive current control (PCC) method using 4 voltage vectors for subspace currents i_α, according to certain embodiments;

FIG. **8**G illustrates a loading response of the electric drive system for the proposed predictive current control (PCC) method using 4 voltage vectors for subspace currents i_x, according to certain embodiments;

FIG. **8**H illustrates a loading response of the electric drive system for the proposed predictive current control (PCC) method using 4 voltage vectors for phase currents i_a, according to certain embodiments;

FIG. **9**A illustrates a reversing response of the electric drive system for conventional predictive current control (PCC) method using 13 voltage vectors for rotation speed, according to certain embodiments;

FIG. **9**B illustrates a reversing response of the electric drive system for conventional predictive current control (PCC) method using 13 voltage vectors for subspace currents i_α, according to certain embodiments;

FIG. **9**C illustrates a reversing response of the electric drive system for conventional predictive current control (PCC) method using 13 voltage vectors for subspace currents i_x, according to certain embodiments;

FIG. **9**D illustrates a reversing response of the electric drive system for conventional predictive current control (PCC) method using 13 voltage vectors for phase currents i_a, according to certain embodiments;

FIG. **9**E illustrates a reversing response of the electric drive system for the proposed predictive current control (PCC) method using 4 voltage vectors for rotation speed, according to certain embodiments;

FIG. **9**F illustrates a reversing response of the electric drive system for the proposed predictive current control (PCC) method using 4 voltage vectors for subspace currents i_α, according to certain embodiments;

FIG. **9**G illustrates a reversing response of the electric drive system for the proposed predictive current control (PCC) method using 4 voltage vectors for subspace currents i_x, according to certain embodiments;

FIG. **9**H illustrates a loading response of the electric drive system for the proposed predictive current control (PCC) method using 4 voltage vectors for phase currents i_a, according to certain embodiments;

FIG. **10**A illustrates a comparative analysis of stator current at 50 rpm and no-load condition for conventional predictive current control (PCC) method using 13 voltage vectors, according to certain embodiments;

FIG. **10**B illustrates a comparative analysis of stator current at 50 rpm and no-load condition for the proposed predictive current control (PCC) method using 4 voltage vectors, according to certain embodiments;

FIG. **10**C illustrates a comparative analysis of stator current at 600 rpm and 3 Nm torque for conventional predictive current control (PCC) method using 13 voltage vectors, according to certain embodiments;

FIG. **10**D illustrates a comparative analysis of stator current at 600 rpm and 3 Nm torque for the proposed

predictive current control (PCC) method using 4 voltage vectors, according to certain embodiments;

FIG. **10**E illustrates a comparative analysis of stator current at 1100 rpm and 4 Nm torque for the conventional predictive current control (PCC) method using 13 voltage vectors, according to certain embodiments;

FIG. **10**F illustrates a comparative analysis of stator current at 1100 rpm and 4 Nm torque for the proposed predictive current control (PCC) method using 4 voltage vectors, according to certain embodiments;

FIG. **11**A illustrates a steady state response of the electric drive system at a low speed of 50 rpm and no-load for the conventional predictive current control (PCC) method using 13 voltage vectors, according to certain embodiments;

FIG. **11**B illustrates a steady state response of the electric drive system for the conventional predictive current control (PCC) method using 13 voltage vectors for subspace currents i_α, according to certain embodiments;

FIG. **11**C illustrates a steady state response of the electric drive system for the conventional predictive current control (PCC) method using 13 voltage vectors for subspace currents i_x, according to certain embodiments;

FIG. **11**D illustrates a steady state response of the electric drive system for the conventional predictive current control (PCC) method using 13 voltage vectors for phase currents i_a, according to certain embodiments;

FIG. **11**E illustrates a steady state response of the electric drive system using a predictive current control (PCC)-deadbeat method for rotation speed, according to certain embodiments;

FIG. **11**F illustrates a steady state response of the electric drive system using a predictive current control (PCC)-deadbeat method for subspace currents i_α, according to certain embodiments;

FIG. **11**G illustrates a steady state response of the electric drive system using a predictive current control (PCC)-deadbeat method for subspace currents i_x, according to an embodiment;

FIG. **11**H illustrates a steady state response of the electric drive system using a predictive current control (PCC)-deadbeat method for subspace phase currents i_a, according to certain embodiments;

FIG. **11**I illustrates a steady state response of the electric drive system for a proposed predictive current control (PCC) method for rotation speed, according to certain embodiments;

FIG. **11**J illustrates a steady state response of the electric drive system for a proposed predictive current control (PCC) method for subspace currents i_α, according to certain embodiments;

FIG. **11**K illustrates a steady state response of the electric drive system for a predictive current control (PCC) method for subspace currents i_x, according to certain embodiments;

FIG. **11**L illustrates a steady state response of the electric drive system for a predictive current control (PCC) method for subspace phase currents i_a, according to certain embodiments;

FIG. **12**A illustrates a variation pattern of average switching frequency at different speeds and 2.5 Nm, according to certain embodiments;

FIG. **12**B illustrates a variation pattern of current THD at different speeds and 2.5 Nm load, according to certain embodiments; and

FIG. **13** illustrates a flowchart of a predictive current control method for a six-phase induction motor driven by a six-phase inverter, according to certain embodiments.

DETAILED DESCRIPTION

In the drawings, like reference numerals designate identical or corresponding parts throughout the several views. Further, as used herein, the words "a," "an" and the like generally carry a meaning of "one or more," unless stated otherwise. The drawings are generally drawn to scale unless specified otherwise or illustrating schematic structures or flowcharts.

Furthermore, the terms "approximately," "approximate," "about," and similar terms generally refer to ranges that include the identified value within a margin of 20%, 10%, or preferably 5%, and any values therebetween.

Furthermore, the terms two level-voltage source inverter, 2-level six-phase inverter, 2-L six-phase inverter, 2-level 6P inverter, six-phase inverter or inverter are used as synonyms throughout the disclosure and used interchangeably.

Furthermore, the terms six-phase induction motor, asynchronous six-phase induction motor, 6PIM, 6-PIM, A6PIM, or induction motor are also used as synonyms throughout the disclosure and used interchangeably.

Aspects of this disclosure are directed to a predictive current control method and system for a six-phase induction motor driven by a six-phase inverter that considerably reduces circulating current, computation cost, and switching frequency. In the PCC method a group of only four candidate voltage vectors (VVs) is formed in each control sample for further examination, based on a lookup table and an optimal voltage vector of the previous control sample. The lookup table is designed such that it allows only one commutation in each control sample.

Turning to drawings, FIG. **1** illustrates a schematic diagram of an electric drive system **100** according to certain embodiments of the present disclosure. The electric drive system **100** comprises an asymmetric six phase-induction motor **102**, herein also referred to as 6PIM in the disclosure, a 2-level six phase inverter **104**, and a controller **106**. The 2-level six phase inverter **104** is configured to convert a DC supply **108** to a six phase outputs through a two level-voltage source inverter (2L-VSI) **104**. The two level-voltage source inverter **104** is further configured to supply the six phase outputs to the 6PIM **102**. The electric drive system **100** further comprises an outer loop **110** and an inner loop **112**. An encoder **114** is attached to the rotor axis of the 6PIM **102** for measuring a rotor angular speed ω_r. A current sensor **132** is coupled to the 6PIM **102**. The current sensor **132** is configured to measure a stator current i_s of the 6PIM **102** and send the measured stator current i_s to the controller **106** via a first transformation block **130**. The controller **106** also receives a rotor angular speed ω_r via the inner loop **112**. In an embodiment, the electric drive system **100** may include a slip calculation block **118** coupled at the output of the encoder **114**.

The 2-level six phase inverter **104** includes a parallel connection of two three-phase two level-voltage source inverters (2L-VSI). The 2L-VSI **104** thus has sixty-four possible switching states by combinations of on/off output states of the six phases. Considering the two on/off switching states of each phase of the six-phase inverter, there are sixty-four (2^6=64) possible combinations of the six phase outputs of the inverter. The six phase outputs are represented by voltage vectors (hereafter "VVs") as V_n(Sa1, Sb1, Sc1, Sa2, Sb2, Sc2) (n=0 to 63), where Sa1, Sb1, Sc1, Sa2, Sb2 and Sc2 each represents an on (1) or an off (0) state of the six phase outputs. The VVs are also denoted by a vector [S] as Sa1Sb1Sc1Sa2Sb2Sc2=$[Sa1\ Sb1\ Sc1\ Sa2\ Sb2\ Sc2]^T$. In the embodiments herein, the VVs representing the switching

states or the six phase outputs of the 2L-VSI **104** are the manipulated variables in the predictive current control (PCC) method for controlling the 6PIM **102**. The output phase voltages of the 2-level six phase inverter **104** can be mathematically expressed as follows:

$$VVs = \begin{bmatrix} v_{a1} \\ v_{b1} \\ v_{c1} \\ v_{a2} \\ v_{b2} \\ v_{c2} \end{bmatrix} = \frac{V_{dc}}{3} \begin{bmatrix} 2 & -1 & -1 & 0 & 0 & 0 \\ -1 & 2 & -1 & 0 & 0 & 0 \\ -1 & -1 & 2 & 0 & 0 & 0 \\ 0 & 0 & 0 & 2 & -1 & -1 \\ 0 & 0 & 0 & -1 & 2 & -1 \\ 0 & 0 & 0 & -1 & -1 & 2 \end{bmatrix} [S] \quad (1)$$

The controller **106** includes a programming code that defines a transformation matrix T_{VSD} as below:

$$T_{VSD} = \frac{1}{\sqrt{3}} \begin{bmatrix} 1 & -\frac{1}{2} & -\frac{1}{2} & \frac{\sqrt{3}}{2} & -\frac{\sqrt{3}}{2} & 0 \\ 0 & \frac{\sqrt{3}}{2} & -\frac{\sqrt{3}}{2} & \frac{1}{2} & \frac{1}{2} & -1 \\ 1 & -\frac{1}{2} & -\frac{1}{2} & -\frac{\sqrt{3}}{2} & \frac{\sqrt{3}}{2} & 0 \\ 0 & -\frac{\sqrt{3}}{2} & \frac{\sqrt{3}}{2} & \frac{1}{2} & \frac{1}{2} & -1 \end{bmatrix} \quad (2)$$

The transformation matrix is used for mapping the resultant voltage vectors from the switching states to αβ and xy subspaces. FIG. **2**A illustrates mapping of the resultant VVs to αβ subspaces, and FIG. **2**B illustrates the mapping of the resultant VVs to xy subspaces. The numbers associated to each VV represent two octal numbers corresponding to the binary numbers [Sa1 Sb1 Sc1] and [Sa2 Sb2 Sc2], respectively. Considering FIG. **2**A and FIG. **2**B, it is to be noted that the 12 largest VVs in the αβ subspace are corresponding to the smallest VVs in the xy subspace. Therefore, the controller **106** is configured to map 12 largest voltage vectors in αβ orthogonal subspace to a plurality of lowest voltage vectors in the xy orthogonal subspace. Furthermore, the twelve possible switching states of the six-phase inverter **104** correspond to twelve largest voltage vectors in αβ orthogonal subspace. The controller **106** is configured to identify resultant voltage vectors (VVs) derived from the stator current i_s, that are illustrated in FIGS. **2**A and **2**B.

Referring back to FIG. **1**, the outer loop **110** is configured to process the rotor angular speed ω_r of the 6PIM **102** as detected by the encoder **114** coupled to the six-phase induction motor **102**. A proportional integral (PI) controller **116** utilizes the rotor angular speed ω_r of the 6PIM **102** in comparison to a reference rotor speed ω_r in estimating a set of rotor variables iq* and id*. Once the set of rotor variables iq* and id* are obtained, they are again converted into an αβ frame and xy frame using a second transformation block **124** and reference rotor current values in a, B and xy subspace, i.e. i_α*, i_β* and i_{xy}* are generated. The second transformation block **124** is coupled at the output of the proportional integral (PI) controller **116**. In an embodiment, the second transformation block **124** may again include a programming code that defines the transformation matrix T_{VSD} as provided in the equation (2) along with other equations to identify the set of rotor variables iq* and id* in the αβ frame and xy frame to generate i_α*, i_β* and i_{xy}*. The transformation matrix T_{VSD} thus uses a plurality of equations to convert the set of rotor variables iq* and id* into three orthogonal subspaces αβ frame, xy frame, and z_1z_2 frame. Components of subspace z_1z_2 are neglected for isolated neutrals of the six-phase induction motor **102**.

The controller **106** of the electric drive system **100** further comprises a prediction block **120** and a cost function minimization block **122**. The prediction block **120** is configured to select in each of the sampling steps a plurality of candidate voltage vectors (CVVs) as candidates for a primary voltage vector V_{opt} to be applied as a switching state of the 2L-VSI **104** in a following sampling step. The prediction block **120** is further configured to predict future values of the control variables corresponding to each of the plurality of CVVs when applied as the switching state of the 2L-VSI **104** in the following sampling step. The cost function minimization block **122** is configured to choose a primary VV giving a minimum value of a predefined cost function from among the plurality of CVVs selected at the prediction block **120**. The predefined cost function adopted in a certain embodiment of the present disclosure represents a squared error between the predicted and reference stator currents of the induction motor, as detailed below in description of the mathematical model of the induction motor.

In a certain embodiment of the present disclosure, the controller **106** is configured to store a predefined lookup table **126** before starting a first sampling step, where the predefined lookup table **126** defines a correlation between a primary voltage vector (VV) that was adopted at a previous sampling step (an optimal voltage vector) or given by an initial condition (denoted as V_{old}) and a voltage vector group (VV_g) comprising four candidate voltage vectors (CVVs). The four candidate voltage vectors (VV_g) comprise three active voltage vectors and one zero voltage vector. Also, the three active voltage vectors correspond to three consecutive switching states of the 2-level six-phase inverter **104**. For example, if the Vold is V_5, the three consecutive switching states corresponding to candidate voltage vectors (VV_g) is [V_{16} V_5 V_6] followed by a zero-voltage vector V_1. Thus, the last optimal voltage vectors V_{old} and its corresponding candidate voltage vectors (VV_g) are thus predefined in the lookup table **126** and is given by Table 1, detail of which is described later. Further, the prediction block **120** of the controller **106** is configured to select a VV_g comprising the four CVVs by referring the lookup table **126** and identifying the VV_g corresponding to a given V_{old}, in each of the sampling steps.

TABLE 1

Lookup table to form the candidate VVs based on the old optimal voltage vector

V_{old} Or(V_{NZ} Last optimal)	Candidate VVs (V_g)
V_5	[V_{16} V_5 V_6 V_1]
V_6	[V_5 V_6 V_7 V_2]
V_7	[V_6 V_7 V_8 V_4]
V_8	[V_7 V_8 V_9 V_3]
V_9	[V_8 V_9 V_{10} V_1]
V_{10}	[V_9 V_{10} V_{11} V_2]
V_{11}	[V_{10} V_{11} V_{12} V_4]
V_{12}	[V_{11} V_{12} V_{13} V_3]
V_{13}	[V_{12} V_{13} V_{14} V_1]
V_{14}	[V_{13} V_{14} V_{15} V_2]
V_{15}	[V_{14} V_{15} V_{16} V_4]
V_{16}	[V_{15} V_{16} V_5 V_3]

FIG. **3**A illustrates selected optimal VVs for the conventional PCC at 1100 rpm and 3 Nm for three electric cycles, according to an embodiment. A first plot **402** depicts a magnitude of voltage vectors with respect to time. FIG. **3**A

shows the selected **12** optimal VV at each sample for the conventional PCC that tends to be selected in successive manner.

FIG. **3**B illustrates a zoomed view of the selected optimal VVs for the conventional PCC at 1100 rpm and 3 Nm for three electric cycles, according to an embodiment. A second plot **404** illustrates a magnified view of the selected optimal VVs with respect to time. The enlarged view indicates that the optimal VV is related to the previously selected one. Thus, the candidate vector group VV_g for the next sample could be formed based on the old optimal voltage vector V_{old}. For example, if the current optimal voltage vector is V_n, the next optimal vectors could be related to its previous optimal voltage vector V_{n-1}, next optimal voltage vector V_{n+1} and one zero vector only. In an embodiment, forming the group of four CCVs (VVg) by the controller **106** is based upon the switching state vectors of the voltage vectors. It is to be noted that, that the optimal VVs are selected in successive manner as illustrated in FIGS. **3**A and **3**B.

Considering FIG. **3**A and FIG. **3**B, the controller **106** is programmed and configured to form the lookup table **126** for each voltage vector based upon old VV (V_{old}), the preceding VV (V_{old-1}), the following VVs (V_{old+1}) in the αβ subspace and one zero VV. The voltage vector V_5-V_{16} are non-zero voltage vector whereas V_1-V_4 are zero voltage vectors. In an embodiment, one zero voltage vector i.e. V_1, V_2, V_3, and V_4 is selected from four zero voltage vectors corresponding to four zero switching states of the 2-level six-phase inverter **104**. This is illustrated in Table 2 as below and shown in FIGS. **3**C and **3**D thereof:

TABLE 2

List of admissible VVs

VV_n	Two octal digits	Switching states $[S_{a1}\ S_{b1}\ S_{c1}\ S_{a2}\ S_{b2}\ S_{c2}]$	|VV| (αβ)
V_1	0 0	[0 0 0 0 0 0]	Zero
V_2	0 7	[0 0 0 1 1 1]	
V_3	7 0	[1 1 1 0 0 0]	
V_4	7 7	[1 1 1 1 1 1]	
V_5	4 4	[1 0 0 1 0 0]	Large
V_6	6 4	[1 1 0 1 0 0]	
V_7	6 6	[1 1 0 1 1 0]	
V_8	2 6	[0 1 0 1 1 0]	
V_9	2 2	[0 1 0 0 1 0]	
V_{10}	3 2	[0 1 1 0 1 0]	
V_{11}	3 3	[0 1 1 0 1 1]	
V_{12}	1 3	[0 0 1 0 1 1]	
V_{13}	1 1	[0 0 1 0 0 1]	
V_{14}	5 1	[1 0 1 0 0 1]	
V_{15}	5 5	[1 0 1 1 0 1]	
V_{16}	4 5	[1 0 0 1 0 1]	

FIG. **3**C illustrate mapping of voltage vectors VVs in αβ subspaces for all 16 VVs (12 Non-zero and four zero vectors) as listed in Table 2, according to an embodiment. If the Vold is V_{12}, the candidate group Vg is [V_g=V_{11}, V_{12}, V_{13}, V_3], where V_3 is a zero vector.

FIG. **3**D illustrate mapping of voltage vectors VVs in the xy subspaces for all 16 VVs (12 Non-zero and four zero vector as listed in Table 1, according to an embodiment. Since 12 largest VVs in the αβ subspace may provide a comparable performance as they are mapped to the smallest VVs in xy subspace, plurality of largest voltage vectors in αβ orthogonal subspace are thus mapped into a plurality of lowest voltage vectors in xy orthogonal subspace in the controller **106**.

Table 2 defines the VV_g correlated with the V_{old} exclusively when the V_{old} is a nonzero voltage vector. The nonzero voltage vector represents one of 12 possible switching states of the 2L-VSI, namely, V_5 to V_{16} of the Table 1, with an on (value 1) state for at least one of but not all of the six phase outputs. As indicated herein, the lookup table as shown in Table 1 covers the correlation between the nonzero voltage vector and the VV_g for all 12 possible cases of the optimal voltage vector. For other situations where the V_{old} was not the nonzero vector, an optimal voltage vector is selected based on last appeared optimal voltage vector V_{NZ} in an earlier sampling step if available, or otherwise given by an initial condition. For example, when the given present voltage vector is V_{old}, for example, V_6 (110100), the four allowable VVs are, for example, V_5 (1 0 0 1 0 0), V_6 (110100), V_7 (110110), and V_2 (000111), as confirmed in Table 2. On the other side, if the present voltage vector is a zero-voltage vector, last appeared non-zero voltage vector is selected as optimal voltage vector for the future sampling.

Initially the 2-level six phase inverter **104** is initialized at a present control sample. The present control sample may refer to the values of stator current i_s. The initial switching state of the inverter **104** corresponds to a present voltage vector VV. For example, the present voltage vector VV may be V_5 at which the inverter **104** is initialized. The inverter **104** uses the present control sample in order to convert a DC input voltage from the DC supply **108** into a set of six-phase outputs for an operation of the 6PIM **102**. Accordingly, initially at any arbitrary voltage vector from the inverter, the 6PIM **102** is initialized.

Mathematically, the model equations for 6PIM **102** required for the estimation, the prediction and the identification made in each of the sampling steps are described below. When a stationary reference frame, commonly called αβ frame is adopted and a stator current i_s is considered as a state variable, the model dynamic equations of the 6PIM **102** can be expressed as follows:

$$\left.\begin{aligned} v_{\alpha\beta s} &= R_s i_{\alpha\beta s} + p\lambda_{\alpha\beta s} \\ v_{xy} &= R_s i_{xy} + p\lambda_{xy} \\ 0 &= R_r i_r + p\lambda_r - j\omega_r \lambda_r \end{aligned}\right\} \tag{3}$$

$$\left.\begin{aligned} \lambda_{\alpha\beta s} &= (L_{ls} + L_{lm} + L_m) i_{\alpha\beta s} + L_m i_r) \\ \lambda_{xy} &= L_{ls} i_{xy} \\ \lambda_r &= L_m i_{\alpha\beta s} + (L_{lr} + L_m) i_r \end{aligned}\right\} \tag{4}$$

$$T_e = \frac{3}{2}\frac{P}{2}\frac{L_m}{L_r}(\lambda_r \times i_{\alpha\beta s}) \tag{5}$$

where $v_{\alpha\beta s}=[v_{\alpha s}\ v_{\beta s}]^T$, $v_{xy}=[v_x\ v_y]^T$, $i_{\alpha\beta s}=[i_{\alpha s}\ i_{\beta s}]^T$, $i_r=[i_{\alpha r}\ i_{\beta r}]^T$, $i_{xy}=[i_x\ i_y]^T$, $\lambda_{\alpha\beta s}=[\lambda_{\alpha s}\ \lambda_{\beta s}]^T$, $\lambda_r=[\lambda_{\alpha r}\ \lambda_{\beta r}]^T$, $\lambda_{xy}=[\lambda_x\ \lambda_y]^T$, R_s and R_r are resistances of stator and rotor, respectively. L_{ls} and L_{lr} are leakage inductances of stator and rotor, respectively. L_m and L_{lm} are the mutual inductance and stator leakage mutual inductance, respectively. ω_r is electrical rotor speed.

$$j = \begin{bmatrix} 0 & -1 \\ 1 & 0 \end{bmatrix}.$$

The stator input voltage vector in an orthogonal αβ frame, at the output of the six-phase inverter is given as equation 1 earlier:

$$\begin{bmatrix} v_{a1} \\ v_{b1} \\ v_{c1} \\ v_{a2} \\ v_{b2} \\ v_{c2} \end{bmatrix} = \frac{V_{dc}}{3} \begin{bmatrix} 2 & -1 & -1 & 0 & 0 & 0 \\ -1 & 2 & -1 & 0 & 0 & 0 \\ -1 & -1 & 2 & 0 & 0 & 0 \\ 0 & 0 & 0 & 2 & -1 & -1 \\ 0 & 0 & 0 & -1 & 2 & -1 \\ 0 & 0 & 0 & -1 & -1 & 2 \end{bmatrix} [S]$$

where V_{dc}=DC link voltage and [S]=[S_{a1} S_{b1} S_{c1} S_{a2} S_{b2} S_{c2}]^T as a switching state vector as 0 or 1.

As such, any arbitrary or initial voltage vector may be applied at the output of the inverter **104** based upon an initial switching state of the inverter **104**.

Now a stator current i_s and a rotor angular speed ω_r of the 6PIM **102** is measured, corresponding to initial switching state of the inverter **104**. For example, the current sensor, such as an ammeter **132** connected at the output of the 2L-6P inverter **104** is configured to measure the stator current i_s. Similarly, the encoder **114** measures the rotor speed ω_r of the 6PIM **104**. Once the stator current i_s is measured, it is transformed into the set of orthogonal subspace current values, i.e. in αβ and xy frames using the first transformation block **130** explained earlier. For example, the first transformation block **130** including the mathematical equation as provided in equation 2 transforms the is into αβ, xy subspace. The output is provided as one of the inputs to the controller **106**.

Further, a set of rotor variables i.e., iq* and id* is estimated. In an embodiment, a difference between the measured rotor speed ω_r and a reference rotor speed ω_r* is measured, for example using a difference measuring circuit (not shown). In an embodiment, the difference between the measured rotor speed or and a reference rotor speed ω_r* is further provided as an input to the PI controller **116**. The PI controller **116** is configured to generate the set of rotor variables i.e. iq* and id*. Once the set of rotor variables i.e., iq* and id* are generated, they are provided as input to the second transformation block **124** such that the set of rotor variables transforms into a pair of current values in αβ frame and xy frame, i.e. iα*, iβ* and ixy*. In an embodiment, the second transformation block **124** may also include mathematical equation as provided in equation 2 to transforms the iq* and id* into αβ, xy subspace.

Now, the model of the 6PIM **102** is arranged in matrix format based on the dynamic model of equations (3) and (4), as follows:

$$\begin{bmatrix} v_{\alpha s} \\ v_{\beta s} \\ 0 \\ 0 \end{bmatrix} = \begin{bmatrix} R_s & 0 & 0 & 0 \\ 0 & R_s & 0 & 0 \\ 0 & \omega_r L_m & R_r & \omega_r L_r \\ -\omega_r L_m & 0 & -\omega_r L_r & R_r \end{bmatrix} \begin{bmatrix} i_{\alpha s} \\ i_{\beta s} \\ i_{\alpha r} \\ i_{\beta r} \end{bmatrix} + \begin{bmatrix} L_s & 0 & L_m & 0 \\ 0 & L_s & 0 & L_m \\ L_m & 0 & L_r & 0 \\ 0 & L_m & 0 & L_r \end{bmatrix} .p. \begin{bmatrix} i_{\alpha s} \\ i_{\beta s} \\ i_{\alpha r} \\ i_{\beta r} \end{bmatrix} \quad (6)$$

$$\begin{bmatrix} v_{xs} \\ v_{ys} \end{bmatrix} = \begin{bmatrix} R_s & 0 \\ 0 & R_s \end{bmatrix} \begin{bmatrix} i_{xs} \\ i_{ys} \end{bmatrix} + \begin{bmatrix} L_{ls} & 0 \\ 0 & L_{ls} \end{bmatrix} .p. \begin{bmatrix} i_{xs} \\ i_{ys} \end{bmatrix} \quad (7)$$

where L_s=L_{ls}+L_{lm}+L_m and L_r=L_{lr}+L_m and stator currents is are considered as the state variables.

Further Discrete model is obtained using first Euler discretization method as follows:

$$X(k+1) = A_d(k)X(k) + B_d U(k) + C(k) \quad (8)$$

where X=[$i_{\alpha s}$ $i_{\beta s}$ i_x i_y]^T and U=[$v_{\alpha s}$ $v_{\beta s}$ v_x v_y]^T can be obtained from the DC link voltage and switching states as given in (5) followed by VSD transformation using equation (1).

$$\text{Also, } A_d = I + T_s \begin{bmatrix} -a_1 & a_2\omega_r & 0 & 0 \\ -a_2\omega_r & -a_1 & 0 & 0 \\ 0 & 0 & -a_3 & 0 \\ 0 & 0 & 0 & -a_3 \end{bmatrix} \quad (9)$$

$$B_d = T_s \begin{bmatrix} b_1 & 0 & 0 & 0 \\ 0 & b_1 & 0 & 0 \\ 0 & 0 & b_2 & 0 \\ 0 & 0 & 0 & b_2 \end{bmatrix} \quad (10)$$

where, where k denotes the k^{th} sampling step, I is the identity matrix and T_s is a duration time of the sampling steps. Also,

$$c_1 = L_s L_r - L_m^2,\ a_1 = \frac{R_s L_r}{c_1},\ a_2 = \frac{L_m^2}{c_1},\ a_3 = \frac{R_s}{L_{ls}},\ b_1 = \frac{L_r}{c_1} \text{ and } b_2 = \frac{1}{L_{ls}},$$

and

$$C(k) = X(k) - (A_d(k)X(k-1) + B_d U(k-1)) \quad (11)$$

is considered as a zero initial condition.

In order to compensate for the time delay caused by calculation process, the variables at the $(k+2)^{th}$ sampling step can be predicted as follows.

$$X(k+2) = A_d(k)X(k+1) + B_d U(k+1) + C(k+1) \quad (12)$$

$$C(k+1) = X(k+1) - (A_d(k)X(k) + B_d U(k)) \quad (13)$$

Based upon the equations 11-13, the prediction block **120** of the controller **106** is configured to predict future stator current X (k+2) for a future control sample of the 6PIM **102**. As such, values of one step ahead of stator currents is are predicted using system model provided in equations 6 through 13. In an embodiment, the prediction block **120** receives the transformed set of orthogonal subspace current values, the estimated set of rotor variables, and the measured rotor speed to predict the future stator current as X (K+2). In an embodiment, future control sample comprises at least two future control samples corresponding to the present control sample.

The controller **106** initially predefines the lookup table **126** as explained in Table 1 and Table 2 containing twelve possible group of VVs. Each group of voltage vector VV corresponds to three neighbor voltage vectors and a zero voltage vector as defined in Table 1 and Table 2 as described previously.

The controller **106** is further configured to select a non-zero voltage vector V_{NZ} or V_{old} from the lookup table **126** described in Table 2. Selecting an optimal VV is now explained with two examples below:

Example I: If the last voltage vector was a non-zero VV as appeared during the last optimal voltage vector selection.

The controller **106** checks if the selected non-zero vector appeared as an optimal voltage vector V_{opt} during the last sampling period V_{old} within the lookup table **126** as stored in a memory block **128**. For example, if the controller **106**

identifies that the present selected voltage vector, for example, is V_5, and during the last sampling period i.e. K^{th} sampling period, the voltage vector V_5 appeared as an optimal voltage vector V_{opt} to be applied as an input for the inverter **104**. If so the controller **106** is configured to select the previous selected optimal voltage vector V_5 as V_{old} for computing the cost function to identify the minimum value of the cost function at the currently identified voltage vector V_5. Since, the new optimal voltage vectors i.e. V_5 for the next sample must corresponds to four neighbor candidate voltage vectors to the optimal voltage vector V_5, as per Table 2 defined in the controller **106**, the controller **106** is configured to identify the group of voltage vectors from the lookup table **126** corresponding to the selected non-zero voltage vector V_5. The candidate voltage vector group V_g corresponding to V_5 are four different voltage vectors, for example [V_{16} V_5 V_6 V_1] as provided in Table 2. It means that the optimal voltage vector must be at least one selected from the candidate voltage vector [V_{16} V_5 V_6 V_1] for the next sampling periods. Accordingly, the controller **106** identifies the group of voltage vector V_g as [V_{16} V_5 V_6 V_1] from the lookup table **126** corresponding to the selected non-zero voltage vector V_5.

Example II: If the present voltage vector is a zero VV as appeared during the last optimal voltage vector selection.

The controller **106** checks if the last appeared optimal voltage vector V_{opt} was a zero-voltage vector during the last sampling period within the lookup table **126** as stored in a memory block **128**. For example, if the controller **120** identifies that the present selected voltage vector, for example, is V_1, and during the last sampling period i.e. K^{th} sampling period, the voltage vector V_1 appeared as an optimal voltage vector V_{opt} to be applied as an input for the inverter **104**. If so the controller **106** is configured to select last active (non-zero) optimal VV referred here as V_{NZ} that was selected as an optimal voltage vector at one step one earlier before the application of the zero-voltage vector for the next step. For example, before the application of zero-voltage vector as an optimal voltage vector for applying as a switching state of the inverter **104**, one more immediate active non-zero voltage vector was, for example V_7, is identified. In this case, the voltage vector for the next step is thus selected as a non-zero voltage vector V_7 since the last voltage vector is a zero-voltage vector. As such, the controller selects V_7 for computing the cost function to identify the voltage vector that yields the minimum value of the cost function at the currently identified voltage vector V_7.

The controller **106** is configured to identify the group of voltage vectors from the lookup table **126** corresponding to the selected non-zero voltage vector V_7. The candidate voltage vector group VV_g corresponding to V_7 are four different voltage vectors, for example [V_6 V_7 V_8 V_4] as provided in Table 2. In other words, the optimal voltage vector must again be at least one selected from the candidate voltage vector [V_6 V_7 V_8 V_4] for the next sampling periods. Accordingly, the controller **106** identifies the group of voltage vector VV_g as [V_6 V_7 V_8 V_4] from the lookup table **126** corresponding to the selected non-zero voltage vector V_7.

Considering both examples 1 and 2, the controller **106** selects four candidate voltage vectors Vg from sixty-four voltage vectors mapped to αβ and xy frames corresponding to sixty-four possible switching states of the six-phase inverter **104**.

The controller **106** implements a predefined mathematical equation (Cost function) for computing a cost function $g(V_s)$ as given in equation 14, in order to identify a voltage vector out of 4 identified candidate voltage vectors in either example 1 or 2, that minimizes the total cost for the predicted future stator current. Here, Vs represents the candidate voltage vectors. In an embodiment, the cost function $g(V_s)$ calculates a squared error between the predicted future stator current and a reference stator current as below:

$$g(V_s) = \left(i_\alpha^* - i_\alpha^P\right)^2 + \left(i_\beta^* - i_\beta^P\right)^2 + K_{xy}\left(\left(i_x^* - i_x^P\right)^2 + \left(i_y^* - i_y^P\right)^2\right) \quad (14)$$

where the superscripts * and P are used for the reference future stator current values and predicted future stator current values, respectively, V_s represents the applied voltage vector or candidate voltage vector, K_{xy} is a weighting factor which reflects the relative priority of αβ components (flux and torque tracking) against the xy components as a current distortion. In an embodiment, the weighing factor is a value selected from a range of 0.01 up to 0.2 that corresponds to control the current in xy orthogonal subspace.

The controller **106** evaluates the value of cost function $g(V_s)$ as defined in equation 14 for each of the plurality of CVVs, i.e., [V_{16} V_5 V_6 V_1] for the first example or [V_6 V_7 V_8 V_4] for the second example, as explained earlier regarding Table 1 and Table 2, particularly in a certain embodiment of the present disclosure,

The controller **106** evaluates the cost function as given in equation (14) to identify plurality of cost function results i.e. at a first voltage vector V_{16}, a second voltage vector V_5, a third voltage vector V_6 and a fourth voltage vector V_1 (zero-voltage vector) corresponding to V_{old} voltage vector for the first example to compute the squared error between the predicted future stator current (for example $i^P\alpha$, $i^P\beta$, i^Px and i^Py) and a reference stator current (for example. $i^*\alpha$, $i^*\beta$, i^*x and i^*_y) as in eq 14. Similarly, for the second example, the controller **106** evaluates the cost function results as given in eq 14 to identify plurality of cost function results i.e., at the fifth voltage vector V_6, a sixth voltage vector V_7, a seventh voltage vector V_8 and an eighth voltage vector V_4 (zero-voltage vector) corresponding to V_{NZ} for the second example to compute the squared error between the predicted future stator current (for example $i^P\alpha$, $i^P\beta$, i^Px and i^Py) and a reference stator current (for example. $i^*\alpha$, $i^*\beta$, i^*x and i^*_y).

Once the controller **106** iteratively computes the cost function results for plurality of candidate voltage vectors as provided in equation 14 corresponding to the V_{16}, V_5, V_6 and V_1, for the first example, or V_6, V_7, V_8 and V_4, for the second example, the controller **106** simultaneously computes equation 16 to identify the minimum value of the cost function for the four CVVs given by the VV_g selected, as below:

$$V_{s-opt} = \underset{\{v_g\}}{\text{argming}}(V_s) \quad (15)$$

The minimum value of the cost function for the four CVVs is determined based on equation 15. For example, the controller **106** identifies that the voltage vector V_6 provides the minimum value of the cost function in case of example 1 or the voltage vector V_7 provides the minimum value of the cost function in case of example 2. Then, a voltage vector corresponding to the minimum value of the cost function, is identified as a primary voltage vector to be applied in the next sample period. For example, Voltage vector V_6 is selected as a primary or a future voltage vector that would

provide a minimum of the calculated plurality of cost function results for the future or next control sample in case of Example 1 or Voltage vector V_7 is selected as a primary or a future voltage vector that would provide a minimum of the calculated plurality of cost function results for the future or next control sample in case of Example 2. The controller thus saves the future voltage vector V_6 in case of first example, or V_7 in case of second example, as an optimal voltage vector to be used as an input to the lookup table **126** for the next control sample. Based upon the identified optimum voltage vector (V_6 in first example or V_7 in second example), that's acts as a switching state of the inverter **104**, plurality of current values in αβ and xy frames of the 6PIM is controlled by applying the future control sample (V_6 in first example or V_7 in second example) as a switching state of the six-phase inverter **104**. Accordingly, the controller **106** need not process all 13 voltage vectors to identify the future or the next voltage vector however, only 4 voltage vectors need to be processed. Thus, evaluating only four VVs in Vg during the optimization step reduces the computation time.

The predictive current control method executed by the controller **106** requires only one commutation to move from one VV to its previous or following one. Also, one of the four redundant zero VV is selected that ensures that only one commutation is required if a zero VV is to be selected among the candidate Vg. In an embodiment, control sample with up to one commutation of the set of switches of the 2-level six-phase inverter **104** is identified. Accordingly, switching frequency is considerably minimized.

FIG. **4** illustrates an exemplary flowchart **200** of main steps of the method of predictive current control for six-phase induction motor driven by six-phase inverter, according to an embodiment. As described with FIG. **1** in a block **202**, an initial value of V_{old}, V_{NZ} and V_{opt} is initialized. In an embodiment, the initial values are predefined in the lookup table **126**. In block **204**, the initial optimum value of the voltage vector is selected and applied as input to the 2L-six phase inverter **104**. Block **206** describes the measuring stator current i_s, rotor speed ω_r and possible V_{dc} value. According, a set of rotor variables (iq* and id*) of the 6PIM **102** is identified using a difference between the measured rotor speed ω_r and a reference rotor speed ω_r*. Based upon the stator current i_s and rotor speed ω_r, a block **208** is configured to predict future stator current for a future control sample of the 6PIM **102** based on the transformed set of orthogonal subspace current values, estimated set of rotor variables, and the measured rotor speed. A Block **210** compensates for the time delay caused by the calculation process. A block **212** computes future control sample (C_{K+1}) using equation 12 and 13 as described earlier. As such, values of one step ahead of stator currents is are predicted using system model provided in Eq. 6-13.

A block **214** selects a non-zero voltage vector from at least one of the present voltage vectors if the present voltage vector is non-zero and a last appeared nonzero voltage vector from the lookup table **126**. If the present voltage vector is same as a last appeared voltage vector and a non-zero VV as appeared during the last optimal voltage vector selection, a block **218** indicates to access the lookup table **126** using the non-zero VV as V_{old}. If the present voltage vector is a zero VV as appeared during the last optimal voltage vector selection, a block **216** indicates to access the lookup table **126** using the last active (non-zero) optimal VV referred here as V_{NZ} that was selected as an optimal voltage vector at one step one earlier before the application of the zero-voltage vector for the next step.

Based upon the selection of the voltage vector as either V_{old} or V_{NZ}, a block **220** indicates to determine candidate voltage vectors V_g corresponding to V_{old} or V_{NZ} as described in Table 1 and Table 2. The candidate voltage vectors V_g includes four voltage vectors. Block **222** indicates to initialize optimum voltage vector as V_{old}. Block **224** and **226**, **228** and **232** in combination indicate to compute the cost function $g(V_s)$ iteratively at each candidate voltage vector Vg to compute the squared error between the predicted future stator current (for example $i^P\alpha$, $i^P\beta$, i^Px and i^P_y) and a reference stator current (for example. i*α, i*β, i*x and i^*_y) as per equation 14. Block **230** indicates the identify of a voltage vector V_{opt} corresponding to the minimum value of the cost function result as a primary voltage vector to be applied in the next sample period that is fed back to the block **204** as a loop.

FIG. **5**A illustrates a comparison between conventional and proposed PCC methods based on average switching frequency, according to an exemplary embodiment. A third plot **502** and a fourth plot **504** illustrates the switching frequency pattern with respect to speed of the rotor and the torque for the convention method and the proposed PCC method, respectively. It is evident that there is an observable reduction in the switching frequency in the proposed PCC method.

FIG. **5**B illustrates a comparison between conventional and proposed PCC methods based on the root mean square (RMS) error of x current, according to an exemplary embodiment. A fifth plot **506** and a sixth plot **508** illustrates a pattern of RMS tracking error of i_x current component with respect to speed of the rotor and the torque for the convention method and the proposed PCC method, respectively. It is evident that there is an observable reduction in the circulating current using the proposed PCC method compared to the conventional method.

FIG. **6** illustrates an experimental set up **600** used to demonstrate the dynamic and steady state analysis of an electric drive system, according to an embodiment of the present disclosure compared with the conventional approach. The predictive current control method is thus performed utilizing a computer module as shown in the experimental setup **600**. The experimental set up **600** was constructed based on FIG. **1**. A six-phase induction motor (6PIM) **618** with 1 kw output power having rating and parameters as listed in Table 3 and Table 4, respectively, was mechanically attached to a 0.75 KW DC generator **614**. The DC generator **614** acted as a load. Terminals of the DC generator **614** were connected to a chroma programmable electronic load **612** to give a controlled load to the 6PIM **618**. The 6PIM **618** was fed by a controlled 2L-VSI **602** from SEMKRON inverter (manufactured by Danfoss, Baltimore, MD) connected with ±15 V DC supply **606**. The PCC technique as described in FIG. **1** and FIG. **4** was implemented in real time using dSPACE **1103** (1 GHz) terminal box platform 608 (manufactured by dSPACE, 50131 Pontiac Trail Wixom, MI, USA 48393-2020) and a host computer **610**. The sampling time for all algorithm was set to 40 usec. The rotor angular speed was measured using a 1024 pulse per revolution incremental encoder **616**. LEM current and voltage sensors **604** were used for measuring the six-phase currents and DC link voltage, respectively.

TABLE 3

Prototype machine specifications

Specification	Value
Rated RMS phase Voltage (V)	110 V
Rated Power (kW)	1
Rated RMS phase current (A)	2.2
Rated frequency (Hz)	60
No. of poles	6
Rated speed (RPM)	1140

TABLE 4

Prototype machine parameters

Parameter (VSD)	Values
R_s	3.1 Ω
R_r	1.94 Ω
L_{ls}	2.05 mH
L_{lr}	6.6 mH
L_{lm}	10.4 mH
L_m	123.4 mH

FIG. **7**A illustrates starting response as a dynamic response of the electric drive system **100** from standstill to 1100 rpm at no-load for conventional method using 13 voltage vectors, according to an embodiment. A PI speed controller was utilized at the time of experimenting. Also, the K_{xy} values were set to 0.2 and 0.05 and tuned to minimize xy currents to best values maintaining good tracking characteristics. In the experiments, in order to demonstrate dynamic characteristics, a step change in the rotor angular speed command from 0 to 1100 rpm was applied. A seventh plot **702** indicates a rotation speed of the 6PIM with respect to time. The transient response settled down at about 0.2 seconds.

FIG. **7**B illustrates starting response as a dynamic response of the electric drive system **100** for a stator current at no-load for conventional method using 13 voltage vectors, according to an embodiment. Same PI controller **116** was utilized at the time of experiment. Also, the K_{xy} values were set to 0.2 and 0.05 and tuned to minimize xy currents to best values maintaining good tracking characteristics. With the applied step change in the rotor angular speed command from 0 to 1100, an eighth plot **704** indicates the transient occurred in the stator current. Here again the transients in the stator current settled down before about 0.2 seconds.

FIG. **7**C illustrates starting response as a dynamic response of the electric drive system **100** from standstill to 1100 rpm at no-load for the proposed method using 4 voltage vectors, according to an embodiment. Similar experimental characteristics as in FIG. **1**A was stablished. A ninth plot **706** indicates a rotation speed of the 6PIM with respect to time. The transient response was again found to be settled down at about 0.2 seconds.

FIG. **7**D illustrates starting response as a dynamic response of the electric drive system **100** for a stator current at no-load for the proposed method using 4 voltage vectors, according to an embodiment. With again similar conditions as in FIG. **7**B, a tenth plot **708** indicates the transient occurred in the stator current. Here again the transients in the stator current settles down before about 0.2 seconds.

Considering FIGS. **7**A, **7**B, **7**C and **7**D, it was observed that both methods have similar transient response and settles down at about 0.2 seconds.

FIG. **8**A illustrates a loading response of the electric drive system **100** for conventional method using 13 voltage vectors for rotation speed, according to an embodiment. A sudden load of 3 Nm was applied to the A6PIM while running at 1000 rpm. An eleventh plot **802** indicates a rotation speed of the 6PIM **102** with respect to time. A twelfth plot **804** indicates a reference rotor speed ω_r*.

FIG. **8**B illustrates a loading response of the electric drive system **100** for conventional method using 13 voltage vectors for subspace currents i_α, according to an embodiment. A thirteenth plot **806** indicates a pattern of subspace current i_α, through the 6PIM **102** with respect to time. A fourteenth plot **808** indicates a reference subspace current i_α.

FIG. **8**C illustrates a loading response of the electric drive system **100** for conventional method using 13 voltage vectors for subspace currents i_x, according to an embodiment. A fifteenth plot **810** indicates a pattern of subspace current i_x, through the 6PIM **102** with respect to time.

FIG. **8**D illustrates a loading response of the electric drive system **100** for conventional method using 13 voltage vectors for phase currents i_a, according to an embodiment. A sixteenth plot **812** indicates a pattern of phase current i_α, through the 6PIM **102** with respect to time.

FIG. **8**E illustrates a loading response of the electric drive system **100** for the proposed method using 4 voltage vectors for rotation speed, according to an embodiment. A sudden load of 3 Nm was again applied to the A6PIM while running at 1000 rpm. A seventeenth plot **814** indicates a rotation speed of the 6PIM **102** with respect to time. An eighteenth plot **816** indicates a reference rotor speed.

FIG. **8**F illustrates a loading response of the electric drive system **100** for the proposed method using 4 voltage vectors for subspace currents i_α, according to an embodiment. A nineteenth plot **818** indicates a pattern of subspace current i_α, through the 6PIM **102** with respect to time. A twentieth plot **820** indicates a reference subspace current i_α.

FIG. **8**G illustrates a loading response of the electric drive system **100** for the proposed method using 4 voltage vectors for subspace currents i_x, according to an embodiment. A twenty-first plot **822** indicates a pattern of subspace current i_x, through the 6PIM **102** with respect to time.

FIG. **8**H illustrates a loading response of the electric drive system **100** for the proposed method using 4 voltage vectors for phase currents i_a, according to an embodiment. A twenty-second plot **824** indicates a pattern of phase current i_α, through the 6PIM **102** with respect to time.

Considering FIG. **8**A-**8**H, it was observed that the speed retained to its reference value after a short transient period for both methods. Further it was noted that i_α in the proposed method using 4 voltage vectors could successfully tracked its reference and the reduction of circulating current i_x was relatively less than the conventional method.

FIG. **9**A illustrates a reversing response of the electric drive system **100** for conventional method using 13 voltage vectors for rotation speed, according to an embodiment. For conducting the reversing test, a command speed was changed from 1000 to −1000 rpm. A twenty-third plot **902** indicates a pattern observed in rotation speed ω_r* of the 6PIM **102** with respect to time. A twenty fourth plot **904** indicates a reference rotor speed ω_r*.

FIG. **9**B illustrates a reversing response of the electric drive system **100** for conventional method using 13 voltage vectors for subspace currents i_α, according to an embodiment. A twenty-fifth plot **906** indicates a pattern of subspace current i_α, through the 6PIM with respect to time. A twenty-sixth plot **908** indicates a reference subspace current i_α.

FIG. **9**C illustrates a reversing response of the electric drive system **100** for conventional method using 13 voltage vectors for subspace currents i_x, according to an embodiment. A twenty seventh plot **910** indicates a pattern of subspace current i_x, through the 6PIM **102** with respect to time.

FIG. **9**D illustrates a reversing response of the electric drive system **100** for conventional method using 13 voltage vectors for phase currents i_a, according to an embodiment. A twenty-eighth plot **912** indicates a pattern of phase current i_α, through the 6PIM **102** with respect to time.

FIG. **9**E illustrates a reversing response of the electric drive system **100** for the proposed method using 4 voltage vectors for rotation speed, according to an embodiment. For conducting the reversing test, a command speed was again changed from 1000 to −1000 rpm. A twenty-ninth plot **914** indicates a rotation speed of the 6PIM **102** with respect to time. A thirtieth plot **916** indicates a reference rotor speed ω_r*.

FIG. **9**F illustrates a reversing response of the electric drive system **100** for the proposed method using 4 voltage vectors for subspace currents i_α, according to an embodiment. A thirty-first plot **918** indicates a pattern of subspace current i_α, through the 6PIM **102** with respect to time. A thirty-second plot **920** indicates a reference subspace current i_α.

FIG. **9**G illustrates a reversing response of the electric drive system **100** for the proposed method using 4 voltage vectors for subspace currents i_x, according to an embodiment. A thirty-third plot **922** indicates a pattern of subspace current i_x, through the 6PIM **102** with respect to time.

FIG. **9**H illustrates a loading response of the electric drive system **100** for the proposed method using 4 voltage vectors for phase currents i_a, according to an embodiment. A thirty-fourth plot **924** indicates a pattern of phase current i_α, through the 6PIM **102** with respect to time.

Considering FIG. **9**A-**9**H, it was observed that the 6PIM **102** successfully followed the command speed for both methods. However, it was observed that there is a very short time for which the actual i_α could not follows its reference at the end of the reversing period for both methods. This behavior attributed to the high circulating current where the optimization step gave more priority to the reduction of circulating current (i_x) than the tracking currents (i_α) at this short period.

FIG. **10**A illustrates a comparative analysis of stator current at 50 rpm and no-load condition for conventional method using 13 voltage vectors, according to an embodiment. Current tracking characteristics were observed at different operating conditions. A thirty-fifth plot **1002** indicates a pattern of $i_{\alpha\beta}$ current. A thirty-sixth plot **1004** indicates a pattern of $i_{\alpha\beta}$* current. A thirty-seventh plot **1006** indicates a pattern of xy current.

FIG. **10**B illustrates a comparative analysis of stator current at 50 rpm and no-load condition for the proposed method using 4 voltage vectors, according to an embodiment. A thirty-eighth plot **1012** indicates a pattern of $i_{\alpha\beta}$ current. A thirty-ninth plot **1010** indicates a pattern of $i_{\alpha\beta}$* current. A fortieth plot **1008** indicates a pattern of xy current.

FIG. **10**C illustrates a comparative analysis of stator current at 600 rpm and 3 Nm torque for conventional method using 13 voltage vectors, according to an embodiment. A forty-first plot **1014** indicates a pattern of $i_{\alpha\beta}$ current. A forty-second plot **1016** indicates a pattern of $i_{\alpha\beta}$* current. A forty-third plot **1018** indicates a pattern of xy current.

FIG. **10**D illustrates a comparative analysis of stator current at 600 rpm and 3 Nm torque for the proposed method using 4 voltage vectors, according to an embodiment. A forty-fourth plot **1024** indicates a pattern of $i_{\alpha\beta}$ current. A forty-fifth plot **1022** indicates a pattern of $i_{\alpha\beta}$* current. A forty-sixth plot **1020** indicates a pattern of xy current.

FIG. **10**E illustrates a comparative analysis of stator current at 1100 rpm and 4 Nm torque for conventional method using 13 voltage vectors, according to an embodiment. A forty-seventh plot **1026** indicates a pattern of $i_{\alpha\beta}$ current. A forty-eighth plot **1028** indicates a pattern of $i_{\alpha\beta}$* current. A forty-ninth plot **1030** indicates a pattern of xy current.

FIG. **10**F illustrates a comparative analysis of stator current at 1100 rpm and 4 Nm torque for the proposed method using 4 voltage vectors, according to an embodiment. A fiftieth plot **1036** indicates a pattern of $i_{\alpha\beta}$ current. A fifty-first plot **1034** indicates a pattern of $i_{\alpha\beta}$* current. A fifty-second plot **1032** indicates a pattern of xy current.

Considering FIG. **10**A-**10**F, it was observed that the proposed PCC method is superior to the conventional one specially at low and medium speeds. The ripple in $\alpha\beta$ currents was observed to be significantly reduced in the proposed method. It indicates an improved performance of the proposed PCC method even by using only 4 voltage vectors compared to the convention method of using 13 voltage vectors.

FIG. **11**A illustrates a steady state response of the electric drive system **100** at low speed 50 rpm and no-load for conventional method using 13 voltage vectors, according to an embodiment. A fifth-third plot **1102** indicates a pattern observed in rotation speed ω_r of the 6PIM **102** with respect to time. A fifth-fourth plot **1104** indicates a reference rotor speed ω_r*.

FIG. **11**B illustrates a steady state response of the electric drive system **100** for conventional method using 13 voltage vectors for subspace currents i_α, according to an embodiment. A fifty-fifth plot **1106** indicates a pattern of subspace current i_α, through the 6PIM **102** with respect to time. A fifty-sixth plot **1108** indicates a reference subspace current i_α.

FIG. **11**C illustrates a steady state response of the electric drive system **100** for conventional method using 13 voltage vectors for subspace currents i_x, according to an embodiment. A fifty-seventh plot **1110** indicates a pattern of subspace current i_x, through the 6PIM **102** with respect to time.

FIG. **11**D illustrates a steady state response of the electric drive system **100** for conventional method using 13 voltage vectors for phase currents i_a, according to an embodiment. A fifty-eighth plot **1112** indicates a pattern of phase current i_α, through the 6PIM **102** with respect to time.

FIG. **11**E illustrates a steady state response of the electric drive system **100** using a PCC-deadbeat method for rotation speed, according to an embodiment. A fifty-ninth plot **1114** indicates a rotation speed of the 6PIM **102** with respect to time. A sixtieth plot **1116** indicates a reference rotor speed ω_r*.

FIG. **11**F illustrates a steady state response of the electric drive system **100** using a PCC-deadbeat method for subspace currents i_α, according to an embodiment. A sixty-first plot **1118** indicates a pattern of subspace current i_α, through the 6PIM **102** with respect to time. A sixty-second plot **1120** indicates a reference subspace current i_α.

FIG. **11**G illustrates a steady state response of the electric drive system **100** using a PCC-deadbeat method for subspace currents i_x, according to an embodiment. A sixty-third plot **1122** indicates a pattern of subspace current i_x, through the 6PIM **102** with respect to time.

FIG. **11**H illustrates a steady state response of the electric drive system **100** using a PCC-deadbeat method for subspace phase currents i_a, according to an embodiment. A sixty-fourth plot **1124** indicates a pattern of phase current i_α, through the 6PIM **102** with respect to time.

FIG. **11**I illustrates a steady state response of the electric drive system **100** for a proposed PCC method for rotation speed, according to an embodiment. A sixth-fifth plot **1126** indicates a rotation speed of the 6PIM **102** with respect to time. A sixty-sixth plot **1128** indicates a reference rotor speed ω_r*.

FIG. **11**J illustrates a steady state response of the electric drive system **100** for a proposed PCC method for subspace currents i_α, according to an embodiment. A sixty-seventh plot **1130** indicates a pattern of subspace current i_α, through the 6PIM **102** with respect to time. A sixty-eighth plot **1132** indicates a reference subspace current i_α.

FIG. **11**K illustrates a steady state response of the electric drive system **100** for a proposed PCC method for subspace currents i_x, according to an embodiment. A sixty-ninth plot **1134** indicates a pattern of subspace current i_x, through the 6PIM **102** with respect to time.

FIG. **11**L illustrates a steady state response of the electric drive system **100** for a proposed PCC method for subspace phase currents i_a, according to an embodiment. A seventieth plot **1136** indicates a pattern of phase current i_α, through the 6PIM **102** with respect to time.

Considering FIG. **11**A-**11**L, the performance of the conventional, the deadbeat (PCC-DB) based method and the proposed PCC methods were investigated at steady state under different operating points. It was observed that both the PCC-DB and proposed methods tracks successfully speed and current references along with reducing the circulating current significantly compared to the conventional method. Also, the PCC-DB method results in the lowest current THD with some sacrifice with higher switching frequency.

FIG. **12**A illustrates variation pattern of average switching frequency at different speed and 2.5 Nm, according to an embodiment. A seventy-first plot **1204** shows a variation in switching frequency for convention method whereas a seventy-second plot **1202** and a seventy-third plot **1206** shows variation in switching frequency for PCC-DB based method and the proposed PCC method, respectively. It is observed that the proposed PCC method is superior from the average switching frequency viewpoint since it utilizes the redundant four zero VVs and limits the maximum switching state change to one time at maximum per sample time. Thus, considerable reduction of about 50% of the average switching frequency was achieved compared to the conventional method. The same is also shown in Table 5. It is to be noted that a 15% reduction in current total harmonic distortion is also achieved using the proposed PCC method.

TABLE 5

Performance comparison between PCC methods

O.P.	Method	e_α^{RMS}(A)	e_x^{RMS}(A)	i_{THD} %	f_{av}(kHz)
300 rpm	Conv	0.35	1.18	43.2	6.0
2 Nm	PCC-DB	0.19	0.76	27.7	4.45
	Proposed	0.27	0.76	27.5	2.7
600 rpm	Conv	0.37	1.13	33.3	5.9
3 Nm	PCC-DB	0.18	0.80	23.3	6.25
	Proposed	0.26	0.82	23.4	3.8
1100 rpm	Conv	0.45	1.10	25.6	4.1
4 Nm	PCC-DB	0.20	0.86	20.5	3.47
	Proposed	0.37	1.06	23.7	2.1

FIG. **12**B illustrates variation pattern of current THD at different speed and 2.5 Nm load, according to an embodiment. A seventy-fourth plot **1208** shows a variation pattern of current THD for convention method whereas a seventy-fifth plot **1212** and a seventy-sixth plot **1210** shows variation in switching frequency for PCC-DB based method and the proposed PCC method, respectively. The relatively high values for current THD of all methods were observed that may be due to the small value of machine leakage reactance which results in high circulating currents or xy components.

In conclusion of all results as observed in FIGS. **7-12** during the experimental tests over the drive system **100**, it was observed that the e^{RMS} for both a and x subspace was calculated at different speed and loading conditions as listed earlier in Table 5. It was also observed that PCC-DB method has the lowest value for RMS errors. The proposed PCC method shows very close values regarding e_x^{RMS} but a little higher value of e_α^{RMS} compared to the PCC-DB method. It was also evident that the proposed PCC method has the lowest average switching frequency.

TABLE 6

Execution times for different PCC methods

Method	Pred &opt (μsec)	Total (μsec)
Conventional	1.31	14.2
PCC-DB	4.68	17.9
Proposed	0.92	13.8

Also, the average execution time of convention method, PCC-DB and the proposed PCC method is shown in Table 6. From Table 6, it is to be noted that the proposed PCC method shows the shortest execution time. Further, the percentage reduction in execution time was not proportional to the reduction of iterations number, as all three algorithms were optimized to reduce the computation burden. Further the constant terms in the predicted variables in the proposed PCC method could be calculated only one time, while the computation of VV dependent term (BU(k+1)) along with the cost function were repeated as many times as the admissible VVs of each method. This shows a considerably reduction in the computation burden for all methods.

FIG. **13** illustrates a flowchart of a method **1300** for predictive current control of a six-phase induction motor driven by a six-phase inverter, according to an embodiment. The method **1300** is described in conjunction with FIGS. **1-4** and plurality of experimental observation depicted in FIGS. **5-12**. Various steps of the method **1300** are included through blocks in FIG. **13**. One or more blocks may be combined or eliminated to achieve predictive current control method for six-phase induction motor **102** driven by six-phase inverter **104**, without departing from the scope of the present disclosure.

At step **1302**, the method **1300** includes initializing the six-phase inverter **104** at a present control sample comprising a present switching state corresponding to a present voltage vector (VV). The six-phase inverter **104** is further configured to employ the present control sample for converting a DC input voltage to a set of six-phase outputs for an operation of the six-phase induction motor **102**.

At step **1304**, the method **1300** includes measuring a stator current i_s and a rotor speed @r of the six-phase induction motor **102**. The stator current i_s may be measured using a current sensor **132** attached at the output of the 6-phase inverter **104**. The rotor speed ω_r may be measured by an encoder **114** coupled with the 6PIM **102**.

At step **1306**, the method **1300** includes transforming the measured stator current i_s to a set of orthogonal subspace

current values. The set of orthogonal subspace current values comprises a set of current values in αβ and xy frames. In an embodiment, the stator current i_s is transformed into αβ and xy frames or subspace using the first transformation block **130**. The first transformation block **130** is coupled at the output of the 2L-6phase inverter **104**.

At step **1308**, the method **1300** includes estimating a set of rotor variables iq* and id* of the six-phase induction motor **102** using a difference between the measured rotor speed ω_r and a reference rotor speed ω_r*. The set of rotor variables comprises a pair of current values in αβ frame and xy frame. In an embodiment, the set of rotor variables iq* and id* are transformed into αβ frame and xy frame using the second transformation block **124**. The second transformation block **124** is coupled at the output of the PI controller **116**. An input of the PI controller **116** is coupled at the output of the difference circuit configured to compute difference between the measured rotor speed ω_r and a reference rotor speed ω_r*.

At step **1310**, the method **1300** includes calculating a future stator current for a future control sample of the six-phase inverter **104** based on the transformed set of orthogonal subspace current values, estimated set of rotor variables, and the measured rotor speed.

At step **1312**, the method **1300** includes selecting four candidate voltage vectors (Vg) from sixty-four voltage vectors mapped to αβ and xy frames corresponding to sixty-four possible switching states of the six-phase inverter. The step **1312** further comprises a step **1314**, **1316** and **1318** sequentially.

At step **1314**, the method **1300** includes predefining a lookup table **126** representing a correlation between twelve possible non-zero voltage vectors and twelve corresponding groups of voltage vectors. The twelve possible non-zero voltage vectors are twelve possible switching states of the six-phase inverter **104** with on state for at least one of but not all of the set of six phase outputs. Each group of the twelve corresponding groups of voltage vectors comprising four voltage vectors.

At step **1316**, the method **1300** includes selecting a non-zero voltage vector (V_{old} or V_{NZ}) from at least one of, (1) the present voltage vector if the present voltage vector is non-zero or (2) a last appeared nonzero voltage vector from the lookup table **126**.

At step **1318**, the method **1300** includes identifying a group of voltage vectors (V_g) from the lookup table **126** corresponding to the selected non-zero voltage vector. The identified group of voltage vectors corresponds to the four candidate voltage vectors.

At step **1320**, the method **1300** includes implementing a cost function $g(V_s)$ to calculate a squared error between the predicted future stator current and a reference stator current. A weighing factor is applied to the cost function. In an embodiment, weighing factor is selected from a range of 0.01 up to 0.2 that corresponds to control a current in xy orthogonal subspace.

At step **1322**, the method **1300** includes calculating a plurality of cost function results corresponding to each of the four candidate voltage vectors (V_g).

At step **1324**, the method **1300** includes identifying a future voltage vector providing a minimum of the calculated plurality of cost function results for the future control sample.

At step **1326**, the method **1300** includes saving the future voltage vector as an optimal voltage vector to be used as an input to the lookup table **126** for the next control sample.

At step **1328**, the method **1300** includes controlling a plurality of current values in αβ and xy frames of the six-phase induction motor **102** by applying the future control sample as a switching state of the six-phase inverter **104**.

Based upon the method of controlling the six-phase induction motor driven by the six-phase inverter followed by a plurality of experimental observations, a simple PCC algorithm for asynchronous six-phase induction motors is proposed. The predictive current control method requires only four VVs to be evaluated during each control sample. Not only the computation cost is reduced but also a considerable reduction of the average switching frequency is achieved. The performance of the proposed PCC method has been investigated at different operating conditions and compared to the conventional method and deadbeat-based PCC method. The proposed method has the lowest average switching frequency with a reduction of about 50% as compared to conventional methods. Compared to the conventional method, the proposed PCC method has considerable reduction in current THD of about 15%, specially at low and medium speed ranges. The current tracking for the proposed PCC method is superior to the conventional one as indicated by the less tracking errors both in αβ and xy subspaces. There are extra calculations involved in the conventional methods that overburden the cost function calculation, especially in the PCC-DB method that is overcome with the proposed PCC method. Further, the execution time required for implementation is shortest for the proposed PCC method. The reduced number of iterations required for the implementation of the proposed PCC method makes it possible for utilizing longer prediction horizon predictive controllers for multi-phase machines.

Numerous modifications and variations of the present disclosure are possible in light of the above teachings. For example, relatively high values for current THD of all methods were observed in the three methods during experiment. The high value may be due to the small value of machine leakage reactance which results in high circulating currents (xy components). It is therefore to be understood that within the scope of the appended claims, the invention may be practiced otherwise than as specifically described herein.

The invention claimed is:

1. A predictive current control method for a six-phase induction motor driven by a six-phase inverter, comprising:

initializing the six-phase inverter at a present control sample comprising a present switching state corresponding to a present voltage vector, wherein the six-phase inverter employs the present control sample for converting a DC input voltage to a set of six-phase outputs for an operation of the six-phase induction motor;

measuring a stator current and a rotor speed of the six-phase induction motor;

transforming the measured stator current to a set of orthogonal subspace current values, wherein the set of orthogonal subspace current values comprising a set of current values in αβ and xy frames;

estimating a set of rotor variables of the six-phase induction motor using a difference between the measured rotor speed and a reference rotor speed, wherein the set of rotor variables comprising a pair of current values in αβ frame and xy frame;

calculating a future stator current for a future control sample of the six-phase inverter based on the trans-

formed set of orthogonal subspace current values, estimated set of rotor variables, and the measured rotor speed;

selecting four candidate voltage vectors from sixty-four voltage vectors mapped to αβ and xy frames corresponding to sixty-four possible switching states of the six-phase inverter, comprising:

predefining a lookup table representing a correlation between twelve possible non-zero voltage vectors and twelve corresponding groups of voltage vectors, wherein the twelve possible non-zero voltage vectors are twelve possible switching states of the six-phase inverter with on state for at least one of but not all of the set of six phase outputs, wherein each group of the twelve corresponding groups of voltage vectors comprising four voltage vectors;

selecting a non-zero voltage vector from at least one of the present voltage vector if the present voltage vector is non-zero and a last appeared nonzero voltage vector from the lookup table; and

identifying a group of voltage vectors from the lookup table corresponding to the selected non-zero voltage vector, wherein the identified group of voltage vectors corresponds to the four candidate voltage vectors;

implementing a cost function to calculate a squared error between the predicted future stator current and a reference stator current, wherein a weighing factor is applied to the cost function;

calculating a plurality of cost function results corresponding to each of the four candidate voltage vectors;

identifying a future voltage vector providing a minimum of the calculated plurality of cost function results for the future control sample;

saving the future voltage vector as an input to the lookup table for a successive control sample; and

controlling a plurality of current values in αβ and xy frames of the six-phase induction motor by applying the future control sample as a switching state of the six-phase inverter.

2. The predictive current control method of claim **1**, wherein the future control sample comprises at least two future control samples corresponding to the present control sample.

3. The predictive current control method of claim **1**, further comprising identifying a control sample with up to one commutation of a set of switches of the six-phase inverter.

4. The predictive current control method of claim **1**, wherein mapping of a plurality of most significant voltage vectors in αβ orthogonal subspace is corresponding to mapping of a plurality of lowest voltage vectors in xy orthogonal subspace.

5. The predictive current control method of claim **1**, wherein the applied weighing factor corresponds to controlling a current in xy orthogonal subspace.

6. The predictive current control method of claim **1**, wherein the weighing factor is a value selected from a range of 0.01 up to 0.2.

7. The predictive current control method of claim **1**, wherein the twelve possible switching states of the six-phase inverter correspond to twelve largest voltage vectors in αβ orthogonal subspace.

8. The predictive current control method of claim **1**, wherein the four candidate voltage vectors comprise three active voltage vectors and one zero voltage vector.

9. The predictive current control method of claim **8**, wherein the three active voltage vectors correspond to three consecutive switching states of the six-phase inverter.

10. The predictive current control method of claim **8**, wherein the one zero voltage vector is selected from four zero voltage vectors corresponding to four zero switching states of the six-phase inverter.

11. The predictive current control method of claim **1**, wherein the six-phase inverter comprises two three-phase two level-voltage source inverters (2L-VSI) connected in parallel.

12. The predictive current control method of claim **1**, wherein the measuring of the rotor speed of the six-phase induction motor utilizing an encoder coupled to the six-phase induction motor.

13. The predictive current control method of claim **1**, wherein the estimating of the set of rotor variables utilizing a proportional-integral controller.

14. The predictive current control method of claim **1**, performed utilizing a computer processor.

* * * * *